Bioreceptivity of 3D Printed Concrete

Encouraging Moss Growth on 3D-Printed Concrete through Material Adjustments

CIEM0500: MSc Thesis

C. C. Jansen



Delft University of Technology

TU Delft

VERTICO

TU Delft | Hortus Botanicus

Bioreceptivity of 3D Printed Concrete

Encouraging Moss Growth on 3D-Printed Concrete through Material Adjustments

by

C. C. Jansen

to obtain the degree of Master of Science

at the Delft University of Technology,

to be defended publicly on Thursday March 20, 2025 at 15:00.

Student number:	4600673	
Thesis committee:	Dr. ir. B. Šavija,	TU Delft, chair supervisor
	Ir. M. I. A. Veeger,	TU Delft, daily supervisor
	Dr. M. Lesueur,	TU Delft
	Ir. K. Leemeijer,	Vertico B.V.

Cover:	Final specimens in Hortus Botanicus (Own Picture)
Style:	TU Delft Report Style, with modifications by Daan Zwaneveld and Coen Jansen

An electronic version of this thesis is available at `http://repository.tudelft.nl/`.

TU Delft

Preface

With the release of this thesis, my study time has come to an end. The master track Construction Materials quickly sparked my interest because of its evident innovative side. The teaching staff and research atmosphere made me develop something you could call a passion for concrete. This eventually led to my, so far, magnum opus that is now in front of you.

This thesis is about 3D printing of concrete, one of the topics that made me enroll for Construction Materials. Bioreceptivity, on the other hand, can help create to a sustainable and habitable future, something that I really value. So I committed. Sometimes it was tough. Physically, when cleaning up for hours after a print while being covered in sweat and concrete. Mentally, when some experiments did not yield expected results. Nonetheless, the process has taught me a lot and I am thankful for all the experiences.

The project would not have been possible without support from others. I would like to express my gratitude to all of the people that have helped and supported me during this academic expedition. First of all, I would like to thank my supervisor Max for providing information about moss and bio-growth, which I had little knowledge of initially, and for planting some key insights into my stubborn head. Also, I would like to thank my supervisors Branko, Martin and Kees for their support and tangible feedback, especially after the green light meeting.

Furthermore, my thanks go out to 'concrete legend' Maiko van Leeuwen, who taught me how to use much of the laboratory equipment and was involved in resurrecting the almost lost knowledge on 3D concrete printing at the faculty. Thanks also to Ton Blom for the numerous hours of sawing and drilling my concrete samples, and to Ron Penners for guidance with the recycling lab machinery. My acknowledgments to John van den Berg and Arjan Thijssen, who taught and assisted me in various laboratory tests, as well as to Patrick Holthuizen, whose microscopic methods I adopted. I am much obliged with James, Lewie, and the other staff of the Hortus Botanicus for letting me use their facility, taking care of my samples and thinking along. It was a pleasant cooperation.

During the 3D printing sessions, I got help from many people at Materials & Environment, to whom my sincerest gratitude goes out: Rowin, Sep, Wouter, Zhaozheng, Burcu, Branko, Laura and Wen. Wen has taught me a lot about operating the printer, and her experience on 3DPC helped me to more effectively make progress.

Much appreciation to my fellow students with whom I shared the same 'afstudeer' journey. Wouter, as we could always discuss anything thesis related. Sabine, Pim and Frederiek, for all the enjoyable times during breaks. Lastly, I genuinely want to thank my friends, Ries and Meike, my family and Tessel, for their unconditional, emotional support.

I consider this thesis to be a contribution to the knowledge base of bioreceptive 3D printed concrete and I wish everyone an insightful and inspirational read.

Coen Jansen
Delft, March 2025

Summary

Due to changes in climate, cities and urban areas are more and more tormented by issues such as the Urban Heat Island Effect and extreme precipitation. One way to tackle these issues is the implementation of green spaces, found to control local climate and improve water management. However, densification within cities threatens the space for green envelope. The application of moss, a type of plant that can adapt to many habitats, directly on the concrete surface of buildings could provide a solution. This requires the concrete to possess certain characteristics that allow and promote moss growth. The general term for a material's ability to be colonized by biological growth is called its bioreceptivity. Surface roughness, surface pH, chemical composition, porosity and water retention have been documented to be strong predictors for bioreceptivity of concrete.

In this thesis, the bioreceptivity of 3D printed concrete (3DPC), an upcoming and promising concrete manufacturing technique with near prospects in urban context, is aimed to be improved by incorporating lightweight aggregates (LWA). A starting 3DPC mixture was adopted. Samples were 3D-printed with sand partially replaced by 30% Crushed Expanded Clay (CEC), Expanded Glass (EG), Expanded Vermiculite (EV), and Pumice (PU). Additionally, a separate set of samples incorporated a 45% replacement using only pumice.

Moss was planted on the specimens and allowed to grow in a climate controlled glass house. After 7 weeks, the green coverage on all specimens had severely decreased. The maximum quantum yield measured by Pulse Amplitude Modulation Fluorometry (PAM-F) suggested decreasing plant health as well. Improper environmental conditions and watering regime were held accountable for this. The results yielded insufficient information to discuss the impact of added LWA on bioreceptivity.

The samples were evaluated on their bioreceptivity factors, compressive and flexural strength. Surface roughness was similar across all the variants. All samples had a surface pH that exceeded 12. Samples withg with 30% replacement of expanded vermiculite (EV30) showed highest porosity, but lowest water retention. Mechanically, EV30 showed weakest compressive and flexural strength, but this can be partially allocated to its curing conditions. Contrarily, CEC30 and PU30 samples showed similar or higher values for compressive and flexural strength than the reference samples without any treatment.

The findings in this research implied that 3DPC open porosity increases with increasing aggregate porosity, and implied a reduced ability to retain water with increasing open porosity, although both these characteristics are reliant on the pore microstructure as well. Of all the LWAs, implementation of EV showed to be most promising in terms of habitat provision for moss growth. However, due to the marginal sample size the statistical significance is questionable.

Contents

Preface i

Summary ii

Nomenclature vi

1 Introduction 1
- 1.1 Background information . . . 1
- 1.2 Problem statement . . . 2
- 1.3 Research aim . . . 3
- 1.4 Scope . . . 3
- 1.5 Task outline . . . 3
  - 1.5.1 Reading guide . . . 4

2 Literature review 5
- 2.1 Mosses . . . 6
  - 2.1.1 Moss benefits in urban areas . . . 6
  - 2.1.2 Moss specifics and nutrients . . . 6
  - 2.1.3 Relationship with pH . . . 7
  - 2.1.4 Relationship with water . . . 7
- 2.2 Bioreceptivity of concrete . . . 8
  - 2.2.1 Types of bioreceptivity . . . 8
  - 2.2.2 Bioreceptivity factors . . . 8
  - 2.2.3 Evaluating biological growth . . . 11
  - 2.2.4 Biological growth and concrete quality . . . 12
- 2.3 3DPC . . . 14
  - 2.3.1 Working principle . . . 14
  - 2.3.2 Fresh characteristics . . . 14
  - 2.3.3 State-of-the-art: bioreceptive 3DPC . . . 17
- 2.4 Experimental exploration . . . 21
  - 2.4.1 Theoretical framework . . . 21
  - 2.4.2 Selected aggregates . . . 22

3 Methods and Materials 23
- 3.1 Experimental outline . . . 24
- 3.2 Tailoring the mix design . . . 25
  - 3.2.1 Reference mix . . . 25
  - 3.2.2 Replacement strategy . . . 26
  - 3.2.3 Material origin . . . 26
- 3.3 Aggregate characterization . . . 28
  - 3.3.1 Grain size distribution . . . 28
  - 3.3.2 Porosity and pore size distribution . . . 29
  - 3.3.3 Water absorption and particle density . . . 29
  - 3.3.4 Water retention . . . 30
- 3.4 Concrete properties - fresh . . . 31
  - 3.4.1 Mixing regime . . . 31
  - 3.4.2 Flowability . . . 31
  - 3.4.3 Extrudability . . . 31
  - 3.4.4 Open time . . . 31
  - 3.4.5 Shape retention . . . 31
- 3.5 Printing . . . 33

3.5.1 Apparatus . . . 33
3.5.2 Print design . . . 33
3.5.3 Print session . . . 35
3.6 Concrete properties - hardened . . . 36
3.6.1 Strength assessment . . . 36
3.6.2 Surface pH . . . 36
3.6.3 Surface roughness . . . 37
3.6.4 Porosity . . . 38
3.6.5 Water retention . . . 40
3.7 Biological Growth . . . 41
3.7.1 Moss harvesting and preparation . . . 41
3.7.2 Planting and storage . . . 41
3.7.3 Assessment of biological growth . . . 42
3.8 Statistical analysis . . . 44

4 Results 45
4.1 Aggregate characterization . . . 46
4.1.1 Chemical composition . . . 46
4.1.2 Particle size distribution . . . 46
4.1.3 Porosity and pore size distribution . . . 46
4.1.4 Water absorption and particle density . . . 47
4.1.5 Water retention . . . 48
4.1.6 Replacement percentages . . . 49
4.2 Concrete properties - fresh . . . 50
4.2.1 Flowability and shape retention . . . 50
4.2.2 Extrudability . . . 51
4.2.3 Open time . . . 51
4.3 Printing . . . 52
4.3.1 Print results . . . 52
4.3.2 Environmental factors . . . 52
4.4 Concrete properties - Hardened . . . 55
4.4.1 Flexural and compressive strength . . . 55
4.4.2 Surface pH . . . 56
4.4.3 Surface roughness . . . 56
4.4.4 Porosity - Water absorption . . . 57
4.4.5 Porosity - CT . . . 57
4.4.6 Water retention . . . 61
4.5 Biological Growth . . . 62
4.5.1 Green cover . . . 62
4.5.2 Quantum yield . . . 72

5 Statistical analysis and Discussion 73
5.1 Growth experiment assessment . . . 74
5.1.1 Initial moss quality . . . 75
5.1.2 Substrate properties . . . 75
5.1.3 Environmental conditions . . . 76
5.2 Influence on intermediate variables . . . 78
5.2.1 Effect of aggregate water absorption . . . 78
5.2.2 Effect of aggregate water retention . . . 78
5.2.3 Effect of water cement ratios . . . 80
5.2.4 Outlier: Expanded Vermiculite . . . 80
5.2.5 Effects of higher LWA content . . . 81
5.2.6 Reflection on Theoretical Framework . . . 81
5.3 Influence on other factors . . . 83
5.3.1 Surface roughness . . . 83
5.3.2 Surface pH . . . 83
5.3.3 Mechanical performance . . . 83

5.4 Quality of printing . . . 86
5.5 Reflection on experiments . . . 87
5.5.1 Porosity approach . . . 87
5.5.2 Statistical significance . . . 87
5.5.3 CT scanning . . . 87

6 Conclusions and recommendations 89
6.1 Conclusive statements . . . 90
6.2 Recommendations . . . 92

References 93

A Geometrical code 102

B CT Acquisition settings 105

Nomenclature

Abbreviations

Abbreviation	Definition
3DCP	Three-Dimensional Concrete Printing
3DPC	Three-Dimensionally Printed Concrete
BFS	Blast Furnace Slag
CEC	Crushed Expanded Clay
CNC	Computer Numerical Control
CT	Computed Tomography
EG	Expanded Glass
EV	Expanded Vermiculite
Fa	Fly Ash
FVM	Focus Variation Microscopy
GSD	Grain Size Distribution
IR	Infra-Red
LOI	Loss on Ignition
LWA	Light-Weight Aggregates
MC	Mold-cast Concrete
MIP	Mercury Intrusion Porosimetry
OPC	Ordinary Portland Cement
PAM	Pulse Amplitude Modulation
PMx	Particulate Matter
PU	Pumice aggregates
RH	Relative Humidity
RS	Reference Sand
SAP	Super Absorbent Polymer
SCM	Supplementary Cementitious Material
SF	Silica Fume
SP	Super Plasticizer
ssd	Saturated and surface dry
UHI	Urban Heat Island
UHPC	Ultra High Performance Concrete
VMA	Viscosity Modifying Agent
w/c	Water cement ratio
w/d	Water to dry ratio
WAM	Water Absorption Method
XRF	X-Ray Fluorescence

1 Introduction

1.1 Background information

Across the globe, people are moving to cities, and urbanization is occurring at large scale [1]. As a response, cities need to expand and increase their capacity by constructing new buildings. It is no surprise that concrete is one of the main building components, as it is a widely available, reliable, and relatively cheap building material and even the second most used material on the planet [2]. However, abundant use of materials like concrete in urban dense areas brings along negative effects as well, some of which are already everyday issues.

Concrete and asphalt dominated cities especially are shown to act as giant heat absorbers during solar rich days, also named the Urban Heat Island (UHI) Effect [3]. Firstly, concrete is able to absorb large amounts of heat energy and emits it over an extended period of time. Secondly, any precipitation water is quickly guided away into the sewer systems, which decreases the rate of heat loss by evaporation. These two dynamics are warming the city to significantly higher temperatures than the area surrounding it. This is an even larger threat considering that temperatures will rise further due to global warming.

Global warming also intensifies sudden and extreme precipitation events, posing an even greater risk to cyclone-prone cities [4]. Cities and their sewer systems are not always able to abduct these large amounts of rainwater, causing overflows and discomfort among the inhabitants [5].

One of the ways to possibly greatly overcome the beforementioned issues, is the implementation of greenery in these cities. Research shows that proper realization of vegetation in cities potentially leads to, among other things, more natural climate control, partly by decreasing high temperatures in the cities [3, 6, 7, 8], but also by saving energy for heating during cooler periods [9]. It could help with water management, since plants and their substrates have the ability to absorb water and release it slowly after [3]. This water retention decreases the load on the sewer systems [5]. Lastly, more vegetation and green areas in cities have a positive effect on the biodiversity in cities [3, 10]. This is often desired, because it contributes to a natural ecosystem.

Although the benefits are widely researched, providing high-quality green areas in densely populated cities is a significant challenge [11, 12]. At the same time, densification of cities is shown to be a major threat to urban green space [13]. These studies indicate that cities must explore new and innovative solutions to integrate green spaces effectively. Utilizing the abundant amounts of concrete in cities as a substrate for vegetative growth could be a pivotal step in this story. To what extent a material is able to house biological growth, is determined by the *bioreceptivity* of that material. Defined by Guillitte [14] (p.216), bioreceptivity is understood as ‘the totality of material properties that contribute to the establishment, anchorage and development of flora and/or fauna’.

The implementation of specifically mosses on concrete is indicated in academic studies as a possible solution to introduce greenery in a city, without occupying more space [15, 16]. Thanks to their little needs and their ability to adapt to a wide variety of substrates and environmental conditions, mosses

can offer a low-cost and low-maintenance alternative green envelope on urban and industrial buildings [16]. When applied at a large scale, this could tackle the before mentioned environment related issues in urban regions as well as bypassing the green implementation dilemma.

Mosses (*Bryophytes*) are the second most species-rich group of plants, with only *Angiosperms* surpassing them in diversity. Mosses are characterized by their mop-like structure, reliance on vegetative reproduction, and so-called rhizoids that enable them to cling to building surfaces [17]. Despite their structural simplicity compared to larger plants, mosses possess unique adaptations that allow them to thrive in a variety of environmental conditions, even the harsh and unfavorable ones. One of moss' most remarkable abilities is their relatively high tolerance for salinity, metals and air pollutants [16]. Their ecological importance is particularly evident in urban and polluted environments, where these traits are very suitable for tracking and mitigating environmental stressors. They require minimal growing substrates, water, and nutrients, while their capacity to absorb liquids up to 20 times their weight further enhances their resilience [18]. Additionally, some mosses exhibit vegetative desiccation tolerance, allowing them to withstand extended dry periods and adapt to challenging habitats [15, 18].

1.2 Problem statement

In recent years, several studies have aimed to map the factors that influence concrete's bioreceptivity and tried to increase its bioreceptivity based on those findings [19, 20, 21], some with a special focus on moss [16, 22, 23]. While this is still a developing field of research, the obtained promoting factors of bioreceptivity are generally similar among the studies. Most of these studies concern conventional mold-cast concrete (MC). However, the attention for three-dimensional printing of concrete (3DPC), a novel manufacturing technique for constructive applications, falls behind in this relation. MC and 3DPC may share the same fundamental ingredients like cement and water, but the proportions in mix design, types of additives, curing regime, structural performance and surface topology cannot be compared.

3D concrete printing has been rapidly advancing over the last years and has emerged as a transformative technology that cannot be overlooked. Compared to traditional mold-cast concrete, 3DPC grants the possibility of freeform of design, allowing the manufacturing of concrete shapes that are much more difficult to achieve with regular formwork. For example, the technique can be used to produce topology optimized constructive elements that are notorious for their rounded and sometimes slender appearance, saving materials and accessory costs [24, 25, 26]. Some other application that sees use is the on-site printing of the entire structure. Corrugated hollow walls are printed with a structural infill, which can sometimes even serve as formwork for additional cast concrete. This is reality rather than concept, as there are numerous examples of multi-story buildings that have been established by employing 3DPC, either by prefabricated assembly or full-size on-site printing [26]. Considering the amount of studies on 3DPC, the rise of companies associated with 3DPC, and the objects made by 3DPC over the last few decades, it is likely a matter of time before the technique is scaled up to a conventional means for larger urban construction projects.

The shape and surface topology of a material are critical factors influencing its bioreceptivity [27]. In the context of 3DPC, the technology's capability to produce a diverse range of shapes and surface designs offers a significant advantage in studying and optimizing bioreceptivity. Consequently, many studies that focus on the bioreceptivity of 3D printed materials have adopted this approach [28, 29, 30]. Water guidance and cavity presence come out as main contributors to enhanced biological growth. Also varying the layer height of the prints, as done by [29], increases local porosity and consequently enhances moss growth rates. This limited amount of studies shows that biological growth on 3D printed structures strongly relies on outer geometry as well as print parameters. Besides the absence of mortar or concrete, a perspective that focuses on intrinsic material characteristics affecting bioreceptivity is missing in these studies.

In order to fully understand the bioreceptivity of 3DPC structures, geometrical as well as inherent materialistic factors should be taken into account. Considering an expected rise of the 3DPC sector in the urban environment, the relevance of this topic is emphasized even more.

1.3 Research aim

The main aim of this research is to explore possibilities to increase bioreceptivy of 3DPC from a material-based perspective, unveiling the current challenges that this material encounters in terms of moss growth and trying to overcome them. While doing so, the concrete should maintain its properties to be 3D printable. This thesis will not only contribute to the knowledge base in this field, but also provide a first foundation for the advanced development of bioreceptive 3DPC. In a research question:

How can 3D printable concrete mix design be altered to promote bioreceptivity, and how does that affect fresh and hardened 3D printed concrete properties?

To achieve the answer to this question, the following objectives are stated:

1. To understand what the factors are that promote biological growth on concrete, moss in particular.
2. To discover to what extent these factors are represented in current development of 3DPC.
3. Combining the findings of the previous two objectives, to forge a strategy of increasing bioreceptivity of the used concrete while maintaining fundamental 3DPC characteristics.
4. To execute this strategy by manufacturing multiple 3DPC structures and comparing them based on bioreceptive properties.

1.4 Scope

In order to ensure the completion of this research within reasonable time, certain limitations have been imposed on its scope.

- Bioreceptivity is attempted to improve from a material perspective rather than a texture or topology perspective.
- 3DPC performance is reviewed for a small scale laboratory setting. Suitability of the 3DPC for large structures is not part of this thesis.
- Only the horizontally placed side surfaces of sample were examined.
- To encourage moss growth, a controlled constant temperature, relative humidity and watering regime are used. Performance in other environments is not investigated.

1.5 Task outline

This thesis has been conducted with guidance by a sequenced task outline that was made at the start of this thesis, see figure 1.1. The steps are based on the research objectives as well as some preliminary research. Smaller tiles below the steps indicate any prerequisite knowledge or skills for that step.

1. *Determine bioreceptivity factors concrete*. This is covered in the first objective and will mostly be done by analyzing literature
2. *Determine bioreceptivity ingredients*. What could be suitable additions to a mix design to theoretically make it more susceptible to moss growth.
3. *Implementation in 3DPC*. Try to include these additions to a starting/base line mix design for 3DPC.
4. *Mixture preparation*. See what the effects are of this inclusion on the printability if the fresh concrete. Reconsider other ingredients if necessary.
5. *3D printing*. Genesis of the final specimens.
6. *Testing printed specimens*. Acquire data from the cured specimens based on bioreceptivity markers and mechanical performance.
7. *Adhesion and growing of moss*. Planting moss on the specimens and monitor their growth to verify to which extent the alterations have effect on the bioreceptivity of the 3DPC.

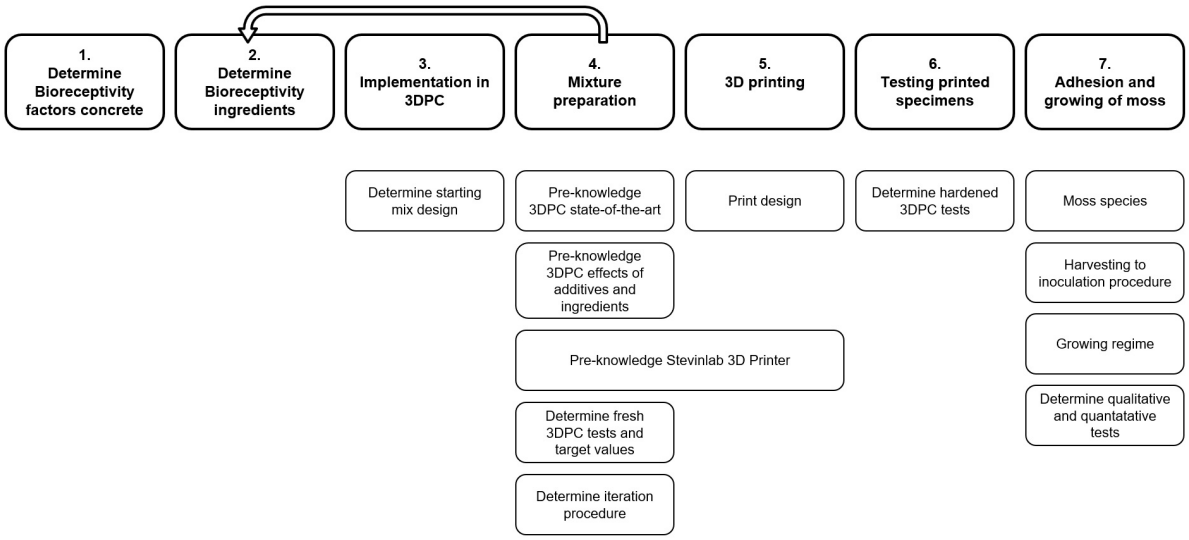


Figure 1.1: Plan of making bioreceptive 3DCP in 7 steps. The tiles in the columns below the steps represent the prerequisites that are needed to properly perform that step.

During this thesis, this task breakdown was used as guidance and followed more or less chronologically. It should be noted that the steps do not necessarily harmonize with the order of chapters and sections in this report.

1.5.1. Reading guide

In this chapter, the reader has gotten acquainted with the topics, the societal relevance, the problem statement and the aims of this thesis. In the next chapter, more information is gathered on mosses, bioreceptivity of concrete and the current state of 3DPC regarding bioreceptivity. The third chapter presents an experimental outline with the goal of developing bioreceptive 3DPC, and lists all the experiments that come with it. The fourth chapter contains the results of all the experiments with some supportive explanation. In chapter 5, the results are interpreted and critically discussed. The last chapter summarizes and concludes the entire thesis, and gives some recommendations for future research.

2

Literature review

This research essentially links the research disciplines of concrete 3D printing to that of concrete bioreceptivity and moss growth. It is necessary to have a thorough understanding of the drivers behind bioreceptivity to eventually design the 3D printed concrete accordingly. On the other hand it is also crucial to be aware of the possibilities and the limitations of 3DCP. Combining the knowledge of both fields, one can estimate what the expected challenges and results could be in terms of both suitability for 3DCP and bioreceptivity.

2.1 Mosses

2.1.1. Moss benefits in urban areas

Mosses are suitable for urban environments due to their ability to provide critical ecosystem services. Their capacity to accumulate particulate matter (PMx) and other airborne pollutants makes them effective natural air filters, with some species serving as bioindicators for air quality [15, 16]. Additionally, mosses excel in stormwater management by retaining significant amounts of water, reducing runoff and improving water quality through pollutant filtration [16, 31]

Mosses' impact on urban climate regulation is equally notable. Mosses help mitigate the Urban Heat Island (UHI) effect by reducing surface temperatures through a phenomenon called evapotranspiration and minimizing heat absorption on concrete surfaces [15, 16, 32]. This function, combined with their desiccation tolerance, allows them to survive on scarce and nutrient-poor surfaces, making them ideal for urban structures such as walls and roofs [15, 16, 31].

Ecologically, mosses contribute to urban biodiversity by creating microhabitats for small organisms. Their ability to colonize extreme environments enhances urban green spaces in locations unsuitable for vascular plants [15, 16]. Economically, mosses present a low-cost, low-maintenance alternative to traditional green infrastructure, requiring minimal water, no soil, and no complex irrigation systems. Their use can be even more supported when they have sufficient bioreceptive area to live on [15, 16].

2.1.2. Moss specifics and nutrients

Although mosses are regarded plants, they possess some mechanisms that differentiates them from vascular plants. Mosses anchor themselves to their substrate making use of so-called rhizoids, which are hair-like filaments that serve mainly for attachment to surfaces such as rock or wood [17]. Regarding reproduction, mosses can do this either sexually, or asexually, of which fragmentation is a possible method [33, 34].

Mosses obtain their nutrients primarily through passive mechanisms, as they lack vascular systems for nutrient uptake They are poikilohydric: possessing a water content equivalent to then of their environment [35]. This feature means that their hydration, and consequently their access to nutrients, depends entirely on environmental conditions [17]. Carbon supply usually comes from the CO_2 in the air, and sometimes from the released CO_2 from the soil. For nutrients, mosses rely heavily on rainwater, absorbing dissolved minerals directly from precipitation. Atmospheric dust and particulate matter deposited on their surfaces also provide essential nutrients [17, 36, 37]. This is especially the case for rock-dwelling colonies.

According to [17], the nutrient requirements of mosses closely resemble those of vascular plants, as they are used for similar cellular processes. However, due to their poikilohydric nature, mosses require nutrient concentrations approximately ten times lower than those needed by vascular plants. This lower requirement stems from their mode of water and nutrient absorption through their external surface, which also makes them highly sensitive to osmotic shock. Exposure to solutions with excessively high concentrations of nutrients or toxic substances can lead to cell damage and localized plant death.

Mosses' nutrient requirements are divided into macronutrients and micronutrients. Macronutrients, required in relatively high concentrations, include nitrogen (N), phosphorus (P), sulfur (S), potassium (K), calcium (Ca), magnesium (Mg), and iron (Fe). Micronutrients, needed in much smaller amounts, include manganese (Mn), copper (Cu), zinc (Zn), molybdenum (Mo), nickel (Ni), chloride (Cl), and boron (B) [17]. Notably, nutrient requirements and tolerance levels can vary even within colonies of the same moss species, as individual plants often develop osmotic potentials adapted to their specific local environments. This balance can be disturbed when the mosses are exposed to a different environment, for which it will take some time to adapt [17].

2.1.3. Relationship with pH

How well nutrients dissolve in water has to do with the pH. Generally, a lower pH allows more nutrients to be dissolved and hence being absorbed by the moss. However, this also is the case for more toxic elements like Aluminum (Al) [17]. Colonies have been observed in low as well as high pH habitats.

2.1.4. Relationship with water

Considering the fact that bryophytes evolved from - and some species still are - submerged organisms, they ideally require a vast sufficient amount of water [31]. As said before, mosses obtain water solved nutrients via their outer surface through osmotic principles. Mosses do therefore benefit from retaining any water they can grasp, which they do by absorbing it into their capillary spaces [31]. However, there is a limit to the amount of moisture surrounding the leaves for extensive periods, as it can become difficult for the moss to obtain CO_2 [17]. Some bryophytes have evolved such that they can survive extremely irregular access of water, which goes by their poikilohydric abilities. In water scarce times, their metabolism will be suspended until water is available again. These mosses are therefore desiccation tolerant.

2.2 Bioreceptivity of concrete

2.2.1. Types of bioreceptivity

The term bioreceptivity can be specified further. In his paper, Guillitte [14] defined six types of bioreceptivity, which were later revised by Sanmartín et al. [38]. The latter defined primary, secondary, tertiary and quaternary bioreceptivity of a material. Primary indicates a new material which is ready to be used for its final function. Secondary indicates that the material has been weathered due to environmental factors. Tertiary: the material has been exposed to cleaning (mechanical, laser, etc.) which affects the material surface. Quaternary: the material has undergone some sort of surface treatment or coating. The latter two specifically imply the interference of humans. Besides these types, intrinsic factors and extrinsic factors also play a role in the bioreceptivity of the material. Intrinsic factors are material specific, whereas extrinsic factors include things like surface deposits and locational properties [38]. Lastly Sanmartín et al. [38] distinguish the setting in which potential biological attachment takes place, which can be in subaerial, submerged or subsoil environment. Regarding this research, intrinsic bioreceptivity factors of 3DCP specimens in a subaerial environment are attempted to be improved, resulting in an increase of the primary bioreceptivity.

2.2.2. Bioreceptivity factors

The bioreceptivity terminology from Sanmartín et al. [38] suggests that there is more than one way in which a materials bioreceptivity can be improved. Over the last three decades, more and more studies have been done that try to pinpoint which factors (intrinsic and extrinsic) influence the bioreceptivity of many materials. Among these concrete is very popular, given that it is the second most used material on earth [2].

Numerous studies on the topic of bioreceptivity of concrete specifically have been reviewed by [27]. Many of these studies were executed in different settings and with diverse methods, making it difficult to fully compare all the results. Storage conditions, cementitious mix design, species for growth, and documentation method of biological staining are some of the parts where the studies greatly differ. This shows that there is still a wide variation of factor combinations that have not been researched yet, and that the field needs some standardizations of testing and methods.

From this meta-analysis from [27], it becomes clear that porosity, water retention, surface roughness, surface pH, and to some extent the chemical/mineralogical composition can contribute to concrete bioreceptivity. This forms some useful insights, but solely based on studies that involved (cyano)bacteria, algae or fungi. No studies considering mosses were included. However, since mosses require similar nutrients, water access and anchorage options, the factors are arguably similar for them as well as for other species. This is further backed up by various studies including moss and concrete/mortar that involve such properties [10, 16, 19, 22, 23, 39, 40].

2.2.2.1. Water management

Some studies on bioreceptivity state that water availability is the single most important factor for biocolonization [22, 29]. As stated before, moss' relation to water is one of their most important regarding the survivability of the species. After periods of precipitation or dew, water supply from within the concrete substrate can be crucial in organism development. The concrete should therefore ideally be able to absorb water when abundant and provide it to the organisms later.

Research showed that a larger content of pores in mortar were reason for increased algal bioreceptivity [41]. Because of the incorporation of coarser aggregates, porosity was increased and the use of recycled super absorbent polymers (SAP) resulted in water retaining pores. Other studies also show a positive relationship between the porosity of the concrete surface region and the observed biological growth [39, 42].

Porous concrete allows water to access the concrete matrix. Higher porosity concrete generally has the ability to absorb more water than nonporous variants. This would suggest that a higher porosity is always better for bioreceptivity. However, the reality is a bit more nuanced.

First of all, water needs to be able to reach the pores in order for the concrete to yield absorbing properties. The open porosity, meaning all the pore spaces that can be accessed from the outer surface of the concrete, is therefore an indicative characteristic for its bioreceptivity. This total volume of open pores can be estimated by immersing and measuring the absorbed water mass [19]. Mercury Intrusion Porosimetry (MIP), a technique where mercury is intruded in the concrete specimen by means of pressure, is also seen in literature [41, 43, 44, 45]. Pores are mathematically approached as cylinders, hence a pore size distribution of the open pores is the result.

What the most important pore size is for water absorption and retention varies a bit among studies. The study from [41] showed that increased content of mesopores was governing for increased algae growth. According to the review from [27], capillary pores are expected to have the most influence on water supply for organisms such as bacteria, fungi and algae. It is not clear if this is the case for mosses too, as mosses are larger multicellular organisms that could require larger amounts of water.

For correct understanding, the pore diameter ranges from the IUPAC are [46]:

- micropores - Ø < 2nm
- mesopores - 2 nm < Ø < 50 nm
- macropores - Ø > 50 nm

The size of capillary pores is not defined, as capillary refers more to a function than to a size.

In the end, the role of the pores in bioreceptive context is to absorb (and retain) water into the concrete. In some studies, water absorption or retention measurements are carried out complementing outcomes of porosity tests [19, 41, 45]. Or water retention is measured directly, without supporting porosity measurement data [20, 22]. Not surprisingly, higher absorbing and retaining specimens performed better on bioreceptivity.

In macroscale, the water retention can also be increased by the shape of the surface and the structure. Crevices or pockets are an example of this, as they can store water as well as dust or sand particles that act as a growth substratum [29].

To conclude, flora can profit from concrete with high water retention. To retain high amounts of water, it should have high water absorption. High water absorption can be achieved with a high open porosity, and pore shapes and sizes that allow this, but no specifics about this are clear.

2.2.2.2. *Surface roughness*

Roughness of a surface describes how much the surface deviates in height over a certain length or surface area. Higher roughness indicates relatively large local peaks and valleys, effectively increasing available surface area. This can act as protective areas for (micro-)organisms as well as mosses. The roughness allows the organisms to attach to the surface better, being able to withstand rain and wind induced stresses [22, 47]. For mosses specifically, surface texture increases their rhizoids effectivity to clamp to the concrete and secure their position [17]. Sometimes, nutrient-rich particles can accumulate in between the tiny crevices which can be additionally beneficial for the organism [48].

The use of surface retarders can significantly play a role in the concretes surface roughness. These substances extend the hardening of the concrete at the surface. After formwork removal, the surface concrete can than be mechanically removed, exposing the aggregates. Used by [20], a surface retarder showed increased bioreceptivity, presumably through increased surface roughness and easier water ingression abilities.

In comparison, a smooth surface tends to be disadvantageous for biological growth. It cannot provide protection nor proper anchorage of the organism. An example of this was researched by [47], where smooth surfaced UHPC-based concrete was compared to bioreceptive concrete by casting it in the same tile. In controlled exterior setting as well as exterior, the smooth surface concrete did not show any algae growth while the bioreceptive part of the tile did.

What a good roughness level is, depends on the species in question. Single-celled organisms likely prefer roughness that is slightly larger than the size of the sort itself. This is not exactly clear for

mosses, but the study from [19] showed that substrates with higher roughness levels exceeding 2500 µm showed more moss growth than specimens with roughness below 150 µm.

That raises the question how roughness is actually measured. A 3D scanning device was used by [19], but optical methods (with digital post-processing) also see use [20, 49]. They all eventually use the observed heights and transfer them to a roughness number. Norms such as ISO 21920-2:2021 and ISO 13565:1996 give equations for roughness parameters that can be used for this. Common ones are the maximum height profile Rz [50, 51] and the (Arithmetical) mean Ra [45, 49, 50, 51, 52]. By the ISO standards, these are defined as:

$$Rz = \max(Z(x)) + |\min(Z(x))| \tag{2.1}$$

$$\mathrm{Ra} = \frac{1}{\ell_\mathrm{r}} \int_0^{\ell_\mathrm{r}} |\mathrm{Z(x)}| \mathrm{dx} \tag{2.2}$$

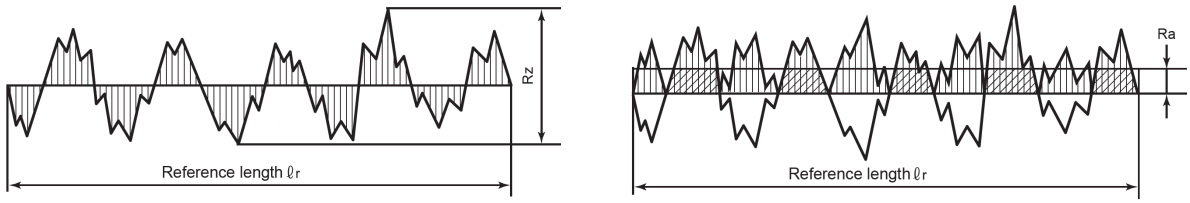


Figure 2.1: Visualization of common roughness definitions, adopted from Keyence VHX-7000 User's manual. (a) Maximum height profile. (b) Arithmetical mean.

In figure 2.1, the visual representations of both roughness definitions are shown. $Z(x)$ is the vertical distance from the average line, ℓ_r refers to the investigated length.

2.2.2.3. *Surface pH*

The pH (*Potential Hydrogen*) of a substrate can be critical for an organisms survival. A pH that is too high or too low can result in disruptions of the integrity of cell membranes of organisms, as well as impede the solubility and uptake of nutrients. The pH is a chemical property that relies on ion concentrations, and is therefore dependent on temperature.

Aside from some alkali tolerant algae and cyanobacteria, there are basically no organisms that prefer extremely alkaline environments [53]. And there have also been no reports of life in such alkaline areas. In the book from [17], it becomes clear that in nature most mosses thrive in slightly acidic to neutral pH regions, most 3.0 to 5.5. This is ofcourse species dependent. Also, due to their great adaptability some mosses can even grow in limestone rich areas with higher pH [17].

Portland cement based concrete is usually also very alkaline, where pH values of 12 or 13 are not uncommon especially in newly made concrete. Over time, carbonation can occur where CO_2 ingress can chemically bond with portlandite and CSH, resulting in lower alkalinity of the surface region of the concrete [54]. Very carbonated concrete can have a surface pH below 9, which is a lot more suitable for many organisms than 12 or higher. Conversely, one must also consider that carbonation is associated with a reduced pore volume, due to the deposition of $CaCO_3$ [54].

Many researchers use therefore accelerated carbonation (or accelerated weathering) methods to drastically decrease the alkalinity when experimenting with bioreceptivity of concrete [21, 42, 55, 56]. One study found algae growth on concrete with pH >10 [20]. This is somewhat supported by [55], who found that carbonation in their in-situ concrete did not play a large role on algal biofouling. Other factors were believed to be stronger reasons for algal growth. These studies implicate that the so-far thought pH limit for growth can be stretched, as long as other bioreceptivity factors make up for it.

It becomes clear that, mostly due to carbonation, concrete's pH is lower at the surface region than in the bulk. The pH of the bulk is of marginal importance to the bioreceptive characteristics of the surface. Therefore, when measuring pH it should concern the surface of the concrete the most.

2.2.2.4. Chemical composition

Compounds in common MC are cement, water, aggregate. Often, supplementary cementitious materials (SCM) such as Blast Furnace Slag (BFS), Fly Ash (FA), Silica Fume (SF), other pozzolans, and additives like super plasticizer (SP) and Viscosity Modifying Agents (VMA) are added. All these ingredients have a different chemical composition, where the surface organism will be in contact with. Cement and (quartz) aggregates contain an excess amount of calcium and silica, including some metals like iron and aluminum [57, 58]. SCMs have a pozzolanic effect, which refers to the secondary reactions during concrete hydration, producing reactive products such as calcium compounds. BFS inclusion can increase the Alumina and Manganese content a bit, where as fly ash does the same for silica, aluminum and iron [59]. Superplasticizers often consist of polymers, consisting of elements like carbon, hydrogen, oxygen, nitrogen and sulfur [60], which can even be of nutritional value to moss [17].

Concluded by [27], the chemical composition affects bioreceptivity the most by affecting other bioreceptivity properties, pH in particular. For example, [21] used specimens based on Magnesium Phosphate Cement (MPC) instead of OPC and found a pH of 6.7 and faster algal biofouling was observed.

The concrete substrate itself does not have to be the main source of nutrients, since organisms like algae or bacteria can get sufficient nutrients from water and the aerosol. However, an element like phosphorus, which is an essential nutrient for mosses [17], is only found relatively low quantities in (polluted) aerosol and water [61]. It can increase plant growth rates significantly and is a common fertilizer in agriculture [61]. The addition of phosphorus rich materials to concrete has shown to also increase algae growth [20], suggesting that the organisms can extract the nutrients from the substrate.

As stated before, some elements can be toxic for mosses, in particular heavy metals and Aluminum [17]. So, although not the largest influence on bioreceptivity, it should be taken into account that the elements inside the substrate are able to stimulate or impede biological growth to some extent.

2.2.3. Evaluating biological growth

2.2.3.1. Biomass

What the effect is of certain changes made to concrete on bioreceptivity can only be assessed by the amount of observed biomass. A solid measurement would be to determine the mass difference before colonization and after some growth took place. However, in order to exclude any weight gain from ingressed moisture, the samples should be oven-dried until constant mass, obtaining the exact gain of dry biomass. The main disadvantage is that measurements should be taken very carefully, as the biomass is often a fraction of the total concrete sample mass. Any mass changes from other chemical processes (like carbonation or hydration) cannot be completely isolated. Besides, this way of measuring is rather destructive for the organisms. That is why researchers employ other methods to assess biological growth.

2.2.3.2. Digital image analysis

So far, there is no non-destructive standard procedure for quantifying of biological growth (on bioreceptive materials). In literature, photographing the specimens and performing various sorts of digital image analysis is a popular method, especially to track biological growth coverage over time [19, 20, 40, 45]. An example is given in figure 2.2, where cover percentage is based on pixels that fall in a pre-specified green range. These methods are sensitive to lightning and camera settings, as the judgment is done based on digital pixel colour and intensity. In the research from [45], some open pores were mistaken for algal growth in the image analysis. Digital adjustment can be done to overcome this, but with the risk of excluding other grown areas as well. Also, this 2D measurement does not take organism height into account, which can be an issue for moss monitoring. Instead of a true value for biomass, image analysis can therefore give more relative results between specimens. The big advantage is that the method is non-destructive, so multiple measurements can be taken over time.

2.2.3.3. PAM-Fluorometry

Aside from basing the organisms prosperity on biomass or coverage alone, growth quality can also be evaluated by looking at a plants stress. Uncomfortable environmental factors can increase vegetative stress, making the organism focus more on surviving rather than growing or reproducing [62]. When the

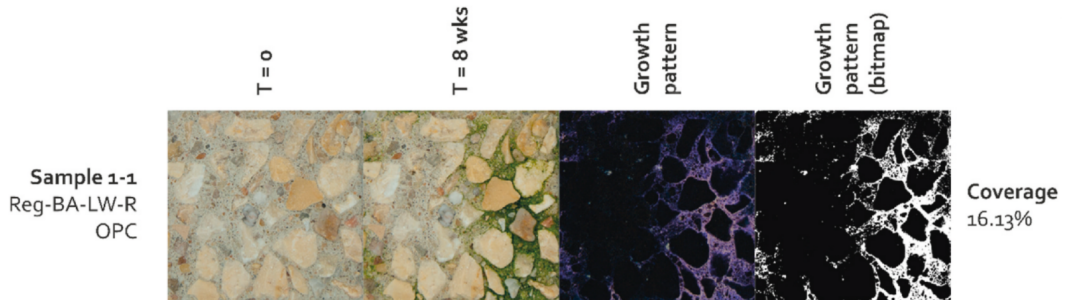


Figure 2.2: Image analysis example from [20] of algae stained sample at 0 and 8 weeks, including digitally obtained growth area and bitmap variant

organism is photosynthetic, such as algae and mosses, a pulse-amplitude modulated fluorometry (PAM-F) test sees use in literature to allocate a number for the stress a plant has based on their chlorophyll response [42, 45, 51, 63].

According to [64], in PAM-F a modulated (low-intensity) light pulse is used as a probe. This light pulse is turned on and off at a frequency of multiple kHz. The modulated light is weak enough not to significantly drive photosynthesis but is sufficient to excite chlorophyll fluorescence. This fluorescence is detected only at the modulation frequency, enabling separation of the weak fluorescence signal from background light. Typically, specimens are kept in the dark for a short amount of time, allowing the organisms to adapt to the dark. In this state, a minimum fluorescence yield F_0 is measured, after which a strong light pulse is saturating the chlorophyll and a maximum fluorescence F_m is measured. More thorough chemical explanations are given by [42, 64]. The variable fluorescence F_v is defined as the difference between the minimal and the maximal state. In the study from [42], F_m was used as a biomarker, but the maximum quantum yield F_v/F_m is also an option to look at the plant health. This unit-less ratio indicates how effectively absorbed light can drive photosynthesis [64]. In practice, values ranging from 0.65-0.75 were found on bryophytes in Japan [65].

From literature it becomes clear that PAM-F is a useful addition to biological growth evaluation. It is a non-invasive method that can reflect on the organisms state real-time, and can even be used as a biomass quantification method.

2.2.4. Biological growth and concrete quality

Before Guillitte [14] published his work, biological growth on buildings was often linked with deterioration of the substrate material: biodeterioration or biodegradation. And this is not entirely untrue: in stone surfaces, it is believed that 20-30% of deterioration is a result of biological activity [66]. This can occur either by the products of the metabolic processes of the organisms (biogeochemical) or by stresses induced by the presence of organisms through e.g. growth, surface penetration or organic volume changes (by dry-moist or freeze-thaw cycles), called biogeophysical deterioration [67, 68]. Although when it is estimated that only around a quarter of deterioration is bio-induced, most of the deterioration comes from other environmental or mechanical factors. Most of the time, undesired biological growth occurs after a certain degree of weathering and degradation already took place [39]. This could, but not does not have to, make biological growth an indicator of worsening material quality.

2.2.4.1. Mechanical performance

It is in that sense understandable that some concrete properties that are beneficial for biological growth, have the opposite effect in mechanical-physical context. For example, strength of the concrete is generally inversely correlated with porosity [44]. Higher porosity makes concrete also more susceptible to freeze-thaw damage [47]. Lowering the pH value can be done by a lower binder content, but this is likely to decrease strength of the concrete too. Lowering the pH can be done by using SCMs as well, for example fly ash [59] or BFS [20]. However, [19] found that their fly-ash containing samples were least susceptible to moss growth, indicating that addition of fly-ash does not enhance bioreceptivity. This might have to do with the filler function of the SCM, decreasing porosity.

Generally it can be stated that concrete types that are highly bioreceptive have a relatively low strength

and durability: the (mechanical) quality is comparatively poor. On the other hand, high quality concretes such as UHPC usually have a low porosity, high alkalinity and are likely to have a very smooth (micro)roughness, making them less bioreceptive [47].

2.2.4.2. *Concrete-moss symbiosis*

In recent years, studies start to encourage the use of moss on concrete rather than reject it. The potential that moss has to mitigate certain environmental issues in cities plays a role in this paradigm shift. Also the protective function of moss to concrete erosion is underscored [32, 69].

2.3 3DPC

Additive manufacturing of concrete has strongly developed over the years. Currently, the focus in this development particularly lies on improving the structural characteristics. These can be divided into design (topology) optimization of structural members, and optimizations of current limitations of 3DPC like mechanical anisotropy [70]. In order to compete with conventional MC, 3DPC should be able to perform equally good or better in terms of mechanical strength. Due to the anisotropy, 3DPC shows different strength in different loading directions.

Although there are many developments in academic research, [70] underscore that many aspects lack sufficient consistency among studies, one of which is strength testing. The absence of unified normative standards for e.g. compressive testing, specimen size, number of layers and curing conditions make studies difficult to compare. In the Netherlands, some guidelines about 3DPC have been newly developed [71], but these are not norms or standards yet. However, where possible these guidelines will be followed in the experimental phase of this thesis.

In this section, a closer look is taken at the working principles of 3DPC, the fresh state and how to handle it when designing a mixture, and lastly what the bioreceptivity related status is in 3DPC currently.

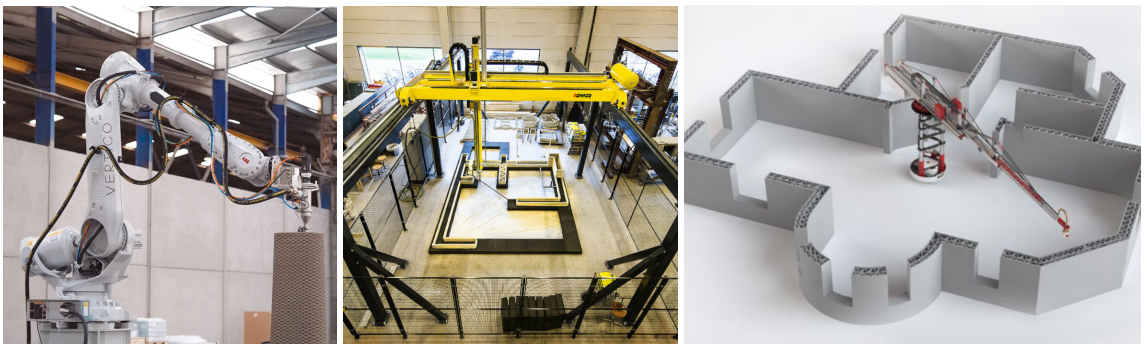
2.3.1. Working principle

Many techniques are considered 3D printing, but in this thesis the focus is on extrusion based additive manufacturing of concrete. Shortly summarized, layers of concrete are deposited on top of eachother. In most cases, a specially made concrete recipe is mixed, pumped through a hose and extruded from a nozzle. A computer controlled device can move the nozzle with attached hose in multiple directions.

There are various types of printers. Three common ones are robotic arm printers, crane printers and gantry printers [72]. For this thesis, a small gantry-like system is used. A concrete mix designed for one printer may not be suitable for another due to differences in pump capacity, pipe length and diameter, and nozzle dimensions [73]. Since in this thesis mix designs will be altered to increase bioreceptivity, it is important to understand what things can be expected when making modifications. The concrete should remain printable, which is considered as the totality of rheological and shape retaining parameters [74].

2.3.2. Fresh characteristics

From previous work it becomes clear that researchers often evaluate their 3D concrete mix based on four aspects flowability/pumpability, extrudability, buildability and open time [74, 75]. The first three aspects can be linked and should be sufficient in the presented order: concrete cannot be properly build if not properly extruded, not extruded well if it cannot be pumped consistently. Additionally, if the open time is too short, it can limit the timeframe in which good printing can be done.



(a) (b) (c)

Figure 2.3: Different types of common 3D printers for all scales (a) Robotic arm printer (Vertico), (b) Gantry system (TU Eindhoven), (c) Rotational crane printer (Compact Apis)

2.3.2.1. Flowability

Flowability is an important parameter giving information about the workability of the concrete. How flowable a mixture is, is determined by its spread diameter from a slump test or flow table test. Previous studies found very diverse ranges for their optimal flowability from a mini-slump test, 150-190 mm [76] or 130-180 mm [77]. An exact optimal number or range is different for every printer and should be acquired separately. Spread diameter indicates to some extent if a mixture is also pumpable, but not all. For example, the implementation of larger aggregates could complicate consistent pumping [74]. For each type and size of pump there are mixtures that will flow and that will not, and vice-versa.

More or less all constituents that can be added or removed from the concrete mix will impact the flowability. Most impactful are arguably changing the water volume [78], or using a water reducer [79]. It was found by [58] that replacing a high content of cement with a limestone and calcined-clay blend reduces the flowability. Adding more viscosity modifying agent (VMA) reduces slump diameter as well [80].

Summed up by [81] are the most common types of SCMs and the effect they have on rheological properties. For example, silica fume addition reduces the flowability. For other SCMs the amount and particle size distribution are governing in effect on workability.

Lastly, just as with the SCMs, an adjustment in the particle size distribution of aggregates and sand can drastically influence the flowability. An optimum for aggregate content has a linear relationship with flowability of just the paste [82]. Rounded aggregate particles are found to improve flowability, while angular ones disrupt it [83].

Concluding, flowability of the concrete can be measured by means of a slump flow test, of which optimal outcomes deviate per application and printer. It should be kept in mind that altering anything about the mix proportions will likely change the flowability characteristics.

2.3.2.2. Extrudability

Extrudability refers to the capability of fresh concrete to be continuously transported from the hopper to the nozzle, forming a continuous filament [84]. A mixture is considered workable when extruded properly, meaning without any blockage, cracking or segregation. During this process, the fresh material is subjected to a certain degree of pressure and friction. This changes the rheological properties compared to the material in the hopper [81]. Extrudability is therefore reliant on the complete printer system, from hose length to nozzle radius to pumping speed.

Mixtures that have a high yield stress when in fresh state can be difficult to extrude [85]. The inclusion of materials like silica fume, viscosity modifying agents, and nanoclay can improve the robustness and reduce variability in yield stress, enhancing extrudability [85]. Implementations of coarser aggregates reduce the workability because it increases the possibility of dewatering of the mixture during extrusion [86].

2.3.2.3. Buildability

Buildability assesses the ability of fresh 3D-printed concrete to support its own weight and the load of upper layers without collapsing during printing [81]. There are generally two failure modes, one of which is in the form of deformation of the bottom layers due to the load of the layers on top. The stress caused by gravity has to be lower than the yield stress of the material in order to retain shape. The other way is the collapse of a multi-layer component caused by structural instability. An overview of common failure mechanisms is shown in figure 2.4.

Models have been developed to estimate the critical height based on the shape retaining properties of only a single layer of filament [81]. Just as with many other facets of 3DPC, there is not yet a standardized method to quantify the buildability. Many studies simply stack layers and measure any deformation [84]. However, buildability can also be estimated by moulding the concrete and applying a load for a certain amount of time. The observed strain or deformation can be indicative of the shape retaining properties of the final structure [87]. Here, it should be noted that the mechanical properties of fresh concrete do not have to be exactly representative before and after extrusion [88].

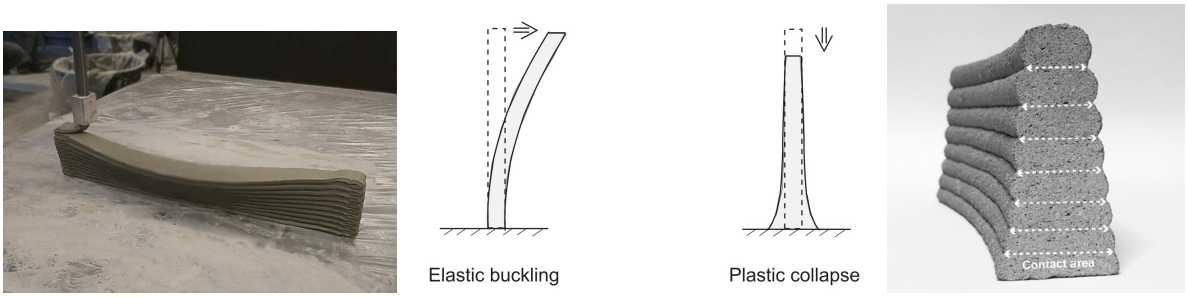


Figure 2.4: Common types of failure mechanisms in 3D printing. (a) buckling (from [89]), (b) schematic failure types (from [89]), (c) plastic deformation (from [58])

Buckling collapse specifically can be overcome by design of the structure. Especially for taller structures, integrity should be maintained. Using an infill or special cross-sectional grid is therefore recommended by [70].

2.3.2.4. Open time

Open time refers to the duration during which the material remains flowable through the nozzle without blockage or clogging [90]. The open time of the material must exceed the time required for finishing the print in order to maintain good printability, and it is much correlated with the initial setting time of the concrete. Extending the open time can be done by adding retarders or other admixtures [91], and is undeniably reliant on the binder type. Furthermore, factors like higher temperatures are known to significantly shorten setting time, and therefore affect the open time as well [92].

It is important to determine the open time for a mixture combined with the printer it is used with. Therefore, a straighforward method is to extrude concrete with a time interval until unbuildable flow comes out, or the pump is no longer able to transfer the mixture [93]. Other methods address the shear strength or flowability over time, or use a Vicat apparatus to determine setting time [94].

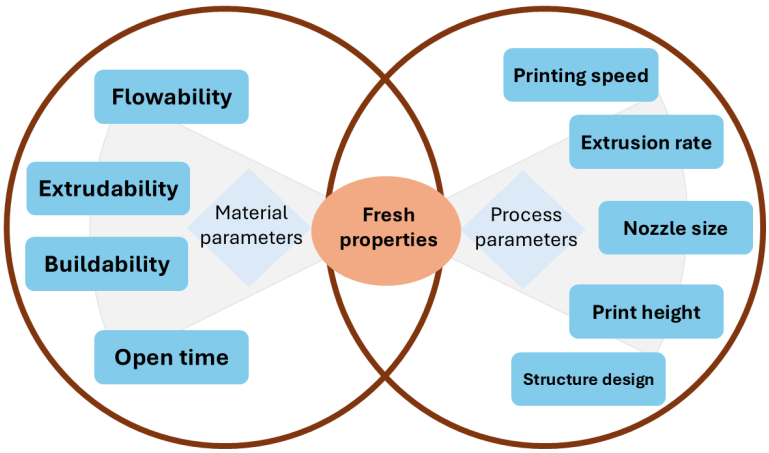


Figure 2.5: Materials and process parameters that affect the fresh properties of a 3DPC mixture summarizing this section. (based on [94])

2.3.3. State-of-the-art: bioreceptive 3DPC

In this section, the bioreceptivity factors as broken down in section 2.2.2 are portrayed against current development of 3DPC. This should help comprehending where improvement can be made regarding bioreceptivity, and how.

2.3.3.1. Porosity and water retention

The pores within the printed structure can generally be categorized into two types: small pores formed within the filament during the extrusion process and entrapped pores created at the interfaces between filaments (both interlayer and intralayer) during the deposition printing process [95].

Pores in 3DPC, their number, their shape and their size, all affect the strength and elastic modulus, which is the main cause for the anisotropy [96]. In other words, pores can mostly be held accountable for the mechanical performance. 3DPC can easily have a higher porosity than MC, having to do with lack of vibration among other things [97].

But vibration is definitely not the only factor. It should be mentioned that virtually any variable has an effect on this. Geometry of the layers and packing for example. Different extrusion shapes and sizes have significant influence on how the layers build up, attach to eachother and the amount of voids they leave between the layers, and hence the mechanical properties [98]. The nozzle shape plays a role in this as well [99]. A larger layer-on-layer time is found to negatively influence the strength [99], due to moisture loss on the layers and consequent inadequate adherence, leaving behind void spaces. A too high nozzle standoff distance can result in improper bonding as well, resulting in larger pore spaces between the layers [100]. X-ray CT analyzed specimens in figure 2.7 show clearly the higher porosity between layers.

All these factors underscore the sensitivity of 3DPC to even small alterations in print parameters. It can be said that achieving a high porosity in 3DPC can be done in many different ways that include printing parameters. This could be beneficial for bioreceptivity. For this research however, the focus lies on enhancing bioreceptivity from a material perspective. Nonetheless, it remains important to not ignore print parameter induced pores.

Regarding this material perspective, there are multiple ways of tailoring the mix design such that it influences overall porosity, which are not surprisingly similar to what is expected with MC. Below, a list is presented with referred literature, variables and what its effect is on fresh properties of 3DPC.

- **Aggregates**. Incorporation of more porous aggregates or a different grade of aggregates does affect the porosity. It was found that adding recycled aggregates to the mix, which were over 35% more porous than the reference aggregates, increased the porosity of the 3D printed layers as well [95]. Their findings even showed a higher early yield stress with a higher replacement ratio, increasing buildability characteristics. The study from [83] replaced 50% and 100% of the sand with pumice and expanded glass, which are lightweight aggregates (LWA). Their altered 3DPC had increased porosity compared to the reference, ranging from 11.37% to 27.9%. On top of that, the additions enhanced flowability and extrudability. Incorporating coarse aggregates at the expense of finer ones could also lead to increased porosity in 3DPC, plus consequent bioreceptivity and is therefore recommended by [75]. But currently, most machinery does not allow coarse aggregates in 3DPC processes since there is a risk of blocking and other impracticalities [73].
- **Water**. It is common knowledge that in MC, adjusting the water content or the water binder ratio has an effect on the pore specifics. In 3DPC, [101] conducted an experiment with three different water to dry ratios (w/d) while keeping other parameters equal. Increasing the water amount increased flowability. However, they found that for mechanical performance, a not too high nor too low w/d ratio was optimal. Lower and higher w/d ratios increased open porosities and water absorption, since it also severely affected the rheological properties of the mix and hence the printability. Seen in figure 2.6.
- **Additives**. The addition of chemical agents to the concrete mix sees use regarding rheological properties. However, some additive chemicals can be used to form entrapped gas bubbles, named as foaming agents [102]. A distinction can be made between physical blowing, where the agent expands upon decompression, or chemical blowing, where the agents forms gas resulting



(a) (b)

Figure 2.6: 3D printed results from [101] with w/d ratios of (a) 0.140 L/kg, (b) 0.145 L/kg

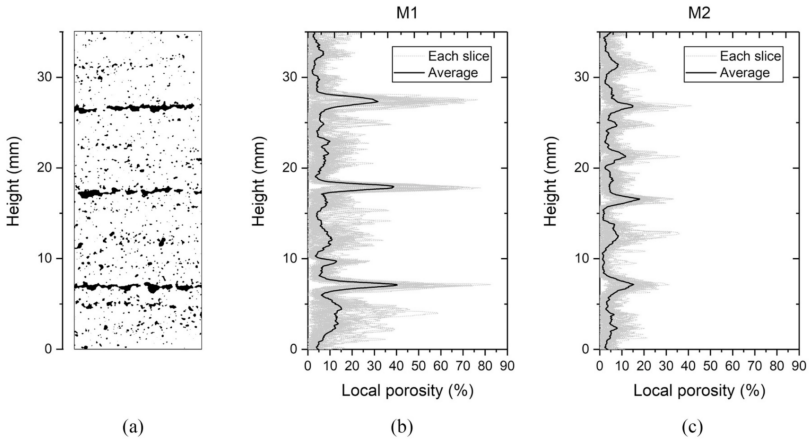


Figure 2.7: Example of CT scan data of 3DCP specimen, porosity between layers clearly visible. (a) After segmentation (b), (c) local porosity over height of two different specimens. Averages are calculated over 40 slices. (from [97])

from a chemical reaction. Both lead to aerated concrete, a foamy structure with high porosity concrete. The manuscript from [102] does not mention water absorption related issues, as insulation and cost-effectiveness are focus points rather than bioreceptivity. Despite possible benefits of aerated concrete for bioreceptivity, the execution can still be a challenge. One research that did use air entraining agents experienced difficulties when trying to extrude 3DPC with this agent: gas bubbles exploded when the material left the nozzle, leaving in a highly inconsistent flow [103]. Ensuring that water does not escape the system easily can be achieved by the addition of super absorbent polymers (SAP) [41]. When mixed, these additives can bond with water, leading to substantial retention of water in concrete.

2.3.3.2. Surface roughness

Surface roughness is represented in multiple ways in 3DPC. On one hand, the layer stacking creates a wavy profile on the side of the structure with a relatively large height-depth deviation, called the staircase effect [52]. Especially in the crevices between the layers, this profile could form a habitat basis for organisms as it can provide environmental protection and is prone to accumulation of (nutrient-rich) particles. A thinner layer leads to a more detailed side profile, which can be achieved through small nozzle bead radius and low standoff distance, among other things [29]. The same study also showed that water adhered better to interlayer regions when channeled over the surface, seen in figure 2.8.

On the other hand, the layers themselves can have a certain degree of roughness embedded. Some researchers have investigated the effect of increased layer surface roughness in order to increase layer bond strength, and found that addition of sand increased surface roughness, but roughness addition through wire brushing was more effective [104]. Contradictory to that, [95, 96] argue that some roughness can be the origin of defects in adhesion between filament, as it entraps air more easily leading to interlayer voids. Addition of materials like carbon fiber was reported to cause surface irregularities hence increasing local texture [52].



Figure 2.8: Water channeling behaviour on 3D printed ceramic structures. A liquid dye has been used to visualize. Apart from in the channels, water is also seen in the interlayer regions (from [29])



Figure 2.9: Crack developments at a corner of a newly printed concrete structure (from [73])

One could argue that surface cracks do enhance local surface roughness. An improper mix design can lead to a severely 'damaged' surface, being extruded as an inconsistent mash with rough finish instead of a steady firm slurry. Figure 2.6a is an example of this. Printing curved sections with a rotating circular or rectangular nozzle deposits more concrete at corners, widening the layers compared to straight sections. This leaves the outer side prone to tearing and cracking as relatively less concrete is extruded. These cracks can expand under the weight of subsequent layers, leading to poor surface finish as seem in figure 2.9. Shrinkage is another contestant in this context, but generally leads to surface microcracks instead of a roughly cracked surface. Shrinkage cracks can be exaggerated by higher binder content or improper curing conditions [73]. Addition of fibers to the concrete could stabilize these shrinkage cracks [79]

Summarizing, in the field of 3DPC, the surface roughness is mostly linked to bonding strength of the filament, and not much to its effect on bioreceptivity. Incorporation of larger aggregates, manual surface treatment, purposefully imperfect curing conditions or addition of other materials like fibers can increase surface roughness. On a geometric level, adjusting layer height or overall shape of the structure can aid surface roughness as well.

2.3.3.3. Composition and pH

Although many different recipes exist for 3D printable concrete, most of them share more or less the same fundamental ingredients and ratios thereof. Compared to MC, a much higher quantity of binder is used since it is a requisite for a workable and printable consistency. A comparison can be seen in figure 2.10. A higher cement content is generally regarded as ill-fated for biological growth: it yields relatively more toxic elements such as aluminum but most of all it enables the hydration reaction that

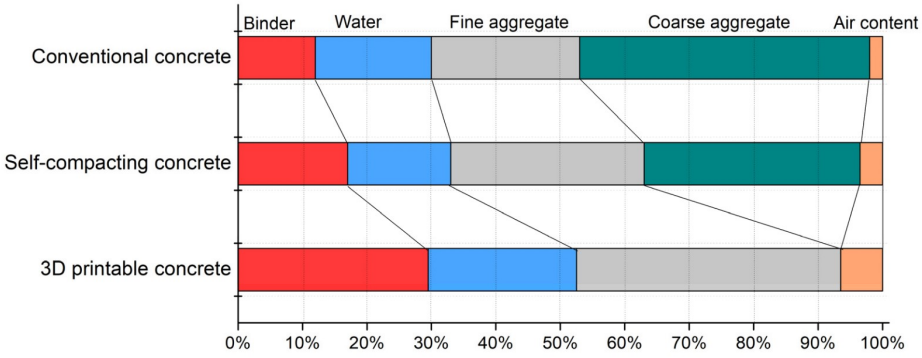


Figure 2.10: An illustrative comparison of percentage of materials (by volume) used in conventional concrete, self-compacting concrete, and 3D-printable concrete (from [73])

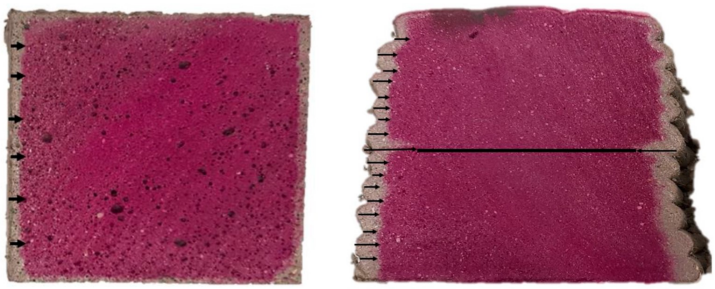


Figure 2.11: Carbonation depth measurement points (black arrows) for the (a) cast and (b) printed samples by means of phenolphthalein indicator after accelerated carbonation. (from [108])

leads to alkalinity. So, a higher pH than for MC is expected, but there are almost no references of common 3DPC pH levels. Only one study was found that assessed the pH of 3DPC with various amounts of pozzolanic replacements [105]. It was found that the incorporation of Incinerated Sewage Sludge Ash (ISSA), which contained high silica iron and aluminum, had the most decreased surface pH value compared to the reference mix (10.12 and 10.89 respectively). Incorporation of slag, however, also lowered the pH but by a smaller margin (10.77). Extensive research is needed to discover more potent methods of lowering the pH in 3DPC directly.

In contrast, some more research has been done regarding carbonation of 3DPC. It is reported that generally, the degree of carbonation is higher in 3DPC than in MC, in both interlayer and intralayer regions [106, 107, 108]. This is illustrated in figure 2.11. Anisotropy plays again a role in the carbonation resistance, as it is reported that carbonation depth differs greatly when measured laterally or perpendicular to the layers [106]. Local porosity variations are appointed as the cause for these differences [109].

Lower pH levels can be achieved by using other binder types as well, such as Magnesium Phosphate Cement (MPC). In the context of 3DPC, however, it has not been investigated much. The rapid setting time of this concrete type makes it challenging to properly extrude and print the material, although the feasibility of 3D printing MPC paste has been documented [110]. In the context of bioreceptivity, no reference research on 3D printable MPC was found. The before mentioned addition of phosphorus to MC is something that has not been investigated either.

Recapulating, there is little known about pH and composition based 3DPC for bioreceptivity. 3DPC generally has a high initial pH, but is also more prone to carbonation than MC. Alternative methods for reducing the pH, as well as the incorporation of phosphorus into the mix design, have been scarcely investigated.

2.4 Experimental exploration

From the collected literature, a rough but broad understanding emerged about moss growth behaviour and habitat, and how bioreceptivity is represented in 3DPC. In this section, the usability of the certain possible improvements is more closely examined. An approach outline for the experimental phase of this thesis is presented.

2.4.1. Theoretical framework

The choice for implementation of lightweight aggregates has been made. This based on the following line of thought, which also presented in figure 2.12.

- Some studies suggest that water availability is the single most important survivability factor for organisms. Mosses also rely heavily on water availability. So increasing the material based water availability could be a key improvement here.
- The water absorption is highly correlated with the porosity of concrete. It is clear that the absorption and permeability are far from uniform over the 3DPC surface due to print parameters. The water absorption of the bulk should also be increased. More ways of increasing bulk porosity were explored
- One approach could be to develop a 3D printable pervious concrete. This involves adjusting the particle packing, which is influenced by the grain size distribution (GSD) of the mix. As a result of the absence of fine aggregates, the pervious concrete is characterized by large open voids in the hardened product. However, most 3D concrete printers, just as the one used for this thesis, cannot handle coarse aggregates. As coarse aggregates form the basis of this type of concrete, it is not investigated further.
- One other method is to pursue the principle of aerated concrete, or foam 3D printing, but has a scarce amount of documentation [102]. One research that did use air entraining agents experienced difficulties when trying to extrude 3DPC with this agent: gas bubbles exploded when the material left the nozzle, leaving in a highly inconsistent flow [103]. It was found difficult to tackle the issues given such a little amount of documentation, hence the investigation into this method was discontinued.
- Another method is the incorporation of porous aggregates in the mix, which could directly contribute to the overall porosity. Lightweight aggregates (LWA) serve a promising role in this, having a bulk density of less than 1200 kg/m^3 and often having highly porous micro structures. Given that LWA incorporation in conventional has been researched often, and literature implies a positive relationship regarding bioreceptivity [20], this method was pursued.
- The choice for replacing original aggregates with LWA was also considered to be convenient for the 'rapid prototyping' of different mix designs when incorporated with the same GSD as the original aggregates. It is expected that compared to using agents, modifying the additive or water ratios, this has the least influence on printability properties, which will likely inhibit the mix designing procedures the least.
- It has been found that porous aggregates lead to higher overall porosity of 3DPC. This finding, combined with the availability of some literature that incorporates lightweight aggregates to 3DPC led to the choice for a similar approach using lightweight aggregates.

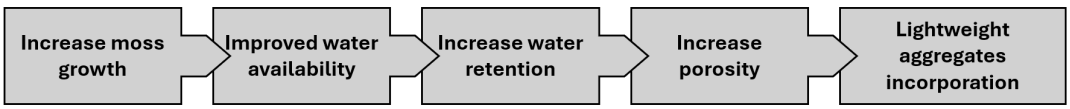


Figure 2.12: Theoretical framework in figuring the experimental phase

2.4.2. Selected aggregates

Four lightweight aggregates were selected for this thesis, which are elaborated on in the paragraphs below. Crushed expanded clay has seen some positive relationship with bioreceptivity in literature [20]. Pumice is a commonly used aggregate for lightweight concrete, and some documentation is available on using it in 3DPC [83, 111]. Expanded vermiculite reportedly has an extremely low density, which is makes it appealing to implement in 3DPC for this thesis' purpose. Lastly, expanded glass is a lightweight material that was a readily available, making it practical to pick. It additionally has some documentation on use in concrete [83, 112]. Out of these four aggregates, expanded vermiculite and crushed expanded clay are most often related to biological growth.

2.4.2.1. Crushed Expanded Clay

Expanded clay is a commonly used lightweight substitute for normal weight aggregate. It is manufactured by letting clay expand and vitrify in a rotary kiln. Gases inside the materials cause a pore system with pores ranging from 5 - 300 µm [113]. There can be some variation, but common constituents of clay are mostly silica, aluminum, iron, magnesium and calcium [114, 115]. Crushed expanded clay (CEC) as a (partial) replacement for aggregate has seen to significantly increase bioreceptivity [20, 45]. It is expected to increase the hydraulic properties of the mix because of its increased porosity [116], making the material inherently bioreceptive. Regarding the printability using expanded clay aggregates, [86] found that for coarse aggregates (up to 10mm) only up to 30% of the original aggregate can be replaced with expanded clay without affecting the extrudability. Higher contents were seen to have phase separation in liquid phase, using a piston-pump based 3D printer. The same study also found that collapse (plastic and buckling type) of the lightweight aggregate concrete print occurred later compared to the reference, increasing the critical height of the print.

2.4.2.2. Crushed Expanded Glass

Expanded glass (EG) beads are made from heating up a mixture of ground glass, binder and certain blowing agents [117]. Just as with expanded clay, gas bubbles will form leading to the creation of porous glass beads. Depending on the temperature regime and the quality of the materials, the glass beads can have varying properties [112]. Elemental investigation usually shows a high silica content, along with some calcium, sodium and traces of magnesium [112]. Water absorption up to 25% has been documented, and varies with the grain size distribution [118]. However, all these findings concern just the spherical granules, whereas in this thesis the beads will be crushed to approach the angular shape of the sand. This could lead to different properties, as the inner pore structure of the beads now becomes surface exposed. Incorporating expanded glass in 3D printable concrete has been done by [83], and found among other things that the mechanical strength was far greater in 'regular' sand based 3DPC compared to the specimens where sand was replaced by expanded glass.

2.4.2.3. Expanded Vermiculite

Vermiculite is a type of mineral that expands greatly when exposed to high temperatures. The density is extremely low, 60 to 160 kg/m3 when dry. This material sees mostly use in the agricultural sector, as an enrichment of soil. One research found that addition of expanded vermiculite (EV) to mortar was beneficial for plant growth compared to the reference [119]. Also, there is documentation about the use of EV as an aggregate in 3DCP, providing some information on how to add to the mixture [120].

2.4.2.4. Pumice

Pumice (PU) is a type of extremely porous volcanic rock. Pumice contains mainly silica and aluminum, and can reach as high as 85% porosity by volume [121]. Implementing this as an alternative aggregate is expected to greatly increase porosity, hence increase water retention and slightly lower the pH value. In the manual from [111], it is stated that pumice implementation improves water absorption, while giving in on mechanical properties and workability. Workability measured by slump flow decreases with an increasing pumice aggregate content, coarse as well as fine [43]. [122] found up to 4 times higher water absorption for mortars with only fine (0-4mm) pumice aggregate compared to the control batch. Regarding the mechanical strength, reductions of over 60% compared to the reference have been reported when all aggregates were replaced by pumice aggregates [123, 124].

3

Methods and Materials

In this chapter, the experiments from this thesis will be described. First, an explanation about the made choices is done and an outline is presented including quantities to be measured. The rest of the chapter specifies the methods and actions about aggregates, fresh concrete properties, 3D concrete printing, hardened tests and moss growth in that order.

3.1 Experimental outline

Based on the broader thesis planning in figure 1.1, an outline for the experimental phase of this research is made, figure 3.1. First, mixtures with incorporated LWA are made and reviewed. When sufficient, samples are 3D printed. When cured, bioreceptive factors of the samples are measured. Moss is planted and growth is monitored. The arrows mark the order of tests, and the dark gray tiles implicate actual measurements. In the discussion chapter, the moss growth progress is linked to findings from the concrete evaluation.

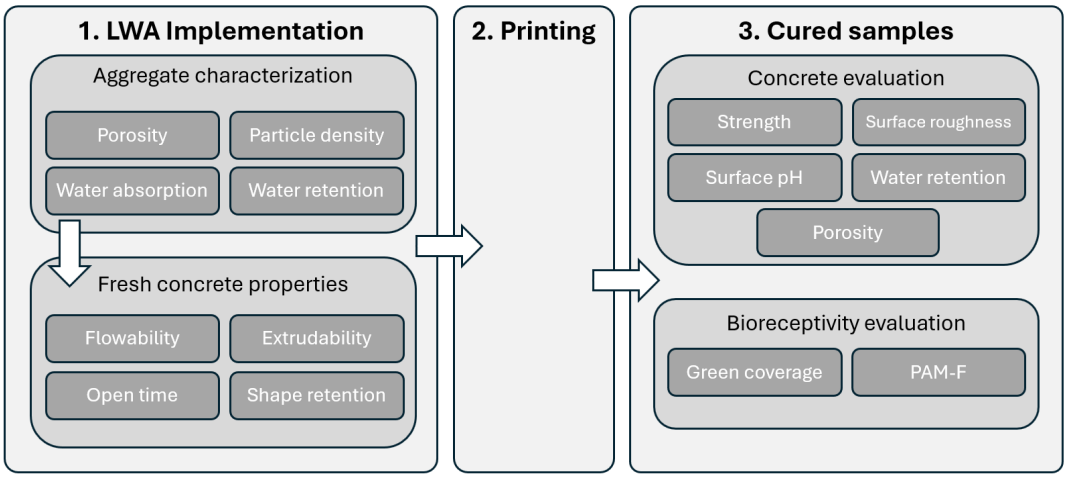


Figure 3.1: Diagram of the experimental phase of this thesis. The gray blocks with white text implicate that a measurement is done for quantification.

3.2 Tailoring the mix design

It would be much work to manufacture a 3DCP mix design from scratch for the purpose of this study. There are many types of printable concrete out there to pick from. The printable concrete is usually optimized for a specific printer and conditions. Previous studies that used the same setup as this thesis have been analyzed to possibly mimic their mix designs [125, 126]. These however often contained extra components like calcined clay or fibers, which are not in the scope of this thesis. Eventually, a mix from 3DCP pioneering company Vertico was chosen. Their mix design is open source, contains of a simple mix of ingredients and have a lot of reference structures to support the printability of this mix. Because Vertico uses state-of-the-art robotic arm printers, which are very different from the setup in this research, the mix will first tested and mimicked to ensure usability here. From there, alterations to the mix will be made.

3.2.1. Reference mix

Vertico's mix design consist of 35 wt% CEM I 52.5 R, 13.2 wt% water, 50 wt% dried sand (fig 3.2 and table 3.1), 1 wt% retention agent (*Cugla ViscoSmart Pure P-50*) and 0.8 wt% accelerator (*MasterRoc SA 167*). This mix is optimized for their 3D concrete printer: a robotic arm based machine with continuous inflow and near-nozzle mixing. Near-nozzle mixing is possible with the TU Delft setup, but was not used for this research since the goal can also be achieved without. On top of that, the accelerator contains some Aluminum compounds which could impede biological growth. For that, the accelerator was left out of the equation and the percentages were adjusted to 35.1% CEM I, 13.8% water, 50.1% dried sand and 1% retention agent. The composition of this mix was mimicked with cement and sand from the TU Delft silos and acts as the reference batch for this research.

Table 3.1: Sand for Vertico mix passing percentage and bounds

Sieve	**passing**[%]	**min** [%]	**max** [%]
C8	100.0	100.0	100.0
C4	100.0	100.0	100.0
2	96.6	100.0	85.0
1	85.2	100.0	50.0
0.5	59.4	90.0	30.0
0.25	17.5	80.0	0.0
0.125	1.1	15.0	0.0
rest	0.0	10.0	0.0

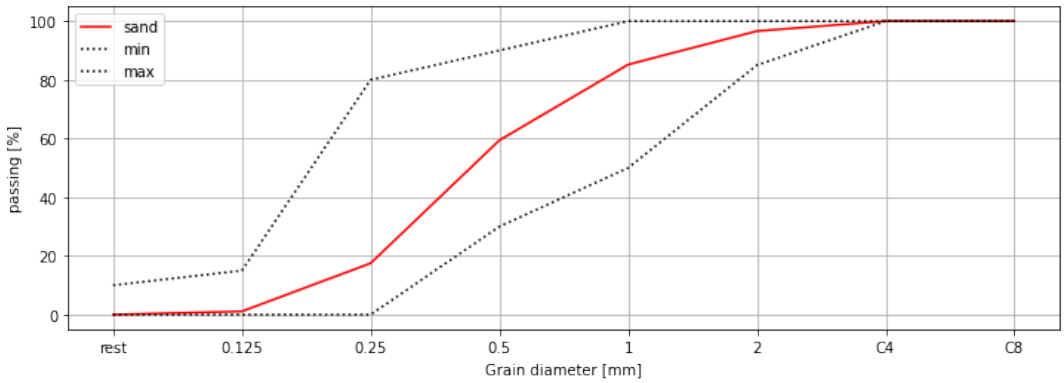


Figure 3.2: Sand sieve curve of Vertico mix design

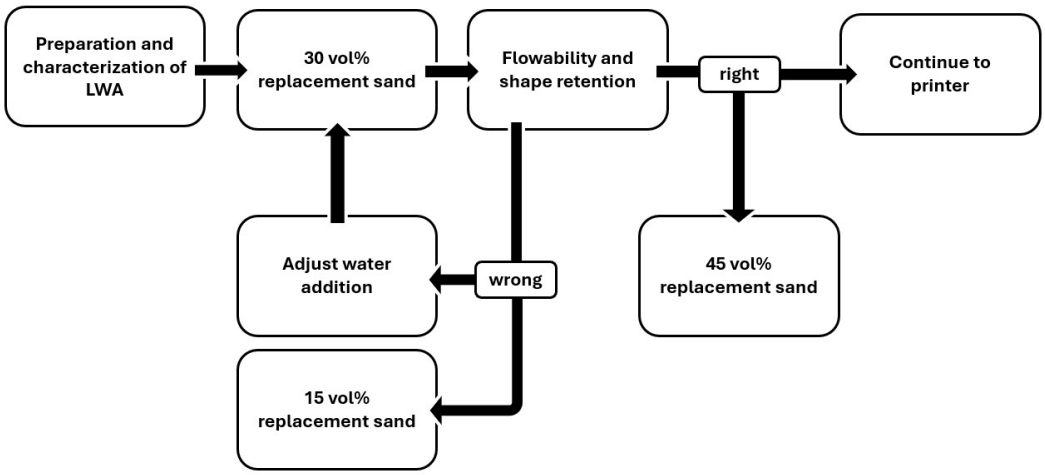


Figure 3.3: Strategy to find best mix design for certain replacement percentages

3.2.2. Replacement strategy

LWAs are characterized by a relatively high water absorption. It is therefore necessary to compensate for this by increasing the amount of water in the mix. This is done by adding the LWA in a saturated surface dry state (ssd), as they do not absorb any more water but do also not add any as to not influence the workability. The mass of the LWA needed is then calculated by:

$$m_{LWA} = replacement[\%] \cdot \frac{\rho_{ssd,LWA}}{\rho_{ssd,sand}} \cdot m_{sand} \tag{3.1}$$

with ρ_{ssd} being the saturated surface dry density of LWA or sand.

Based on some literature, up to 30% replacement will not significantly interact with the printability [86]. To ensure the level of printability that is similar to the reference, for every LWA it is investigated whether a 30% replacement is possible, and if some adjustment of the water addition is necessary.

Results from the flowability test (section 3.4.2) and shape retention test (section 3.4.5) are governing in determining a proper replacement percentage and water addition. When no feasible combination can be found, the replacement percentage is lowered to 15%. On the other hand, when no issues arise, a replacement of 45% is explored. It is desired that least one set of samples has a 45% replacement, as a more distinct comparison can be made about the influence of higher amount LWA on bioreceptivity. The strategy is depicted in figure 3.3.

The developed iterative mixtures are named as follows:

1. **Aggregate type**. CEC, EG, EV, PU, RS
2. **Replacement percentage**. 30 or 45
3. **Water decrease**. Which percentage of saturation water is decreased from the mixing water amount.

3.2.3. Material origin

A total of 8 materials were used in for the mixtures.

- **Pumice** Picked up at a depot, origin and GSD are unknown.
- **Expanded vermiculite** Agra-Vermiculiet, F2/0-3 mm, 100L. Bought from Agrifield.
- **Crushed expanded clay** Liapor® Sand K 0/2.
- **Expanded glass** From batch at Vertico storage. Origin unknown.
- **Sand** 0-2 mm dried riversand from TU Delft provision

- **CEM I 52.5 R** from TU Delft provision
- **VMA** CUGLA VISCOSMART PURE P-50

3.2.3.1. Chemical composition

X-ray fluorescence (XRF) was carried out to observe the compounds of all LWA, sand, CEM I and VMA. First, material was dried in an oven at 105°C until constant mass. Then, it was ground using a ball mill machine (*Retsch MM 301*) for 5 minutes at a frequency of 20/s. From the powders, 4 grams of material was taken to be made into a compressed pallet for XRF analysis (*Bruker*). Of all the substances, the loss on ignition (LOI) was determined since XRF cannot observe elements that have lower atomic number than sodium. To determine the LOI, around 2 grams of the ground powder was put into a small crucible and carefully weighted with a 4-decimal scale. The crucibles were transferred to an oven. The oven heats up to 800°C at a rate of 10°C/min. It remains this temperature for 10 mins, after which it heats up again to 950°C at 5°C/min. This temperature is kept for 60 mins. Then the oven turns off and cools down slowly. After a few hours, the crucibles are carefully removed and placed into a glass container with sealed lit. This allows the substances to cool down further without gaining any mass from the air. After some time the crucibles are weighted again. The LOI is calculated as the percentage of mass loss, which accounts for the elements that are not traceable by the XRF machine. Method according to *NEN-EN 196-2: 2013* [127].

3.3 Aggregate characterization

The grain size distribution can have influence on the flowability and printability [86]. To not interfere and to exclude these factors, the LWA has been assimilated to fit the sieve curve from 3.2 as much as possible. More accurately, the grain size distribution has been adjusted slightly in order to neglect the >2 mm and <0.125 mm particles. The objective sieve curve is displayed in figure 3.4.

3.3.1. Grain size distribution

Dried sand, or reference sand (RS), was available in fractions 0.125-0.25, 0.25-0.5, 0.5-1, and 1-2 mm. The 0.125-0.25 and 1-2 mm batches were first manually sieved to limit the amount of <0.125 and >2 mm sand respectively. The fractions were merged by according weight to satisfy the objective GSD (figure 3.4).

In order to convert the raw LWA batch to the GSD as depicted in figure 3.4, the material was sieved in a sieving tower and the different sizes particles were merged accordingly by weight fraction. For PU and CEC the water content was too high to sieve properly, so both were dried in an oven at 110°C until constant mass. PU and EG contained many particles that were too large and needed to be crushed. This was done using a *SIMPSON Mix-Muller* rotational crusher.

The final batches with correct GSD were verified by doing an additional sieve check according to *NEN-EN 993-1* [128], albeit without the washing phase. When the LWA GSD showed a large difference with the calculated GSD (fig 3.4) the entire batch was sieved and merged by correct weight fraction again.

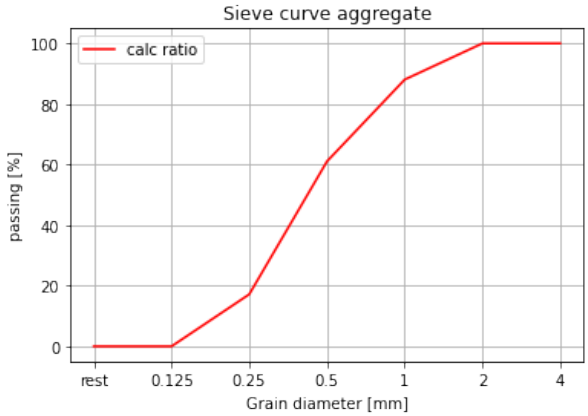


Figure 3.4: Sieve curve similar to Vertico premix dried sand sieve curve



(a) **(b)**

Figure 3.5: (a) Old model SIMPSON rotational crusher (in Dutch: Kluitenbreker), (b) Multiple sieves and sieving tower



(a) (b)

Figure 3.6: (a) Setup for determining water absorption. The vacuum pump on the left is connected with a hose to an Erlenmeyer flask in which the Büchner funnel is placed, (b) LWA being soaked in sealed containers

3.3.2. Porosity and pore size distribution

Mercury Intrusion Porosimetry (MIP) was employed to characterize the pore related specifics of the lightweight aggregates. A small amount was taken from the correct-GSD batch and freeze-dried for several weeks until constant mass. Since the inspected samples consist of many particles, it should be taken into account that some mercury will also occupy the inter-particle spaces in the lower pressure region. The porosity of the LWA itself is therefore lower than what is derived directly from the needed amount of mercury. Both Low-vac and High-vac measurements were done on the MIP device (*Micromeretics AutoPore IV 9500*).

3.3.3. Water absorption and particle density

Water absorption, apparent particle density, oven dried particle density and saturated surface dry particle density of the sand are done according to EN 1097-6 [129]. For the correctly distributed LWA, a modified method of EN 1097-6 Annex D was carried out, at least four times for every material: a quantity of material, with a volume of 200 mL to 400 mL, was weighted using a digital scale to the nearest 0.1g (M_{dry}) and soaked in water in a sealed plastic container for at least 20 hours (fig 3.6b). The next day, a filter paper (*Whatman 93 Wet Strengthened, diameter 110 mm, CAT No. 1093-110*) was placed in a Büchner funnel of diameter 120 mm and height 63 mm and soaked with water. The funnel was placed in an Erlenmeyer flask with tap, which was connected via a hose to a vacuum pump. The soaking water was drained using the pump. The weight of the Büchner funnel with wet filter paper was measured and denoted as M_1. After placing the funnel back to the Erlenmeyer flask, the entire content of the sealed container was poured into the Büchner funnel. During this pouring, the vacuum pump was turned on in order to prevent detachment of the filter paper. Remaining material in the plastic container was carefully removed using a glass rod, additional water and a soft disposable pipette. When all the material was transferred into the funnel, occasionally more water was added to make sure the soaked aggregate was leveled. Then the water was drained using the vacuum pump with pressure gauge for 5 minutes, after which the specimen approached saturated surface dry state. The pressure was recorded and often decreased slightly over the duration of the drainage. The funnel including filter paper and specimen was transferred to the scale and the total mass was noted as $M_3(t)$. The water absorption could now be calculated, but some additional measurements were done to estimate the densities of the material. So immediately after this, a 1000 mL measuring cylinder was filled with 500 mL water and weighted as M_4. After this, the specimen in the Büchner funnel was transferred into this beaker, using a glass rod and a regular plastic funnel. Remaining material was carefully rinsed away into the beaker, using a soft plastic pipette with water from the measuring cylinder, as to not add to the 500 mL. The residue in the Büchner funnel was kept at a minimum and the volume of the total content was read from the cylinders measuring lines. Finally, the beaker with water-specimen mix was weighted and noted as $M_5(t)$. This process from M_3 to $M_5(t)$ took about 5 minutes.

Water absorption, apparent particle density, oven dried particle density and saturated surface dry particle density could then be calculated through the equations given in *NEN-EN 1097-6 Annex D* [129]. However, M_2 is defined as:



Figure 3.7: LWA in small metal trays ready to be placed in the climate cabinet

$$M_2 = M_1 + M_{dry} \tag{3.2}$$

3.3.4. Water retention

This test is not necessary for implementation, but outcomes can be linked to possible corresponding behaviour in the 3DPC samples. Based on the method from [20], water retention of the LWA was tested similarly. The aggregates were dried at 100-110°C. Per aggregate, water was added until reaching the saturated surface dry state, as found by the water absorption test. Per type, the LWAs were divided over three small trays, filled up to similar volume, and placed in a climate cabinet (*Nuve TK 120*) at 37°C and 40 % RH (figure 3.7). Mass was measured at 1, 2, 4, 8 and 24 hours.

3.4 Concrete properties - fresh

As stated before, the mixes are developed such that the workability and printability properties are very similar to the reference. The fresh reference mix was qualified for its flowability, extrudability, open time and shape retaining characteristics. Extrudability was not investigated for the other mixes during the iterative process like presented in figure 3.3, since there was no quantity to measure when extruding aside from visual inspection. Based on results from primarily flowability and shape retention, there was confidence that the mixes would behave very similarly to the reference mix extrusion-wise. Flowability and shape retention tests, on the other hand, were carried out for the developed mixes with LWA.

3.4.1. Mixing regime

For the small tests, mixing the concrete was done with a *Hobart N50* Planetary Mixer. For larger batches, a *Hobart A200* Planetary Mixer was used. The mixing protocol:

1. **2 min**: mixing dry ingredients (lvl 1)
2. **1 min**: while mixing, add water (lvl 1)
3. **1 min**: mixing wet material (lvl 1)
4. *(turn mixer off, add saturated LWA)*
5. *(**1 min**: mix (lvl 1))*
6. turn mixer off, scoop material manually
7. **1 min**: mix (lvl 2)

The abbreviation *lvl* means Level, and corresponds to one of the three rotational speed levels of the machines. Step 4 and 5 were only performed when LWAs were added to the mix.

3.4.2. Flowability

Flowability over time was determined by carrying out the minislump test (figure 3.8a) with time intervals of 20 mins, up to 60 min max. The test was done similar to *EN 1015-3* [130], with some alterations: The used tamper rod had dimensions 6 mm diameter and length 215 mm. The cone was filled up in 3 layers of similar height, after the first and second of which tampering was done 20 times. After lifting the cone, the table was dropped 20 times instead of 15. Spread diameters will therefore be larger compared to other studies doing the same experiment.

3.4.3. Extrudability

This property was investigated only once, using the reference mix. 4 kilograms of mix were prepared using the Hobart A200 and transferred into the hopper. With just the worm and stator connected, it was inspected whether the pump was able to properly extrude the material, without pumping issues. This was not investigated further, because of the labour intensity of setting up and cleaning the pump.

3.4.4. Open time

Vicat needle penetration (fig 3.8b), as described by *EN 480-2* [131], tests were done to measure the initial setting of the mixtures, and hence get an idea about the open time. Ideally, the open time should be not less than 50 minutes, as it is estimated that mixing and printing can be completed within that time, including some margin.

3.4.5. Shape retention

Vertical strain and aspect ratio are so-called direct approaches to assessing buildability of 3DPC [94]. One of the ways to evaluate this as a primary investigation without printing the layers is by means of a shape retention test. For every 20 minutes after finishing mixing the mortar, up to 1 hour max, a shape retention test similar to the one from [87] was carried out. An inverted half cone with a top



(a) (b)

Figure 3.8: (a) Drop table used for the minislump test, (b) Vicat apparati in operation

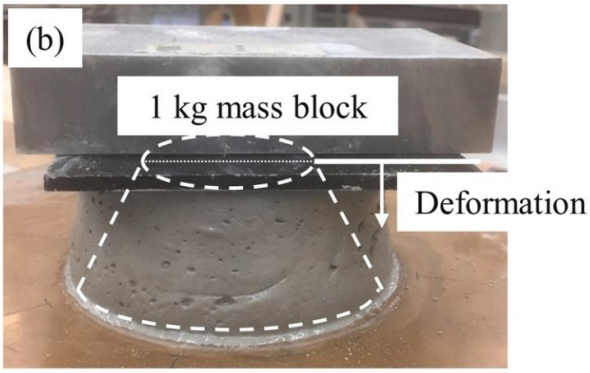


Figure 3.9: A measurement technique where the a weight induced vertical deformation of a concrete inverted half cone over 1 minute is measured, adopted from [87]

diameter of 70 mm, bottom diameter of 100 mm and a height of 60 mm was made wet on the inside, filled with the mortar and gently compacted by hand, as to simulate pressure from the pumping process. Excess mortar was removed by skimming on top of the cone using a metal rod. The cone was removed carefully, after which a 1010.5 grams piece of metal was gently put on top of the mortar cone. After 1 minute, the weight was removed and the vertical deformation was measured at multiple locations over the top surface. The average was noted down and used as an indicator for the shape retaining abilities of the mix.

This method is not yet perfectly suitable for evaluating all deformation that may occur during printing, like buckling. For that, the retention capacities of the fresh concrete were additionally assessed through manual compression and manipulation, as well as by constructing small layered structures to observe any significant deformation. Here it should be kept in mind that this is still not a perfect representation since the mechanical properties of the fresh mix could also change after pumping, even increase for flexural and tensile strength [88].

3.5 Printing

3.5.1. Apparatus

The TU Delft concrete printer is a small gantry system with a printable region of around 1000 x 700 mm. It is operated through computer numerical controlled (CNC) software, hence the machine input can be geometrical coding (G-code). The hopper-pump system (*PFT SWING M FC-230V*) and included stator/rotor (*PFT C4-2*) can pump material with a grainsize of max 3 mm. A pressure gauge is attached (*PFT DN25*) right after the stator. After, a 5m hose (*SEMPERIT SM40*) is attached to the z-axis of the CNC, guided by a support hook at 1.45 m above the print bed. See figure 3.10. At the end of the hose, a 20 mm diameter PLA 3D printed nozzle is attached using bolts and tape as can be seen in figure 3.13. This nozzle shape makes it possible to print curves, as there is no option for z-axis rotation in this setup. Using this nozzle shape, there is a chance of inhomogeneous deposition of filament when printing a corner, but this was not observed during test runs.

3.5.2. Print design

The eventual printed structures have to be suitable for the desired tests, which are described in section 3.6. To prevent severe plastic collapse or buckling, first a design with triangular mesh inside was investigated, recommended by [70]. Also structures with trusses were explored. However after some test prints with the reference material, it was observed that after printing the material possesses enough

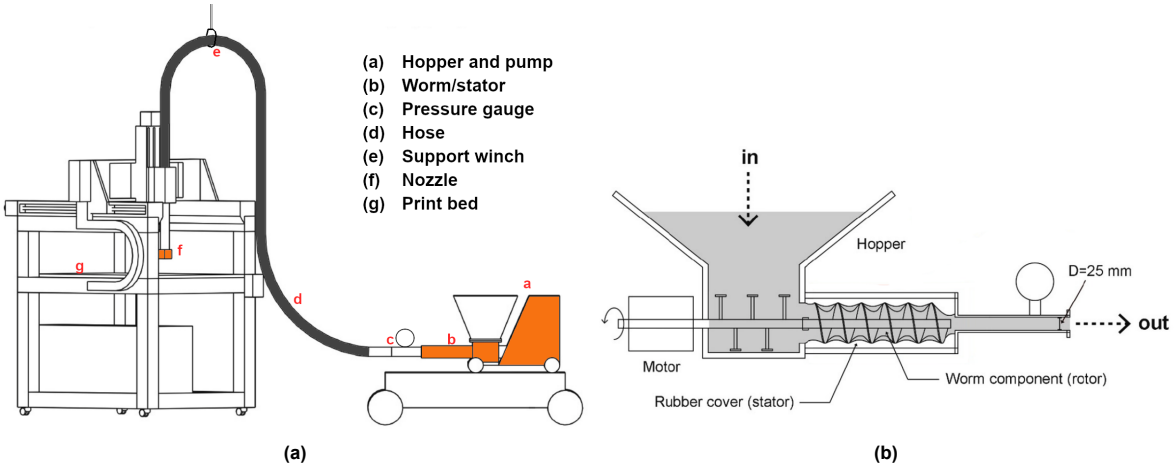


Figure 3.10: (a) Schematic image of TU Delft 3DPC installation. Computer numerical control (adapted from [97]). (b) Detailed drawing of hopper, pump and worm (adapted from [58])



Figure 3.11: (a) CNC and printbed, (b) PFT Swing-M pump with attached worm/stator and pressure gauge

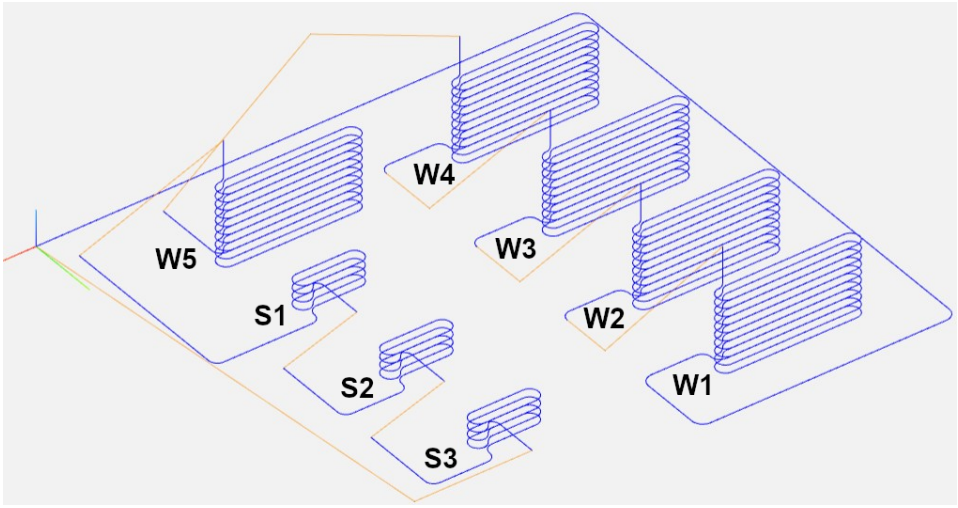
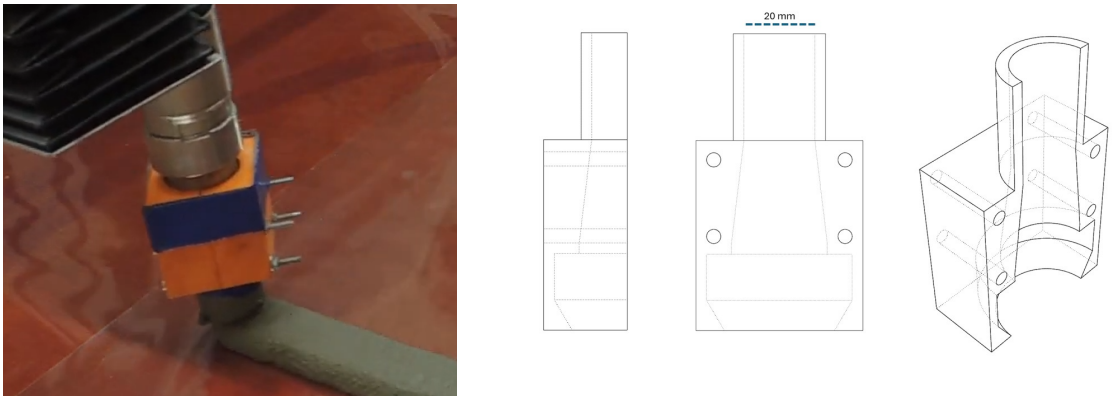


Figure 3.12: Toolpath of final print: five wall structures and three small structures. Visualized by ncviewer.



(a) **(b)**

Figure 3.13: (a) PLA nozzle attached with bolts and tape during a print, (b) Technical representation of circular nozzle halves

shape retention that unsupported walls of 12 layers height did not buckle or show elastic failure. Therefore it was decided that no support system was needed.

For convenient and optimal monitoring of biological growth, the printed structures needed to have at least one 'flat' side where the moss is planted, in other words a wall. A total of three walls were printed per variant to carry out biological growing.

An additional two of the same walls were printed to do mechanical testing. Finally, three smaller structures were printed to carry out tests for water retention, absorption and surface roughness as described in section 3.6.

Summarizing, a total of 8 structures were printed for each mix. Toolpath dimensions:

- 5 x Wall: 194 mm x 24 mm x 99 mm (referred to as W1-5). Layer height 11 mm, total of 10 layers
- 3 x Small: 94 mm x 24 mm x 33 mm (referred to as S1-3). Layer height 11 mm, total of 4 layers

The eventual print design is shown in figure 3.12, of which the code can be seen by the link in appendix A. It should be noted that all structures were printed directly after eachother rather than one layer everywhere, followed by the second layer everywhere, etc. This minimizes the layer-on-layer time, and could result in more pronounced vertical deformation.

3.5.3. Print session

Before a printing session, the installation needs to be set up. The worm is lubed with vaseline, and all components are assembled. The system is rinsed with water to check and ensure extrusion without obstruction. This removes any dust and also lubes the inside of the hose. The printbed was covered with transparent foil to avoid damaging the printbed. Through operating the CNC, the nozzle tip was homed to $\sim$11 mm above the printbed, at which location it starts the toolpath.

Lastly, a data logger (*EL-USB-2*) was attached at a location close to the nozzle. This will track the temperature and relative humidity while printing and curing. Also, a digital camera was placed to record the printing process.

Per print, the material is prepared in four batches. Two large mixers (*Hobart A200*) are simultaneously operated following the protocol described in section 3.4. After the mix is done, it is transferred into the hopper and covered with a piece of foil to prevent drying. When the last two batches are ready, they are disposed into the hopper as well. Finally, one batch (labeled 'sacrificial') is prepared, which is put into the hopper when the print is running. This purpose of this batch is to stimulate a consistent inflow of the 'usable' concrete, hence continuous extrusion at the nozzle. This concrete is similar to the reference mixture, but has some brown color agent added as an indicator. When brown colored concrete is extruded from the nozzle, no more usable concrete remains: the print should be stopped.

The pump operates at a rotational speed of 2, which corresponds to 35 rotations per minute. During prior test runs it was found that this rotational speed is properly aligned with designated printhead velocity.

After the print finished, excess concrete was carefully cut off using a putty knife and removed. The remaining structures were covered with transparent plastic foil to prevent evaporation. The samples were removed the morning after, labeled and transferred to the curing room at 96% RH and 20°C.

To minimize the influence of external factors that influence the concrete, the specimens were made all on consecutive days except for one batch that was printed after the weekend.

3.6 Concrete properties - hardened

After hardening for 28 days, the 3DPC specimens were taken out of the curing room and transferred to a climate chamber, at 20°C and 55% RH. W1 and W2 were cut to prisms one week prior, as they were used to assess the mechanical properties. Out of the remaining material, cores were drilled for CT scanning (figure 3.14). The remaining three wall structures were used to monitor biological growth and for pH measurements. The three smaller rectangles were used to determine the water retention, surface roughness and absorption.

3.6.1. Strength assessment

W1 and W2 were cut into four 40x40x160 mm prisms total, as can be seen in figure 3.14. Flexural and compressive strength tests based on *EN 1015-11* were carried out [132]. Flexural: 50 N/s, start load 0.001 kN, stop load 20%, A = 426.667 mm^2. Compressive: 400 N/s, start load 0.001 kN, stop load 20%, A = 1600 mm^2. All specimens were placed with the top side facing up, ensuring that the loading was applied perpendicular to the layers.

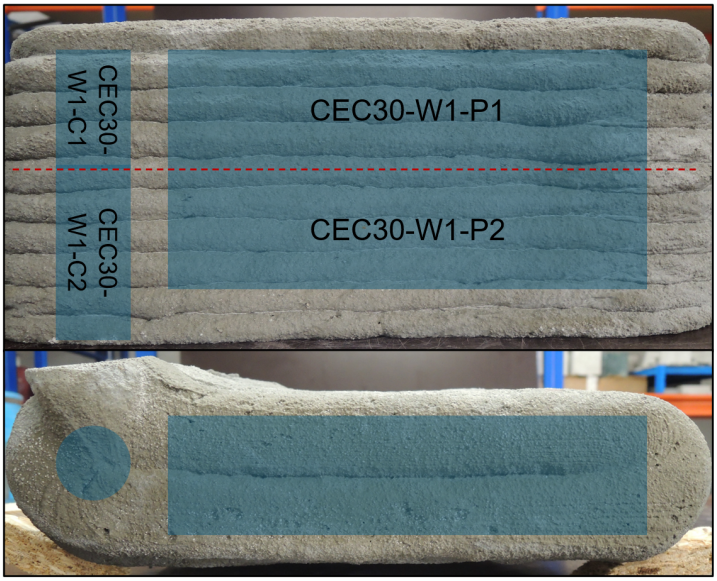


Figure 3.14: From a wall structure, two cores are drilled (C1, C2) and two prisms are cut (P1,P2) in the presented way. Example with CEC30-W1.

3.6.2. Surface pH

Based on the methods from [19, 20], pH measurements were done by obtaining some surface material using a file and chisel. For the first measurement, material was obtained from W3 of each variant at 30-37 days after printing. The second measurement was done on W4 after removal of moss from the growing experiment, at around 19 weeks after printing. At the second measurement, also a cast bioreceptive piece of concrete (bioref) was tested, which was over 1 year old. More on this in section 3.7.2.1.

Any large pieces of concrete were first crushed with an impact mortar (figure 3.15b), and further reduced by grinding for 2.5 minutes with a mortar and pestle. Then, the amount was weighted and demineralized water was added in a ratio of 10 grams powder : 20 mL water. The mixtures were blended for 30 seconds with a stirring magnet, after which it was allowed to settle for 5 minutes. Around 8 mL of the supernatant fluid was extracted using a pipette. From this liquid, the pH value was measured using a Metrohm 827 lab pH meter, calibrated with pH 7.00 and pH 10.01 buffer fluids, seen in figure 3.15a.



(a) (b)

Figure 3.15: (a) Metrohm 827 lab pH meter in operation. (b) impact mortar for crushing pieces of mortar that are too large for the mortar and pestle

3.6.3. Surface roughness

The surface profile of the specimens was analyzed using the Focus Variation Microscopy (FVM) method, as described by [49, 50]. This technique enabled the characterization of surface roughness across three distinct scales: macro-waviness, macro-roughness, and micro-roughness.

Macro-waviness refers to surface irregularities observed over longer spatial intervals, often attributed to phenomena such as layer stacking or significant profile changes within individual layers. In contrast, roughness represents shorter spatial variations that contribute to the overall surface profile when combined with waviness. To further refine the analysis, roughness was classified into macro-roughness and micro-roughness, depending on the field of view and resolution employed during measurement.

A *Keyence VHX-7000* optical microscope was used. After constructing a 3-dimensional representation of the surface in question, roughness and waviness parameters are computed according to the equations from *ISO 21920-2:2021* and *ISO 13565:1996*.The Arithmetical Mean (Ra, Wa), indicating the average of the absolute value over the sampling length, was employed to express the roughness:

$$\mathrm{Ra, Wa} = \frac{1}{\ell_\mathrm{r}} \int_0^{\ell_\mathrm{r}} |\mathrm{Z(x)}| \mathrm{dx} \tag{3.3}$$

Whether a value for the Roughness (Ra) or the Waviness (Wa) is obtained depends on the applied cutoff filters. To acquire roughness, longer wavelengths should be removed while the opposite is true when interested in the waviness. In figure 3.17 from the microscopes user manual, λs, λc and λf represent shorter to longer cutoff values respectively, that bound the roughness and waviness profiles. The *Keyence* software provided with the microscope uses a Gaussian filter.



(a) (b)

Figure 3.16: (a) The samples were cut diagonally, parallel to the outer surface. (b) Half a sample analyzed with optical microscopy.

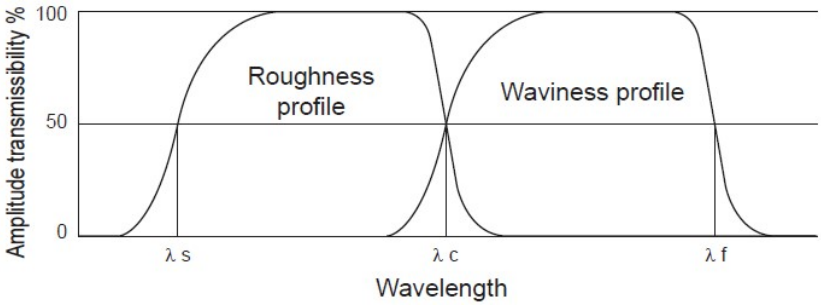


Figure 3.17: Example graph to show which profiles are bounded by certain cutoff values (adopted from VHX-7000 User's Manual)

Table 3.2: Cutoff and microscope settings. FRL = full ring lighting

	Lens and Magnification	height step size	λ_s	λ_c	λ_f	End effect correction
Macro waviness	E100:X100, FRL	40 µm	-	2.5 mm	25 mm	On
Macro roughness	E100:X100, FRL	40 µm	None	8 mm	-	On
Micro roughness	E500:X700, FRL	2 µm	None	0.8 mm	-	On

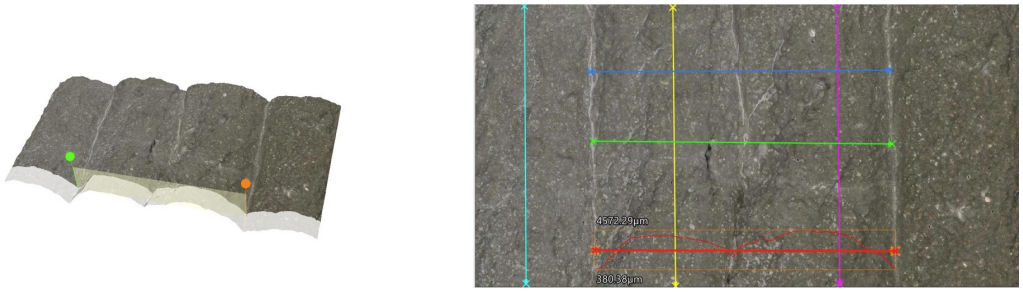
For each of the 6 mortar types, specimen S2 was cut parallel to one of the sides. This allowed proper placement under the lens and finer analysis (figure 3.16). With a magnification of X100, a 40 mm x 20 mm serial 3D stitch image was made over the surface, each with a vertical step size of 40 µm. Employing the *Line Roughness* function in the software, three horizontal line segments were drawn crossing exactly two layers (waviness). The same was done for three vertical line segments over and parallel to the layers (macro-roughness). See figure 3.18. The various cutoff values are based on the lengths of the line segments, depicted in table 3.2.

After, at two arbitrary locations on the layers, a depth-up image was created with a step size of only 2 µm and a magnification of X700. Two horizontal and two vertical line segments per location gave the micro-roughness parameters (figure 3.18). The cutoff value and other settings are depicted in table 3.2.

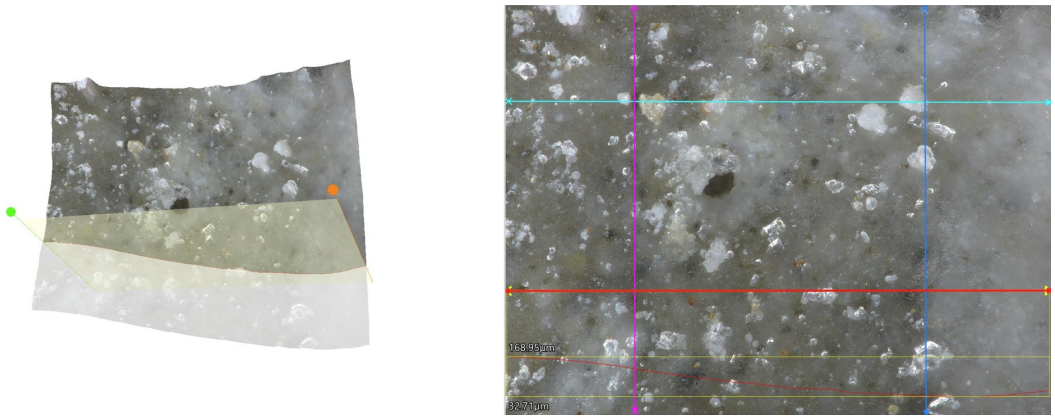
3.6.4. Porosity

Open porosity was determined by immersing S3 samples in water. This is a straightforward method that sees some use in existing literature [109]. First, the samples were dried in an oven at 100°C until constant mass, making sure that all the free water had evaporated without losing any chemically bound water. Then, the samples were immersed in water to absorb it. Multiple times, the samples were taken out, surface moisture was removed with a towel and the mass was measured. This was done at 23hr, 48hr and 77hr after immersion. Then, an estimation of the S3 samples volume was made through approaching the shapes as a trapezoidagons as seen in figure 3.19. The volume of the absorbed water divided by the estimated total volume is the open porosity.

The water absorption method does give an open porosity quantification, but is obviously heavily influenced by topological features. To see if the LWA addition did also increase the inner (bulk) porosity, the specimens were scanned using X-ray computed tomography (CT). Scanning was done with a *Tescan CoreTOM*. Cores were obtained with a 25mm diameter hollow core drill, using material from end pieces from the cutting process. Cylinders W1-C1 and W2-C2 were picked to serve as test samples, see figure 3.14. A voxel size of 25 microns was used. For cylinder EG30-W1-C1, an additional scan with a voxel size of 12.5 microns was done to compare results with a finer scan resolution. In appendix B, all settings for the scanning of EG30-W1-C1 are presented.



(a) Line segments on 40 x 20 mm serial stitch of EV30-S2. Horizontal segments cover two layers for waviness. Vertical segments for macro-roughness.



(b) Line segments on 420 x 315 µm image of PU30-S2. Both horizontal and vertical are used to determine micro roughness.

Figure 3.18

In Dragonfly the reconstructed images were filtered using *Gaussian Smoothing* - 3D smoothing and size 5, with a standard deviation of 1.00. After, the images were segmented based on lower and higher Otsu, in other words the voxel intensity. This roughly divides pores and very porous regions from the inner matrix structure. A cylindrical Region of Interest (ROI) was created that covered the inside of the image. Using a boolean subtraction, the ROI contained the inner pores of the sample as segmented by Lower Otsu and Higher Otsu. To compensate for the noise in the image, the pores with a voxel size of fewer than 9 were removed from the region of interest. Where the original theoretical smallest pore size was 25 microns, it now has increased to an equivalent diameter of at least 50 microns, or 25 microns for the high resolution scan.

The pore assigned voxels could now be added up and expressed as a percentage of the full cylinder ROI, giving a first indication about the total porosity. The pore-ROI was then converted to a Multi-ROI, indexing all individual pores. Individual pore volume and equivalent spherical diameter were computed, as well as locational data of the pores centers of mass.



(a) (b)

Figure 3.19: (a) Printed S3 piece (b) trapezoidagon volume approach of S3 piece

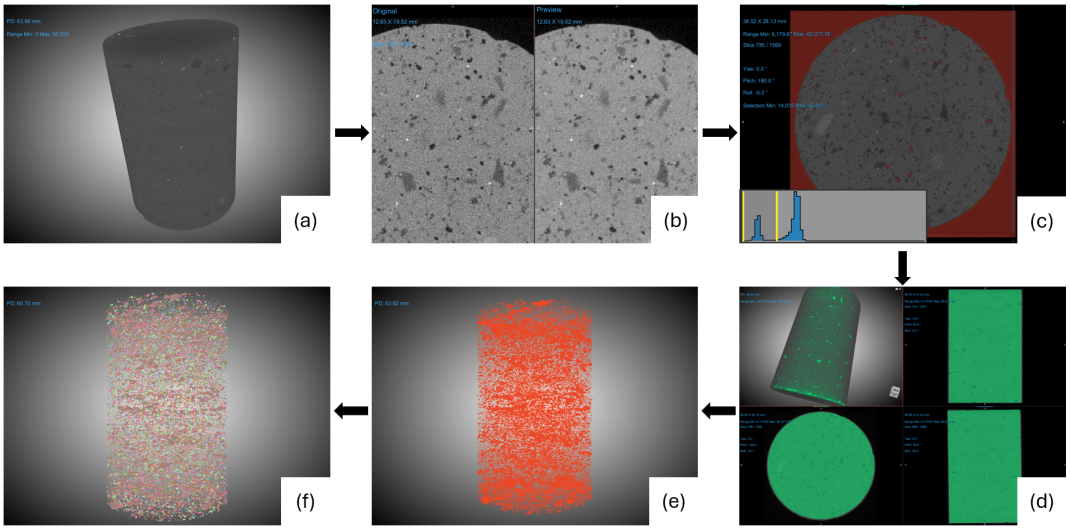


Figure 3.20: Order of steps for CT analysis. (a) Scanned CT image. (b) Noise reduction by Gaussian smoothing. (c) Segmenting Lower and Upper Otsu. (d) Cylindrical ROI. (e) All pores. (f) Index pores.

3.6.5. Water retention

To assess the hydraulic property water retention of the samples, the method from [20] was employed. S1 samples were dried in a climate cabinet at 37°C until mass difference between two consecutive days was less than 0.2%. Then, the specimens were immersed in water for 168 hours to ensure that the specimens were fully saturated. The samples were then placed in the climate cabinet again at 37°C and RH 40%. Their mass was recorded after 1, 2, 4, 8, 24, 47, 73, 101, and 169 hours as they slowly dried. Based on the trapezoidagon method explained in section 3.6.4, an estimation was done of the outer surface area as this plays a role in how effectively the water can evaporate.

3.7 Biological Growth

3.7.1. Moss harvesting and preparation

Based on information from the supervisors, feather-like mosses (Hypnales) that grew on stoney surfaces were collected [37]. Hypnales grow relatively fast as a species, and the stoney surfaces likely make them more quickly adapted to their new concrete substrate. All mosses were collected on and around the a parking lot in Delft (figure 3.21), mainly from concrete edge beams. The mosses were pried loose with a putty knife and kept in a sealed plastic bag. The species were identified as *Hypnum cupressiforme* (Cypress-leaved plaitmoss) and *Brachythecium rutabulum* (Rough-stalked feather-moss).

The mosses were gently washed with water to remove sand. A first batch of moss was then dipped in a 96% alcohol solution in order to rid any unwanted algae or bacteria. However, these mosses started to demise slowly after a while, possibly due to the intense osmotic shock. It was therefore decided to only wash with water. The mosses were placed indoors to dry for some days. The mass of the mosses greatly reduced while drying, emphasizing the water absorption capabilities of the organism. About 120 grams of air-dry moss remained. On the day before planting, the mosses were cut to small size with a knife.

3.7.2. Planting and storage

3.7.2.1. Bioreceptive reference samples

Besides W3, W4 and W5 of all 3DPC types, three more cast concrete specimens (referred to as *bioref*) were placed, which were proven bioreceptive in work from the supervisor [unpublished]. Putting these samples with the 3DPC samples is important. In the same conditions, chances of moss growth on these specimens are theoretically higher than growth on the 3DPC ones. In case no growth is observed on the 3DPC ones, but there is on the *bioref* samples, one can say that the 3DPC samples are not bioreceptive (enough). If moss does not grow on either, there might be an issue with the initial moss quality or some environmental factors. Aside from a single surface pH measurement, no bioreceptive markers have been measured for the *bioref* samples for this thesis, thus most information relies on measurements from previous work.

3.7.2.2. Environment and cultivation

The 3D printed specimens were transferred to a glass house in the Hortus Botanicus of the TU Delft. Here, temperature and humidity are kept fairly constant at 17-21°C and 85% respectively. Temperature and humidity in the near area of the specimens are measured too, using a datalogger (*EL-USB-2*). The specimens were placed horizontally and sprayed with rainwater.



(a) (b)

Figure 3.21: Locations where the mosses for this research were collected: (a) Delft Parking lot (52.00686416315744, 4.367789334382523), (b) Concrete edge beam with moss in the parking lot.

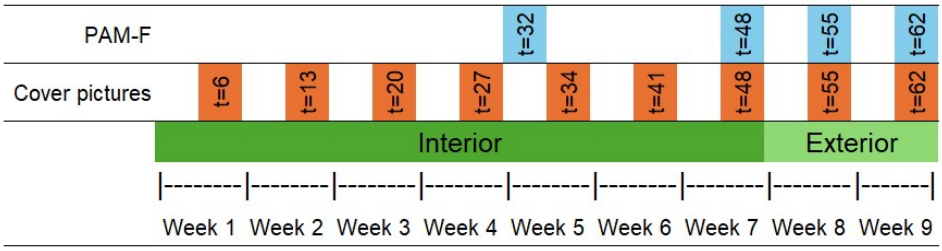


Figure 3.22: Timeline of moss growth experiment, including timestamps for pictures and PAM-F measurements.

The moss was spread over the samples. Around 6 grams for the 3DPC structures and 3-4 grams for the smaller *bioref* ones. Water mixed with nutrients (*Peters 2000 professional 10-52-10, 1.5 g/L*) was sprayed onto the samples to propel the growth. See figure 3.23. The staff of the botanical garden waters the specimens for 7 weeks.

The glass house direction is pointed to the South, meaning sunlight can come in all day through the foiled window roofs. However, at night there is no artificial light, meaning that all the vegetation is exposed to a day-night cycle. The experiment was done in the winter, making the time in which the moss receives daylight not more than 9 hours per day.

3.7.2.3. Exterior

After the 7 week period, all samples were transferred to a semi-indoor location where the outside temperature is closely resembled. The specimens are only watered once a week. This 'exterior phase' lasted for 2 weeks and is done to see to what extent the specimens can keep providing water for the mosses without being watered daily. It also addresses the adaptability of the moss to a less constant, colder and dryer climate. It is likely that the biological colonization will be quickly affected by the different conditions, as [67] points out. A timeline of the entire growth experiment is depicted in figure 3.22.

3.7.3. Assessment of biological growth

Weekly pictures were taken of the samples with identical lighting conditions and similar humidity of the moss. The samples were placed in a light box with embedded ring light (*Puluz 30cm Foldable LED Ring Light Studio*) on highest brightness and color rendering index of 95. Pictures were taken from above, at a height of $\sim$30 cm from the base the photo box. The camera (*Nikon Coolpix P310*) settings were ISO 200, 1/200, f/3.2 with a centered focus. See figure 3.24 for the setup.



Figure 3.23: Horizontally placed samples after inoculation. Location: glass house of Hortus Botanicus

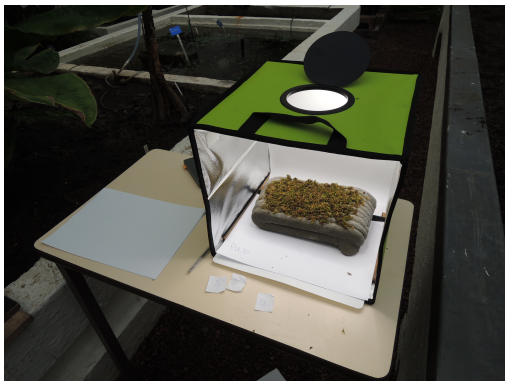


Figure 3.24: Overview image of a photo session, including lightbox with sample placed inside

3.7.3.1. Green cover

The images were digitally cropped with ImageJ and GIMP, ensuring a similar region of interest for every sample. The MATLAB app Canopeo is a tool that is designed to rapidly and accurately measure the canopy cover of farmland [133]. It gives a certain canopy cover percentage based on the green colored regions in the image, depending on the settings. Although it does not give information about the amount of biomass that is actually attached to the surface, the method was still employed because of its simple use and consistent outcomes. Final settings after manual sensitivity analysis: R/G 1.1, B/G 1.1, noise reduction 500.

3.7.3.2. Quantum yield

A PAM-F test (*Walz Mini-PAM II*) is also carried out complementary to the weekly photographs. The measurements were done on the 32nd day, and weekly from 48th day onwards. First, the samples were sprayed with a small amount of water, after which they were covered with a paper sheet to bring the mosses into a dark-adapted state which is necessary for this test. After not less than 30 minutes, the sheet was carefully removed. Measurements, more specifically the maximum quantum yield F_v/F_m, were done at three locations on each sample. One left, one middle, one right as seen in figure 3.25.



Figure 3.25: Three point locations on a sample where a PAM-F measurement was taken.

3.8 Statistical analysis

An Independent Samples Kruskal-Wallis test was done on the green cover and PAM-F results. This method compares the groups of the concrete types and computes whether differences are significant. The calculated F-statistic is the ratio of the variance between the groups over the variance within the groups. The p-value associated with the F-stat outcome should be <0.05 in order to state statistical significance and a possible rejection of the null hypothesis. In this case, the null hypothesis is that there is no difference between growth or PAM-F values between the 3DPC types.

Any significant differences can then be linked to outcomes of other tests by employing a General Linear Model (GLM) or more simple regression analyses such as Kendall's Tau. SPSS, Python and MS Excel were used to execute these methods.

4

Results

In this chapter, the characterization of the lightweight aggregates is presented. The process of developing printable mixtures with LWAs is also documented. The outcomes of the bioreceptivity and strength tests are shown by means of images, graphs and tables.

4.1 Aggregate characterization

4.1.1. Chemical composition

The materials used in this thesis have composition as presented in table 4.1.

Table 4.1: Normalized chemical concentration of all constituents in wt.%. n.d. = not determinable. Empty = not detected

Formula	PU	EV	CEC	EG	Sand	CEM I	P-50
Na2O	2.980	0.080	0.310	11.860		0.200	
MgO	0.270	21.170	3.090	2.170	0.120	1.810	0.331
Al2O3	12.320	7.850	22.030	2.070	2.540	4.000	0.181
SiO2	72.730	35.670	48.630	70.450	95.170	17.000	0.403
P2O5		2.476	0.253	n.d.	0.010	n.d.	n.d.
SO3		9.70E-05	1.580	0.154	0.057	4.840	
Cl	0.248	0.050		0.020	9.90E-05	0.018	0.030
K2O	4.490	4.370	3.290	0.750	0.830	0.590	0.034
CaO	1.058	8.740	4.270	10.930	0.170	65.730	48.690
MnO	0.043	0.081	0.212	0.029	5.40E-05	0.061	0.031
Fe2O3	1.507	11.200	14.850	0.500	0.743	3.570	0.117
ZnO	3.20E-05	0.013	0.048	0.027		0.112	1.70E-05
other	0.224	1.540	1.317	0.410	0.110	0.599	0.023
LOI	**4.130**	**6.760**	**0.120**	**0.630**	**0.250**	**1.470**	**50.160**

4.1.2. Particle size distribution

Final grain size distributions of the aggregates are plotted in the sieve curve in figure 4.1. These are the averages of three tests. Particles with size 0.5 mm and above are mostly equally well represented in all materials. Fine fractions are more divergent, with EG off by a maximum of 8.5 wt% at the 0.125 mm diameter. Overall, these distributions were considered similar and not altered anymore.

4.1.3. Porosity and pore size distribution

The results are plotted in figure 4.2 as the log differential intrusion over the logarithmic pore size, including cumulative intrusion. For all LWA, a high peak in range $\sim$ 100-300 µm is observed, indicating a large total pore volume from pores in this range. A broad peak in EV is observed around 1 µm pore

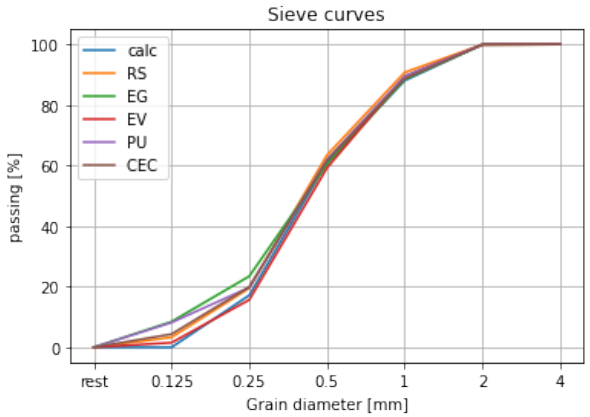


Figure 4.1: Average sieve curves of RS, LWA and objective curve (calc)

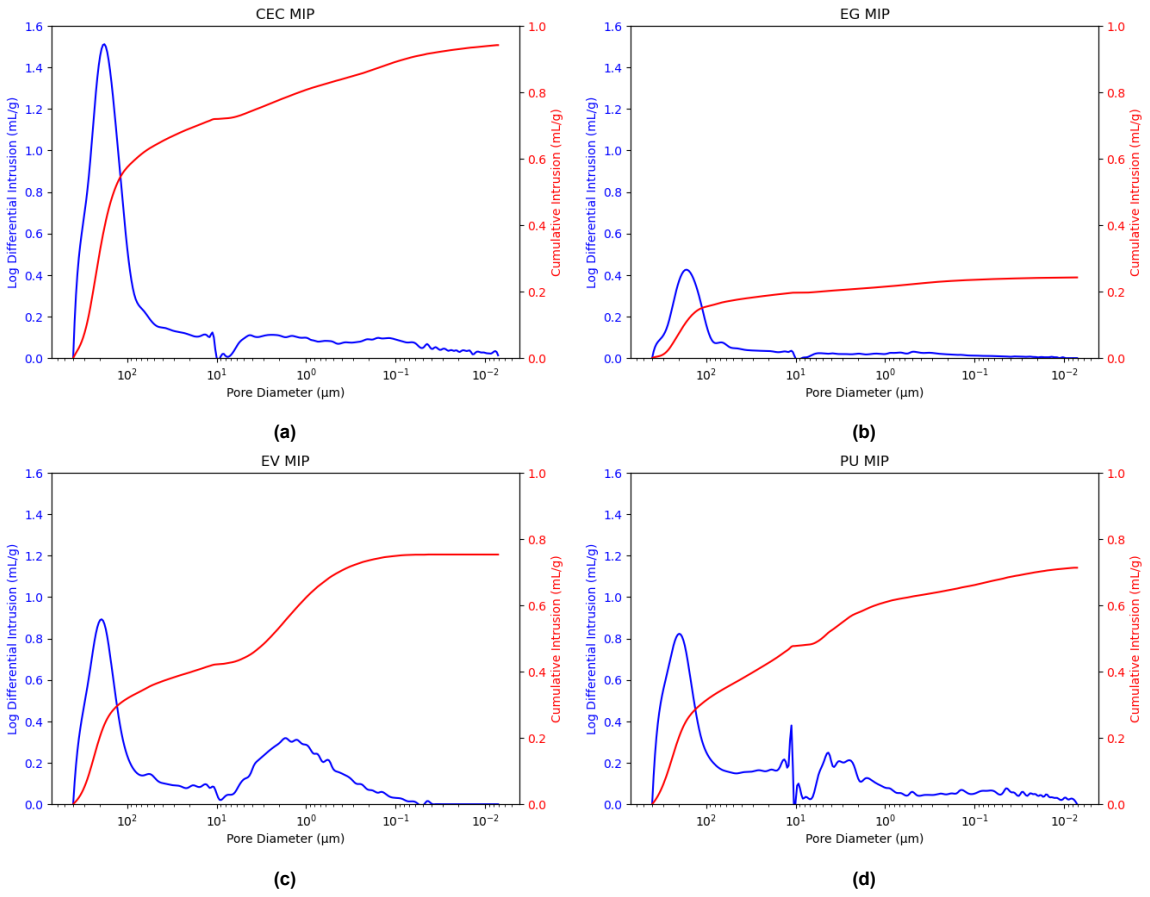


Figure 4.2: The differential mercury intrusion over the pore size of LWAs.

diameter. For PU, a slight peak is observed after the valley, at 4 microns. The other LWAs do not show distinct peaks, indicating that there is no particular pore size governing.

4.1.4. Water absorption and particle density

The method described in section 3.3.3 was carried out 4 or 5 times for each LWA. It was observed that PU and CEC particles descended quickly after soaking, but EV and EG did not. When water was added to EV, the mixture became a slurry and it took a few hours before water was absorbed by most particles and a clear layer of sediment was observed. For EG, some of the larger particles most likely had some closed, non permeable pores since they remained on the water surface even after 20+ hours. For both of these LWA the deviation between test results remained significantly larger than for PU and CEC. The results are depicted in table 4.2 and boxplots in figure 4.3. In the table, the corresponding values of the vacuum pump pressure are also given. Especially with pumice, the filter paper seemed blocked because of the fraction of (ultra) fines, hence the pump pressure gauge displayed its maximum value. For the other LWA, the pressure often decreased slightly over time. Regarding RS, the pycnometer method was used [129], which does not require a vacuum pump.

Table 4.2: Water absorption and ssd density of sand and LWA. P = vaccuum underpressure

	RS		EV		EG		CEC		PU	
	avg	stdev	avg	stdev	avg	stdev	avg	stdev	avg	stdev
$WA\ (t > 20hr)\ [\%]$	0.179	0.104	240.8	9.88	112.7	9.23	44.2	1.42	49.4	1.54
$\rho_{ssd}\ [Mg/m^3]$	2.625	0.024	1.228	0.025	1.097	0.013	1.605	0.006	1.482	0.003
$P\ [mmHg]$	-		725		525-625		650-750		760 (max)	

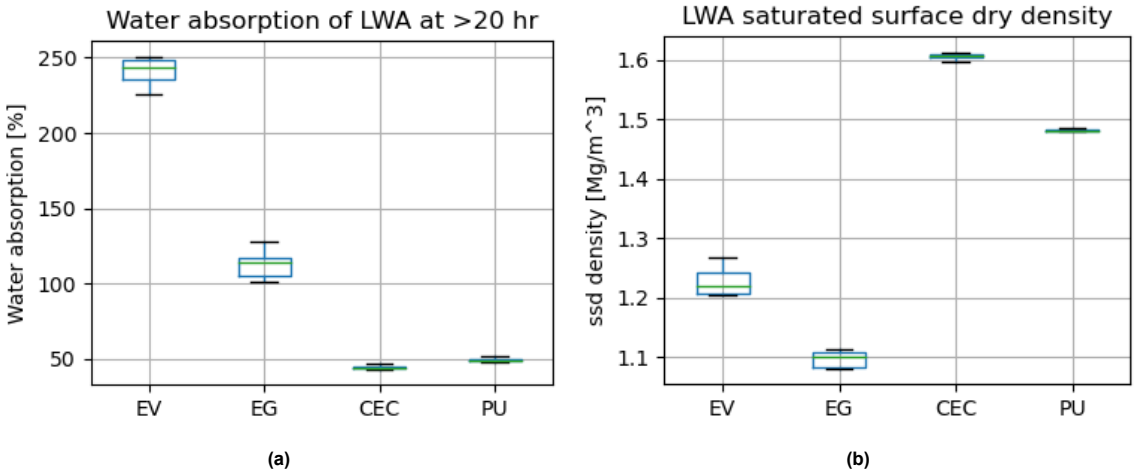


Figure 4.3: Boxplots of (a) water absorption of LWA at >20 hr, (b) LWA saturated surface dry density

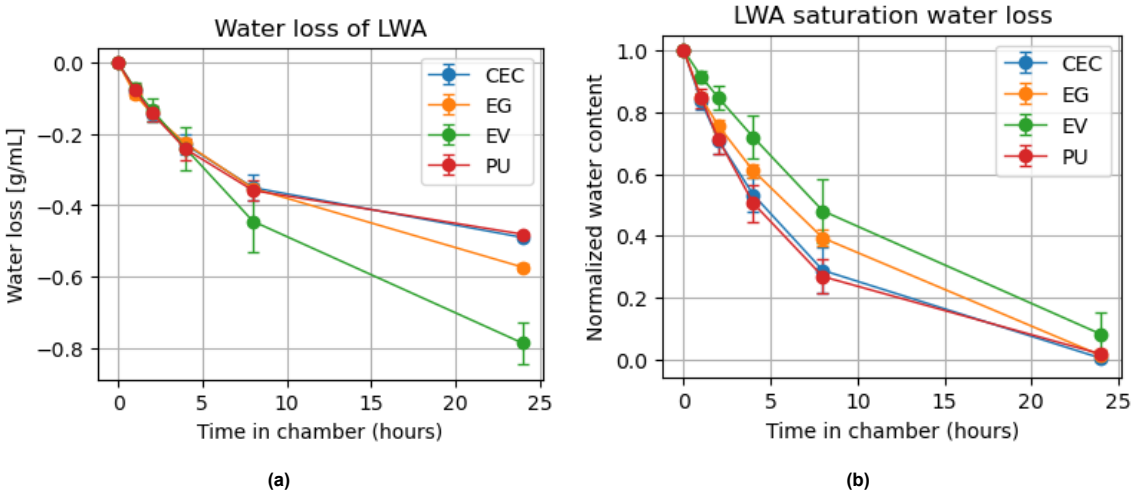


Figure 4.4: Water retention of LWAs expressed in water loss over 24 hours, at 37°C and 40% RH. (a) Grams of water evaporated per mL of LWA. (b) Saturation water content, normalized to content at t=0. At 24 hr, almost all saturation water had evaporated.

4.1.5. Water retention

The water retaining abilities of LWA are presented in figure 4.4. Over the test duration of 24 hours, CEC and PU lose water at a similar rate, while EG and EV lose more over the same period. After 24 hrs, EV lost the most water relative to its volume of aggregate. But because of its enormous absorbance, EV had still on average the most water left at 24hrs: around 10%. EV can absorb the most water and, when completely saturated, will likely take the longest to lose all of it. Testing with larger volumes of LWA will likely yield other results in terms of leftover water mass at 24hr.

Table 4.3: Mix designs for 30% replacement of sand. Quantities are based on 1 kg of RS concrete.

ID	CEM I 52.5R [g]	Water [g]	Sand [g]	P-50 [g]	ssd LWA [g]	mixing w/c	total w/c
RS	351.00	138.00	501.00	10.00	0.00	0.393	0.393
EV30	351.00	137.73	350.70	10.00	70.33	0.392	0.532
EG30	351.00	137.73	350.70	10.00	62.81	0.392	0.487
CEC30	351.00	137.73	350.70	10.00	91.87	0.392	0.473
PU30	351.00	137.73	350.70	10.00	84.87	0.392	0.472

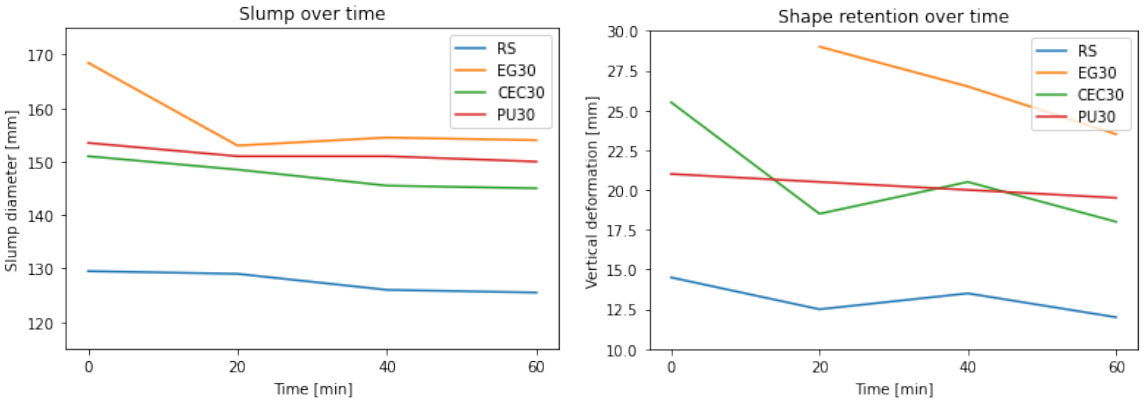
4.1.6. Replacement percentages

As described in section 3.2.2, 30% replacement of sand was first investigated. In table 4.3, the recipes are depicted based on 1 kg concrete of RS. Since the sand is replaced by volume, the summed mass of all ingredients for LWA mixtures is lower. The given quantities should therefore be seen as ratios. The corresponding w/c ratios for added water and total water are also shown. Total water includes LWA saturation water.

4.2 Concrete properties - fresh

4.2.1. Flowability and shape retention

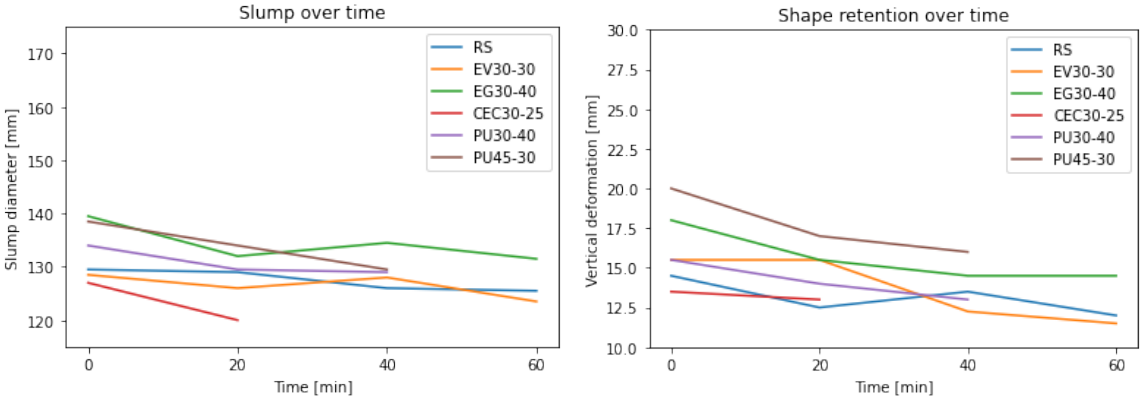
Due to the limited time available, slump and shape retention interval measurements were done only once. Displayed values in figures 4.5a and 4.5b consequently do not have a great statistical significance, and accuracy will increase when tests are done multiple times. The test was not carried out for EV, as this was estimated to behave similarly to EG in terms of flowability and shape retention because of the high water absorption. It can be seen that the concrete with LWA are significantly more workable than RS. They were considered too workable and not suitable for 3DCP. Additional slump and buildability tests were carried out with lower amounts of added water.



(a) Minislump spread diameters over time

(b) Vertical deformation of inverted half cone over time

Figure 4.5: Flowability and buildability results of non-adjusted 30% replacement LWA. Tests with EV were not carried out



(a) Minislump spread diameters over time

(b) Vertical deformation of inverted half cone over time

Figure 4.6: Flowability and buildability results of final 30% replacement LWA.

To tackle this, iterative testing was done with lower mixing water amounts. The ID's of the mixtures follow the form as described in 3.2.2. In the forthcoming sections and chapters, the ID's are often shortened to just the LWA and replacement percentage.

The iterative testing eventually led to the results in table 4.4. All 30% replacement recipes showed promising behaviour in the context of flowability and shape retention. For PU, 45% aggregate replacement was explored and adjusted with the correct water amount. Limited time and resources were the reason to not look into higher replacement for other LWA. Flowability and buildability of the final mixes

Table 4.4: Final mix designs for 30% replacement and PU 45% replacement. Quantities are based on 1kg of RS. The last number of the ID indicates the percentage of saturation water by which the added water has been diminished.

ID	CEM I 52.5R [g]	Water [g]	Sand [g]	P-50 [g]	ssd LWA [g]	mixing w/c	total w/c
RS	351.00	138.00	501.00	10.00	0.00	0.393	0.393
EV30-30	351.00	123.01	350.70	10.00	70.33	0.350	0.490
EG30-40	351.00	124.42	350.70	10.00	62.81	0.354	0.449
CEC30-20	351.00	132.10	350.70	10.00	91.87	0.376	0.457
PU30-40	351.00	126.51	350.70	10.00	84.87	0.360	0.440
PU45-30	351.00	124.98	275.55	10.00	127.30	0.356	0.476

did approach behaviour of RS, as can be seen in figure 4.6b. It should be mentioned that aside from attempting to mimic the RS behaviour numberwise, experience also played a role in judging whether the LWA concrete mixtures were suitable for the 3D concrete printer.

4.2.2. Extrudability

4 kilograms of reference mix (RS) were prepared and put into the hopper of the pump. The mixture was extruded and disposed in a metal tray without any distress. The digitally displayed current on the pump did not exceed the maximum allowable value of 5.8A, above a certain rpm speed. These were the only markers for this test.

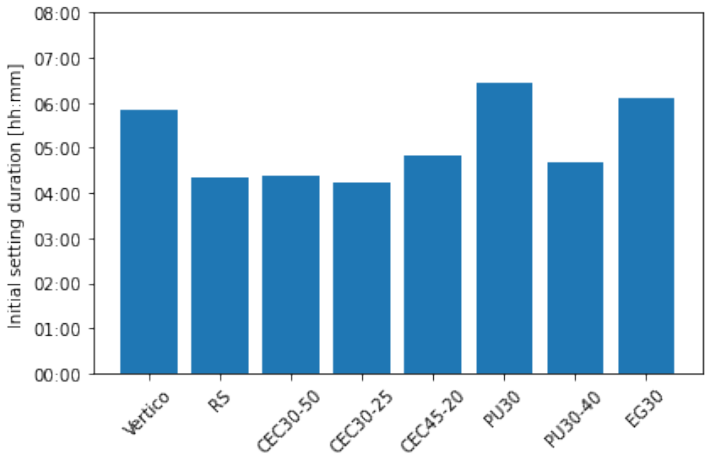


Figure 4.7: Vicat apparatus initial setting times [Ti] of Vertico's adopted mix, RS, and some mixtures from iterative testing. Due to limited time, the final mixtures were not tested. The binder type and content are equal across all mixtures.

4.2.3. Open time

The Vicat apparatus gives an estimation of the setting time. A substantial amount of concrete mixes have been tested, and because of limited time, the Vicat test was often carried out only once or twice per batch. Due to temporary unavailability of the device, some mixtures could not be tested. Relevant results are depicted in figure 4.7. The mixtures represented here are not the final mixtures, but ones that were carried out in the process. Although the open time of the final mixtures was not inspected exactly, the previous results suggest that initial setting will not occur within around 4 hours after mixing, which is a sufficient amount of time for printing. This is further backed up by the fact that the amount and type of binder remains the same, and total w/c ratios are over 10% higher than the RS equivalent (tables 4.3 and 4.4).

4.3 Printing

Based on prior results, total amounts for each print are reported in table 4.5. The samples of EV30 cured for a weekend in the printing area before being transferred to the curing room.

Table 4.5: Total amounts of ingredients used per print. In lightgray the constituents of ssd LWA. The date of printing is also displayed

ID	CEM I 52.5R [g]	Water [g]	Sand [g]	P-50 [g]	ssd LWA [g]	Dry LWA [g]	Saturation water [g]	Date
RS	14040	5520	20040	400	0	0	0	14-10
EV30-30	14040	4920	14028	400	2813	850	1963	18-10
EG30-40	14040	4977	14028	400	2512	1181	1331	16-10
CEC30-20	14040	5284	14028	400	3675	2549	1126	15-10
PU30-40	14040	5061	14028	400	3395	2273	1122	17-10
PU45-30	14040	4999	11022	400	5092	3409	1683	21-10

4.3.1. Print results

All specimens were printed according to plan. It was noticeable that RS print lines seemed slightly more stable after extrusion, whereas mixes with LWA replacement tend to show more pronounced vertical spreading deformation. The EG30 samples had this the most extreme compared to RS, as seen in figure 4.8. The masses of the specimens were divergent as well: despite EG30 having a lower density than RS as a fresh mixture, the mass of EG30-W4 was 3535.7 grams compared to 3168.4 grams for RS-W4. This suggests that the extrusion rate was higher when printing EG30, possibly due to better flowability.

The morning after a print, fair amounts of (evaporation) water were also visible on the specimens and the printbed. This was the case for all final mixtures, where a previous print (not part of this thesis) that was done with Vertico premix did not show this issue. Some IR temperature measurements of the specimens at ∼20 hours after printing showed the exothermic chemical reactions, with temperatures reaching over 25°C (figure 4.9e) while room temperature was only 21.5°C (figure 4.10). This increased temperature does enhance evaporation.

4.3.2. Environmental factors

The datalogger tracked relative humidity and temperature every 15 minutes, and the resulting graph is shown in figure 4.10. Temperature remained fairly constant over the entire week, while humidity ranged between roughly 40% and 70%.

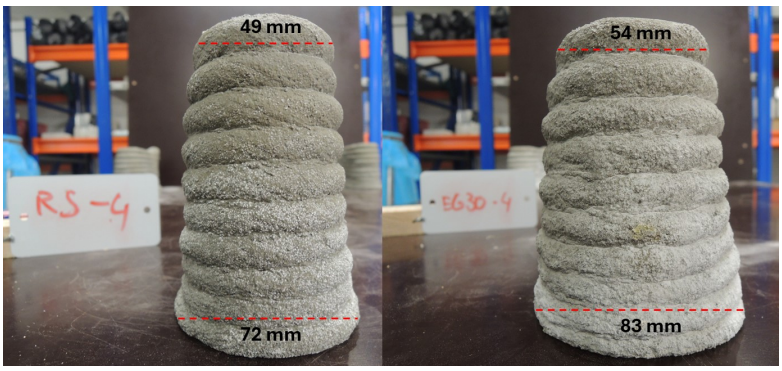


Figure 4.8: Example of printability differences between RS-W4 and EG30-W4. Although the height difference is marginal, the EG30 sample is much wider under the same printing conditions.



Figure 4.9: (a) EV30 directly after printing, (b) PU45 after one night curing, condensation clearly visible, (c) EG30 after removal of plastic cover, (d) CEC30 after removal of plastic cover, (e) IR temperature of PU45 after removal of plastic cover shows 25.2°C, (f) Putty knife cutting surface of PU30 directly after print

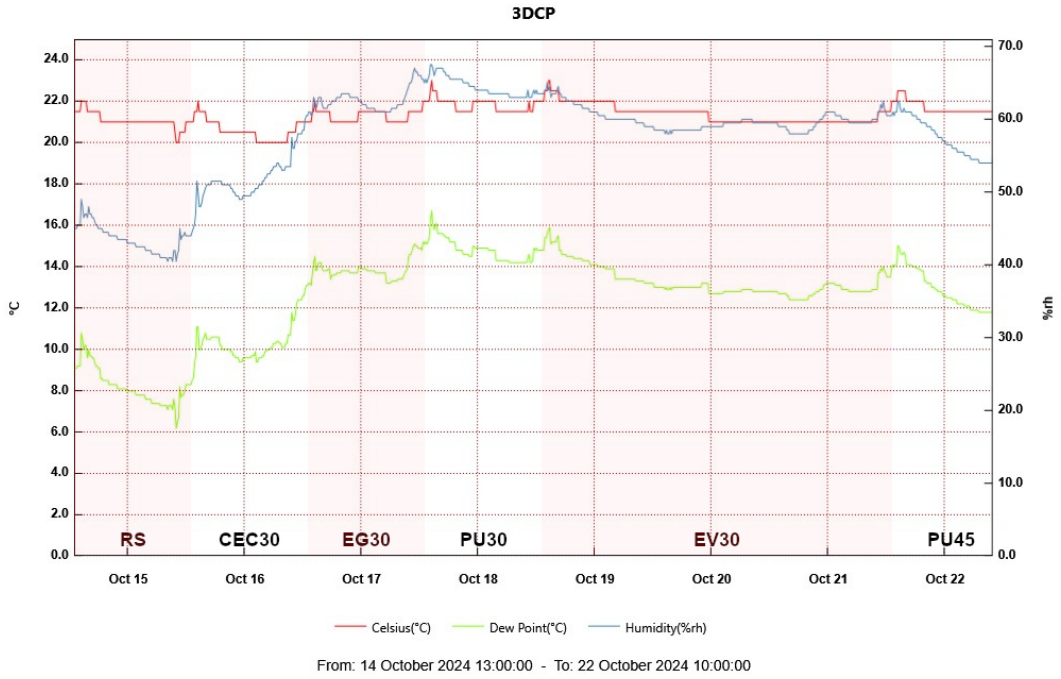


Figure 4.10: Temperature, relative humidity and dew point as measured by the data logger. Printing and curing durations of the six prints are indicated

4.4 Concrete properties - Hardened

4.4.1. Flexural and compressive strength

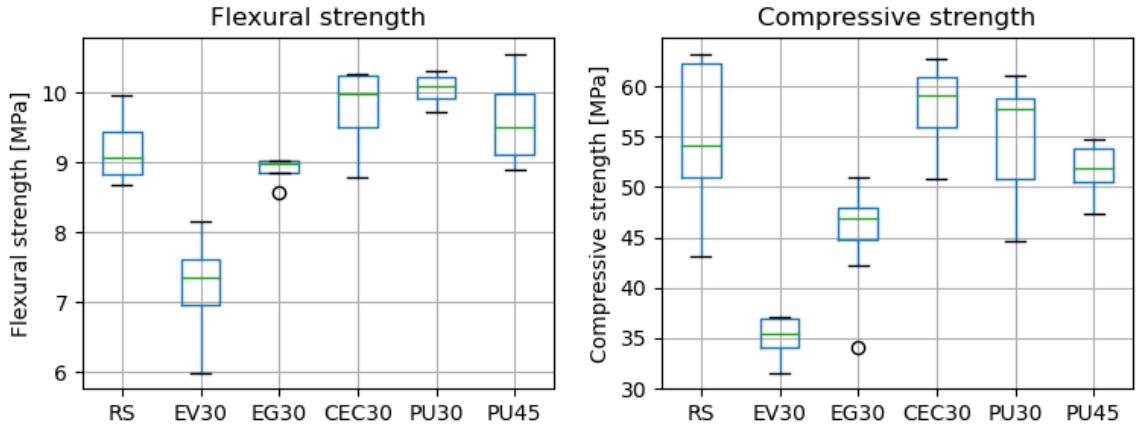
One halve of a prism of RS was slightly too large to fit into the compressive device, hence it was discarded. After the compression, it seemed that some dry or powdered material was present inside the specimens, suggesting either improper mixing or abduction of the water. This was most present at EG30 and PU45 samples which are displayed in figure 4.11, although in the images not visible too well.



(a) (b)

Figure 4.11: 3DPC specimens after compression testing. (a) EG30. (b) PU45. At both types dry material was observed after compression

Regarding the results in figure 4.12, the highest median flexural strength was observed at PU30, whereas the the highest median for compressive strength was at CEC30. Although porous aggregates are expected to decrease the mechanical properties of the mortar, this was not significant for most of the mixtures. CEC30, PU30 and PU45 have very similar or even better strength characteristics than the reference. Lowest strength of all specimens is for EV30 by a significant margin. Furthermore, the increase of pumice aggregates for PU30 and PU45 showed slight decrease in strength.



(a) (b)

Figure 4.12: Mechanical properties of 40 x 40 x 160 mm prisms cut from 3DCP wall structures 1 and 2. (a) Flexural strength, (b) Compressive strength

4.4.2. Surface pH

Around five weeks after printing, the surface showed extremely basic pH values. Some months later, a drop in surface pH was visible. See image 4.13. The control samples RS showed the highest pH, albeit by a small margin. Since only one pH measurement per concrete type was done, measurement- or experimental errors could be more pronounced than when averaged over multiple readings. However, it is unlikely that more statistically reliable results are far off the ones above, given the logarithmic nature of the measurement. Furthermore, the surface pH of all 3DPC samples decreased over time.

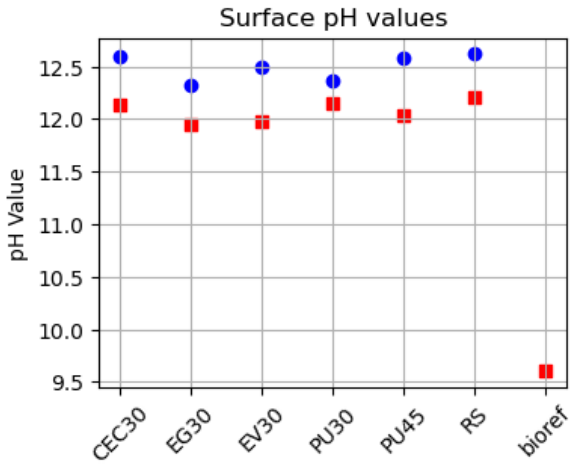


Figure 4.13: pH values measured at around 5 weeks after printing (blue circle) and a second measurement around 19 weeks after printing (red square), except for bioref which was over 1 year old. The second measurement was done on the moss-planted surface after the growing experiment.

4.4.3. Surface roughness

All results can be seen in figure 4.14. The waviness of most samples seems to be quite similar. The Gini number for the waviness is Gini = 0.0690, which indicates a quite uniform distribution across all samples, hence indicating that the surface deviation as a result from layer stacking and possible deformation are similar across all mixtures.

Regarding macro roughness, which was measured along the middles of layers, some pronounced differences can be seen. For all observations, the sampling lengths were between 20 and 25 mm. PU45 shows a large range of values, suggesting smooth as well as rougher measurements. But most medians are around 70 µm.

For microroughness, total of 8 measurements per sample were taken at 2 locations. All having a length of either 315 (vertical) or 420 µm (horizontal). Some deviations are visible, with EV30 having the largest percentile range.

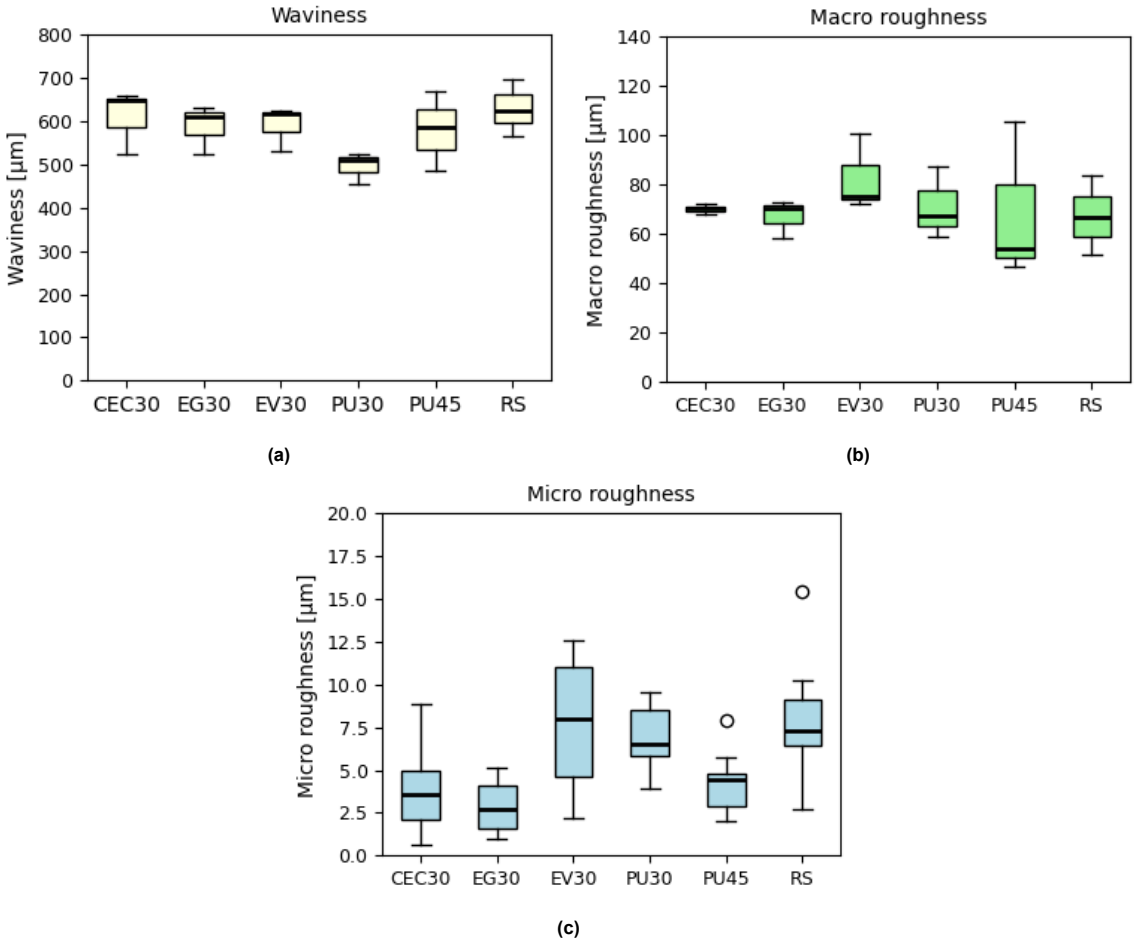


Figure 4.14: Boxplots of surface roughness results divided over Waviness, macro-roughness and micro-roughness.

4.4.4. Porosity - Water absorption

The volume of absorbed water is displayed in table 4.6, along with the estimated volume of the S3 samples approaching them as trapezoidagons. The water volume fraction of the total volume was assumed the open porosity. It is clear that RS is not able to absorb as much water despite having slightly larger volume than some other samples. EG absorbed the most water but also has the highest volume. Per unit of volume, EV absorbed the most, hence it is believed that its open porosity is highest. Based on PU30 and PU45 it can be said that a higher content of LWA does increase the accessible pore volume.

4.4.5. Porosity - CT

The porosities per sample are shown in figure 4.15. The two variants with the lowest density aggregate, EG and EV, show also the highest pore percentage. Not unexpected, EG30-W1-C1-h shows a

Table 4.6: Open porosity through water absorption of S3

	Absorbed water [mL]	Estimated volume [mL]	Open pores
CEC30-S3	79.53	451.78	17.60%
EG30-S3	90.00	518.13	17.37%
EV30-S3	84.11	426.12	19.74%
PU30-S3	77.88	464.64	16.76%
PU45-S3	82.94	456.20	18.18%
RS-S3	66.20	471.71	14.03%

significantly higher porosity than the other samples. This is because its smaller voxel size allows to detect smaller pores, and slightly larger pores are not filtered out as much by Gaussian Smoothing and ROI refinement. This result shows that the accuracy is highly dependent on the voxel size. The smallest included pore volumes of EG30-W1-C1-h are 0.000018mm^3 while the other samples only include volumes of 0.000141mm^3 and larger. To highlight the differences even more, figure 4.16 shows the counted pores per pore range. The pore volumes have been transformed to their related equivalent spherical diameter and grouped in intervals inspired by [134]. The highest amount of pores was discovered below the threshold of the initial minimum pore size. Up to a pore diameter of 250 µm, more pores have been observed using a higher resolution. From 500 µm and above, more pores were discovered in the normal resolution specimen. This could indicate that some larger pores were mislabeled and in reality consisted of multiple small pores close together.

Since the findings are significantly resolution dependent, the percentages in figure 4.15 give only limited insight about the true porosity of the concrete. However, these findings do implicate that a higher replacement percentage PU do give a slight porosity increase as well. The porosity in CEC30 did not seem to have increased by adding the LWA, based on these results. Their porosity is even somewhat below RS.

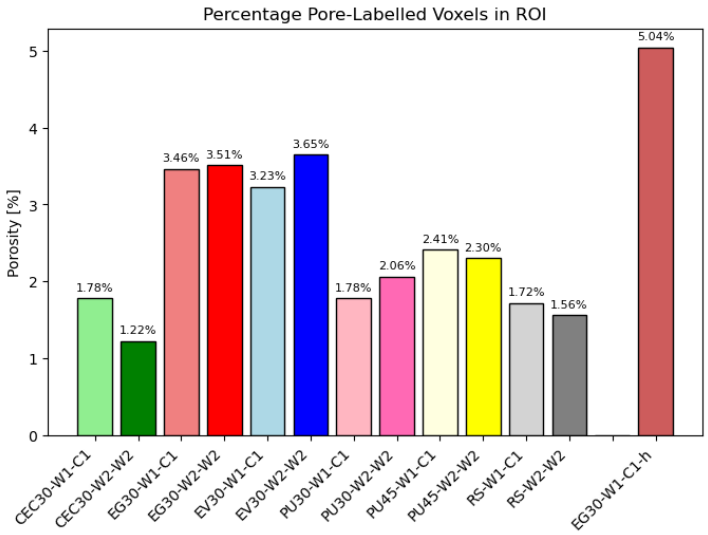


Figure 4.15: Porosity percentage of cores

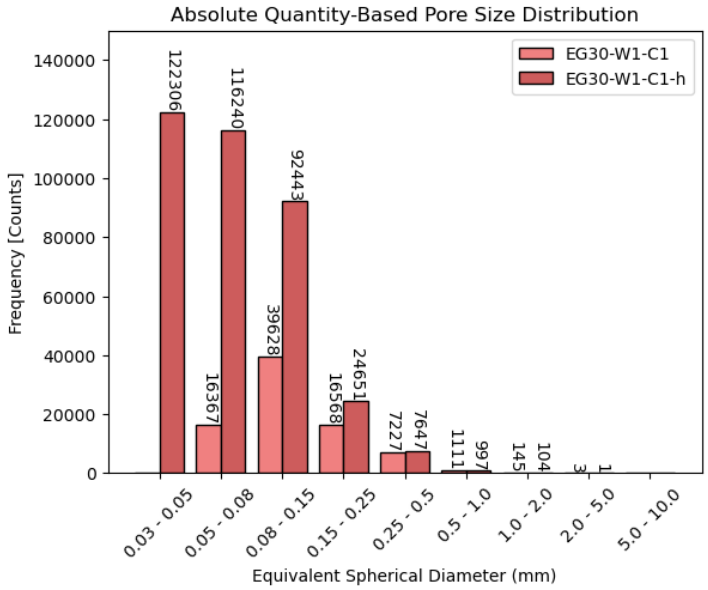


Figure 4.16: Comparison of pore count EG30-W1-C1 with 25 µm and 12.5 µm voxel size

Looking at how many pores were observed per sample (figure 4.17) it can be seen that it is not the smallest size pores that govern in frequency. Again, this could have to do with mislabeling pores, as they might consist of many smaller ones that are not distinguishable. Above the diameter of 2 mm, a very small amount of pores was represented.

However, all cores have slightly different sizes, consequently their region of interest is not equal in volume across all cores. Because of this, it might be more insightful to examine the relative size distribution. This is showed in figure 4.18. It can be seen that relative to all specimens, CEC30-W1-C1 contains a high amount of pores 50-80 microns, and lower amount at pores >150 microns. Contrarily, in EV30 samples the relative amount of smaller pores is lower, and larger pores (>150 microns) is higher compared to the other categories.

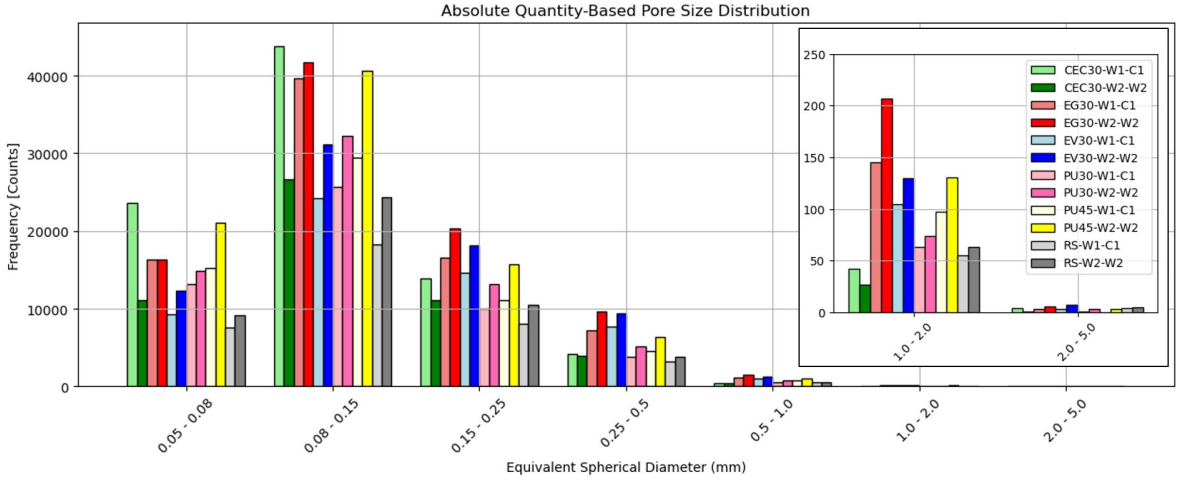


Figure 4.17: Amount of pores per diameter found in each core

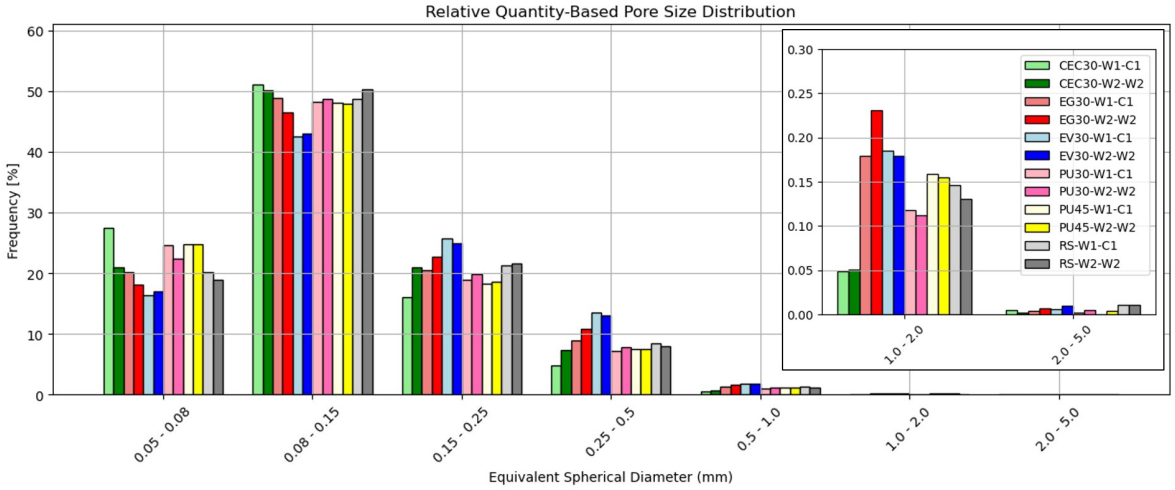


Figure 4.18: Percentage-wise pore-size histogram

The total porosity difference cannot be justified by pore counts alone. When looking at the corresponding pore volume in figure 4.19 things become more clear. Even though EG30-W1-C1-h had over 120000 pores in the 30 - 50 µm region, these pores account for only a couple percent of its total pore volume. Contrarily, large pores (>1 mm) make up less than half a percent of the pore count, yet their combined volumetric presence is significant. This states that porosity is very unequally divided in 3DPC, even regardless of any LWA incorporation.

The combination of figures 4.18 and 4.19 show that for both CEC30 cores, there is a remarkably lower relative amount of >1 mm pores compared to other samples, and consequently a lower relative porosity in that pore size region. This suggest that the scanned cores for CEC30 (simply) did not have the large pores to make their total porosity compete with the other cores.

Furthermore, there was no explicit porosity difference found between -C1 and -C2 of each set, which correspond to the upper or lower layers in the structure. Despite the lower layers being prone to some deformation, the CT scanner did not observe smaller pores or lower porosity compared to the non-compressed upper layers.

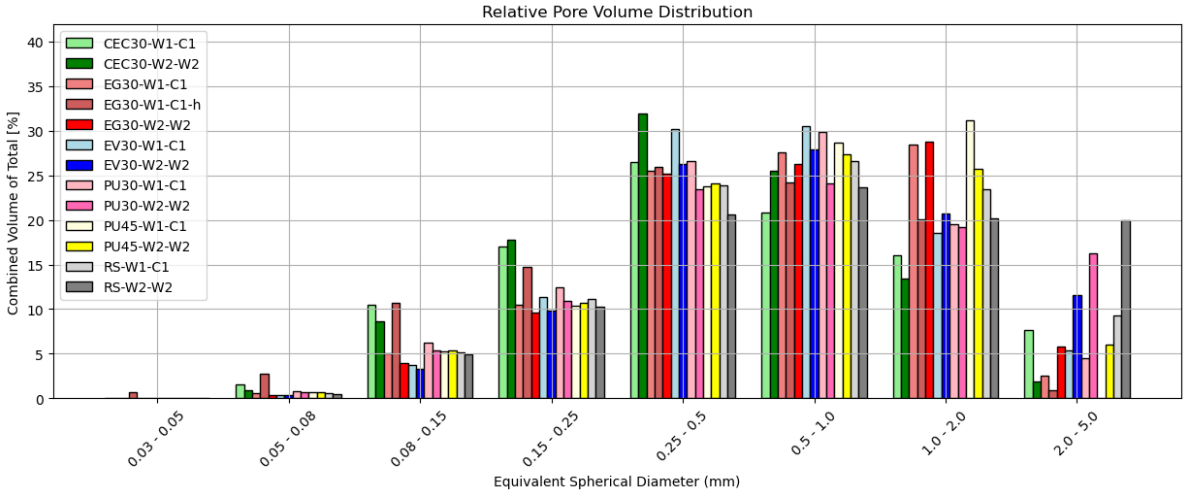


Figure 4.19: Percentage-wise distribution of the volume over the pores in each core, including the high resolution sample EG30-W1-C1-h.

4.4.6. Water retention

Quickly after being exposed to a warm and low humidity environment, the samples lost some water. The fastest rate was observed at EV30-S1 and CEC30-S1 (figure 4.20). At the last measuring point, EV30-S1 has lost the most water in absolute terms, which is not surprising given that EV has the highest water absorption from all LWA: it could potentially yield more water hence also lose more. The normalized curves follow more or less the same downward trend at the last data points, meaning water is still being evaporated at a constant pace. However, where the EV sample already lost over 60% of its absorbed water at 160 hours, the EG sample has still over 55% of its water retained. To be more precise, the water mass loss was divided over the estimated surface area. Based on this, EV retains the least water again. Also note that at 169 hours, RS has lost the least water relative to its evaporative area.

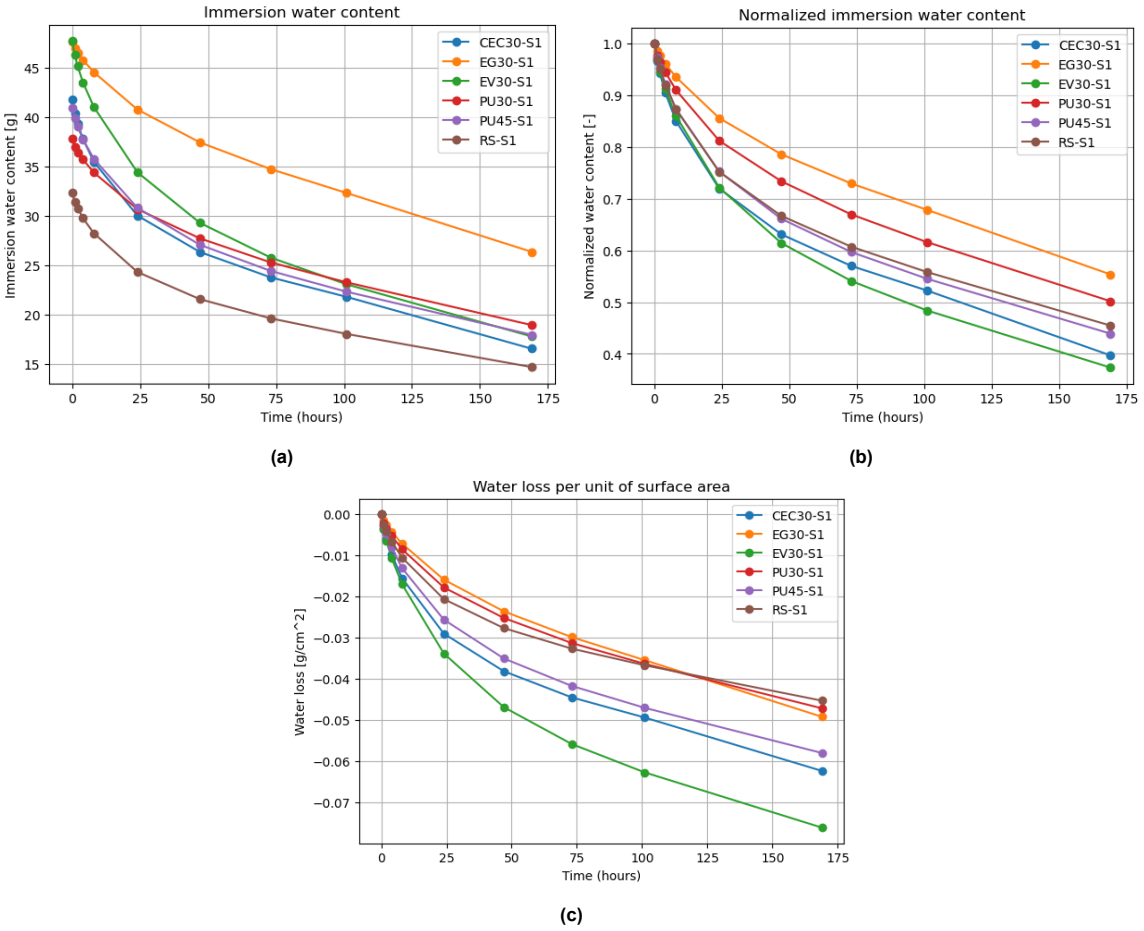


Figure 4.20: Water retention curves of S1 at 37°C and 40% RH. (a) Absolute absorbed water and its mass loss over time. (b) Normalized to initially absorbed water mass. (c) Water loss divided by the estimated surface area of the sample.

4.5 Biological Growth

4.5.1. Green cover

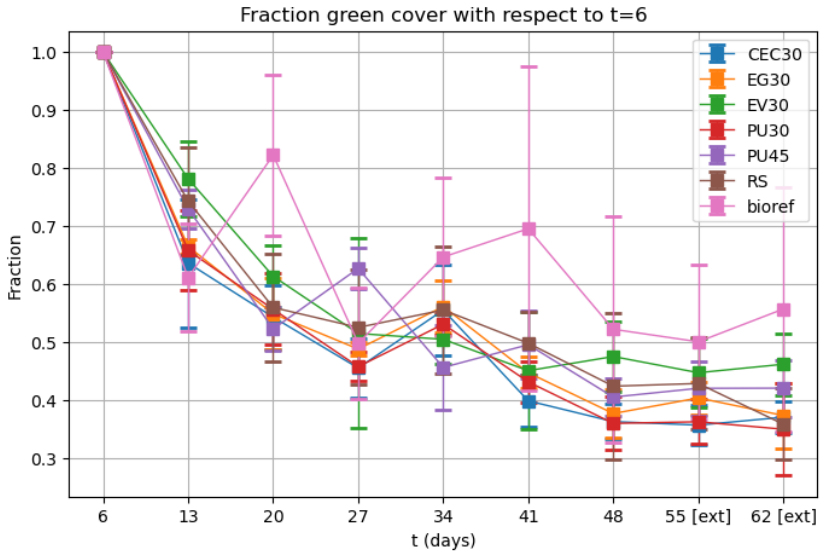
Over the weeks, the planted moss coverage did decrease on all samples. The average cover from all 3 samples per variant was calculated and normalized to the coverage at the first timestamp t=6 days. At 6 days, all samples were slightly more wet than in the weeks after. This can be seen clearly in figures 4.23 to 4.29 and could have resulted in a different green cover than when dry. Due to actions like moving the samples for pictures, watering and PAM measurements some of the moss at the border areas did fall off the samples over time. To minimize this in terms of green cover, the images in figures 4.23 to 4.29 are therefore cropped sections from the middle region of the samples. Each picture is accompanied by its fractional green cover black-white image, where the white pixels represent the green cover. Please note that for EV30, PU45, RS and bioref from 27 days onward and for CEC30, PU30 and EG30 from 34 days onward the images are toned slightly different. A longer camera shutter speed of 1/160 instead of 1/200 was used here, without notice of the author. Since the color range is different on these pictures, so is the indicated green cover. This is made visible in figure 4.22b which represents the derivative of the normalized green cover fraction over time. It displays whether there is any increase with respect to the week before, in other words when the values are above 0. This seen for some samples at t=34, and for PU45 at t=27. The most remarkable behaviour is shown by bioref in figure 4.22a. At three weeks after planting, the moss green cover significantly increased, only to fall back again one week later. Despite a different camera setting for half of the duration, it is clear that the coverages are overall strongly decreasing. Thus, any possible new growth did not outdo the decease of the initially planted moss. This is even the case for bioref samples, although their final green cover is still the relative largest compared to the other variants. There was, however, a visible (natural) colonization of algae on two of the bioref samples, which are cropped out of the image in figure 4.29 but can be seen in 4.21. These colonies were captured effortlessly by Canopeo. No algae were seen on the 3DPC samples.

The temperature and relative humidity were more or less constant and variated mostly with the day night cycles. Logged measurements are shown in figure 4.30. Temperature ranged between 16 and 22.5°C, with an average of 18.2°C. The relative humidity was quite high, ranging from 68 to 100%, averaging 87.8%. At 100%, water had been sprayed over the logger as well as the moss. When the samples were transferred to the second location, the temperature and humidity dropped significantly compared to the glass house. Temperature was on average 6.1°C, where even -0.5°C was measured for a short period. The humidity averaged 74.9%.

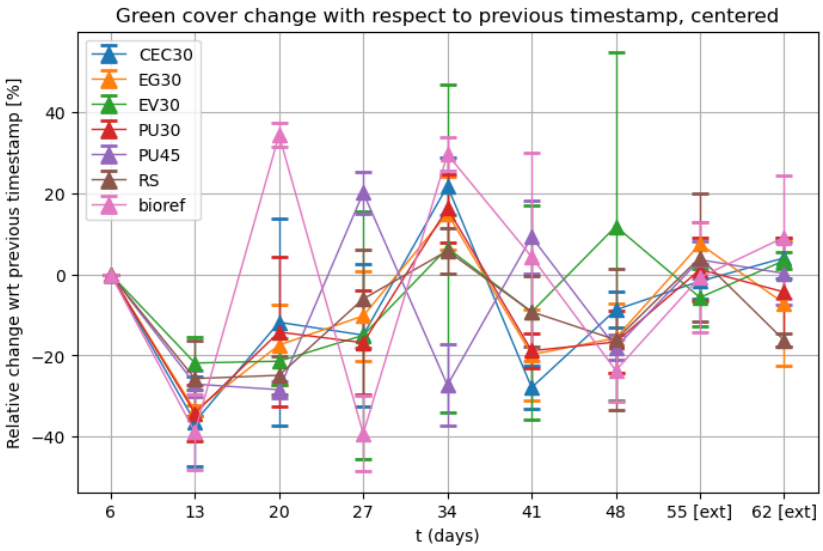
The pictures taken at t=55 and t=62 represent 1 and 2 weeks in the exterior setting respectively. Despite being exposed a less constant climate and being sprayed with water less, the green cover remained fairly constant for most samples. The largest decrease was seen at RS, while some green cover increased for bioref.



Figure 4.21: Algae growth of bioref-5 and green cover interpretation by Canopeo



(a)



(b)

Figure 4.22: (a) Green cover fraction with respect to first image (t=6), (b) Green cover percentile change with respect to previous timestamp

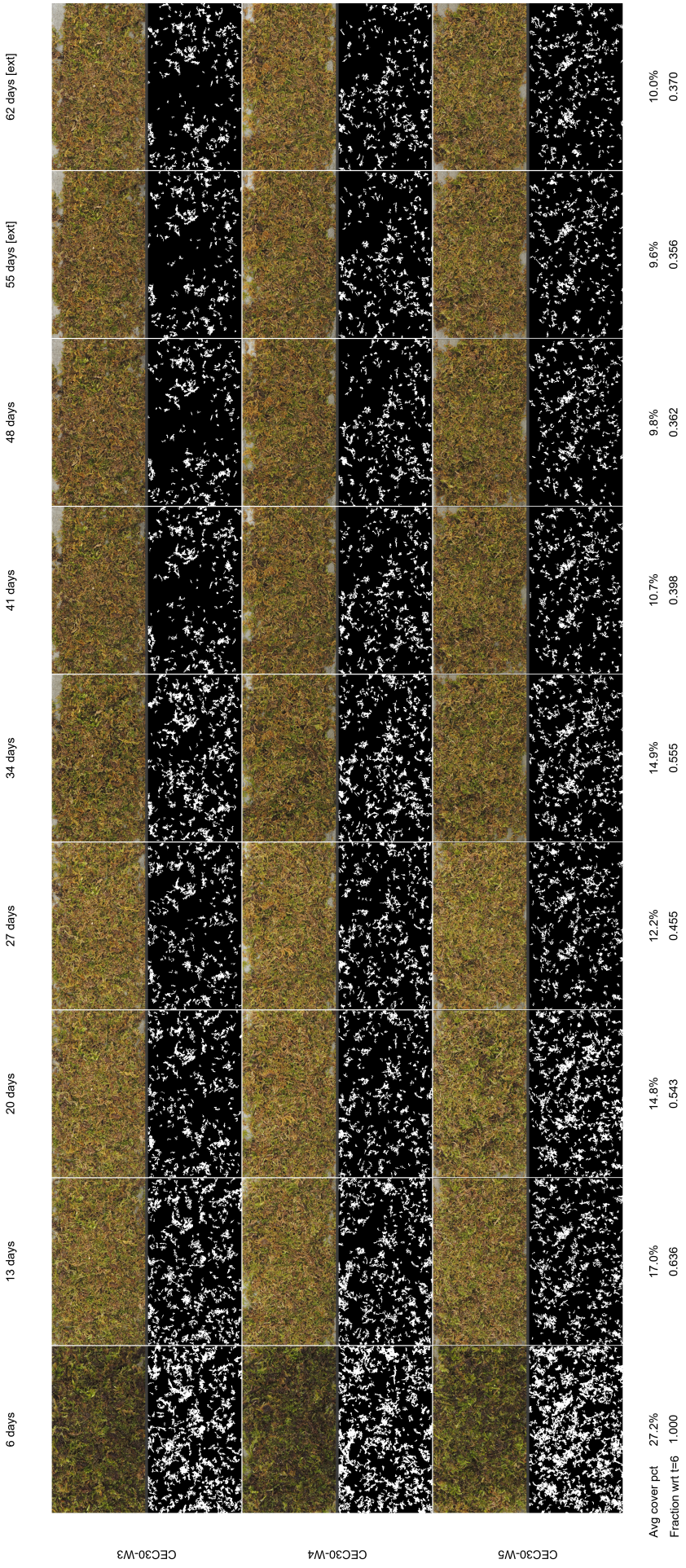


Figure 4.23: CEC growth pictures and black-white image of green-indexed pixels by Canopeo

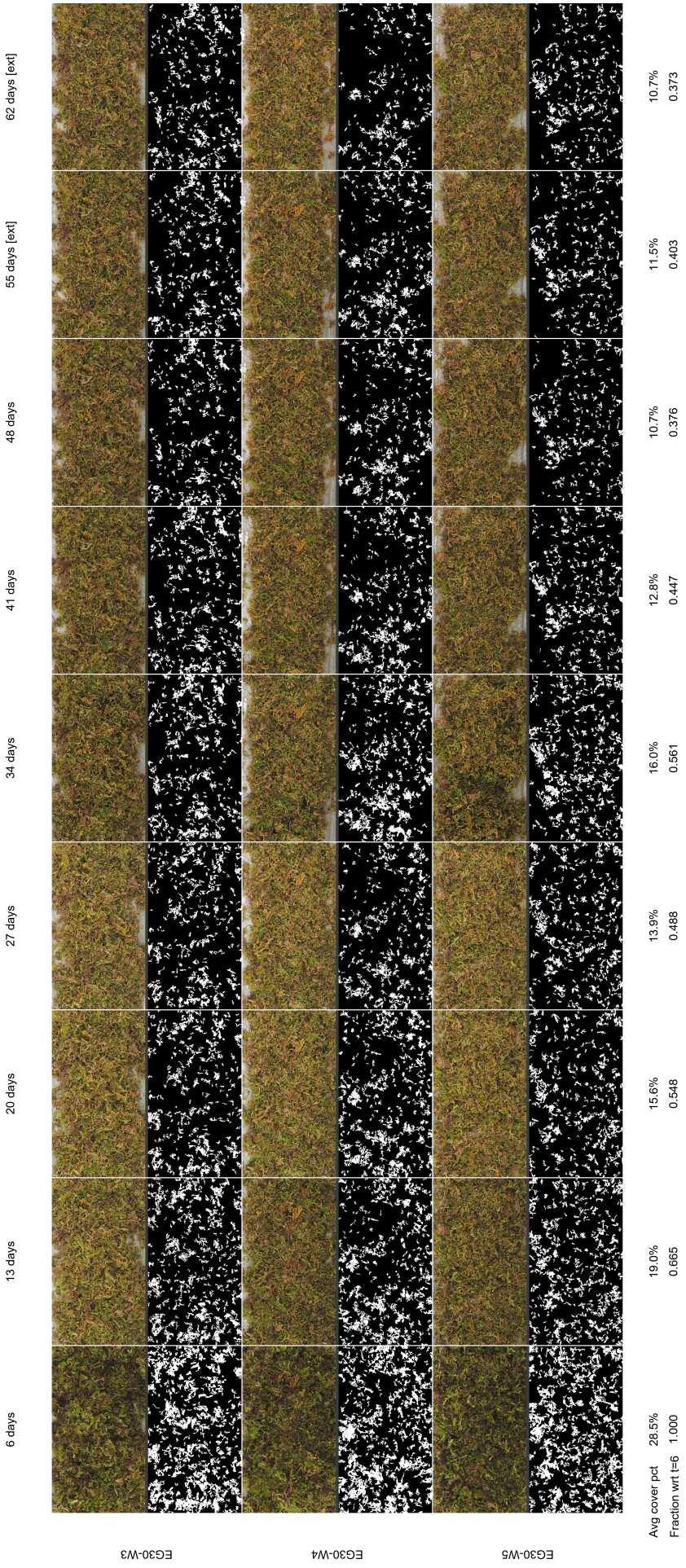


Figure 4.24: EG growth pictures and black-white image of green-indexed pixels by Canopeo

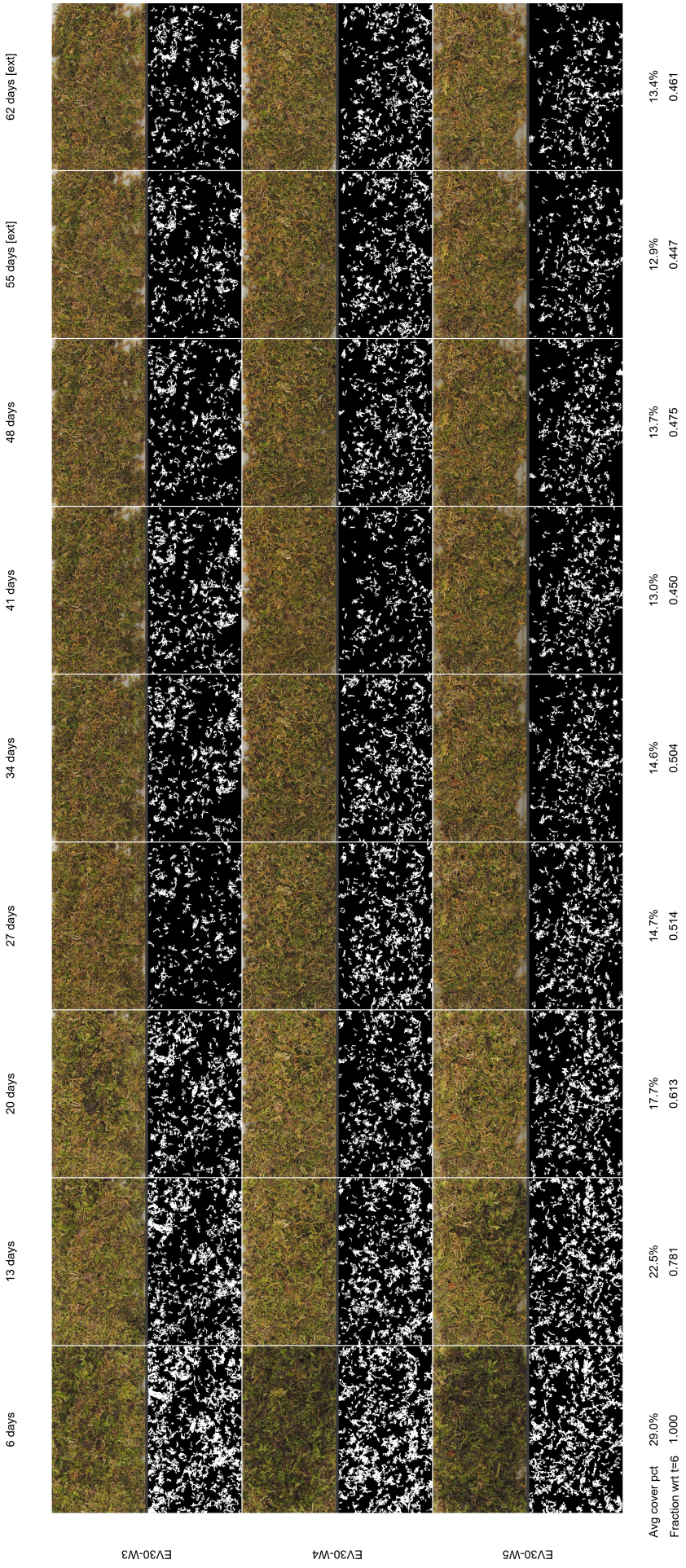


Figure 4.25: EV growth pictures and black-white image of green-indexed pixels by Canopeo

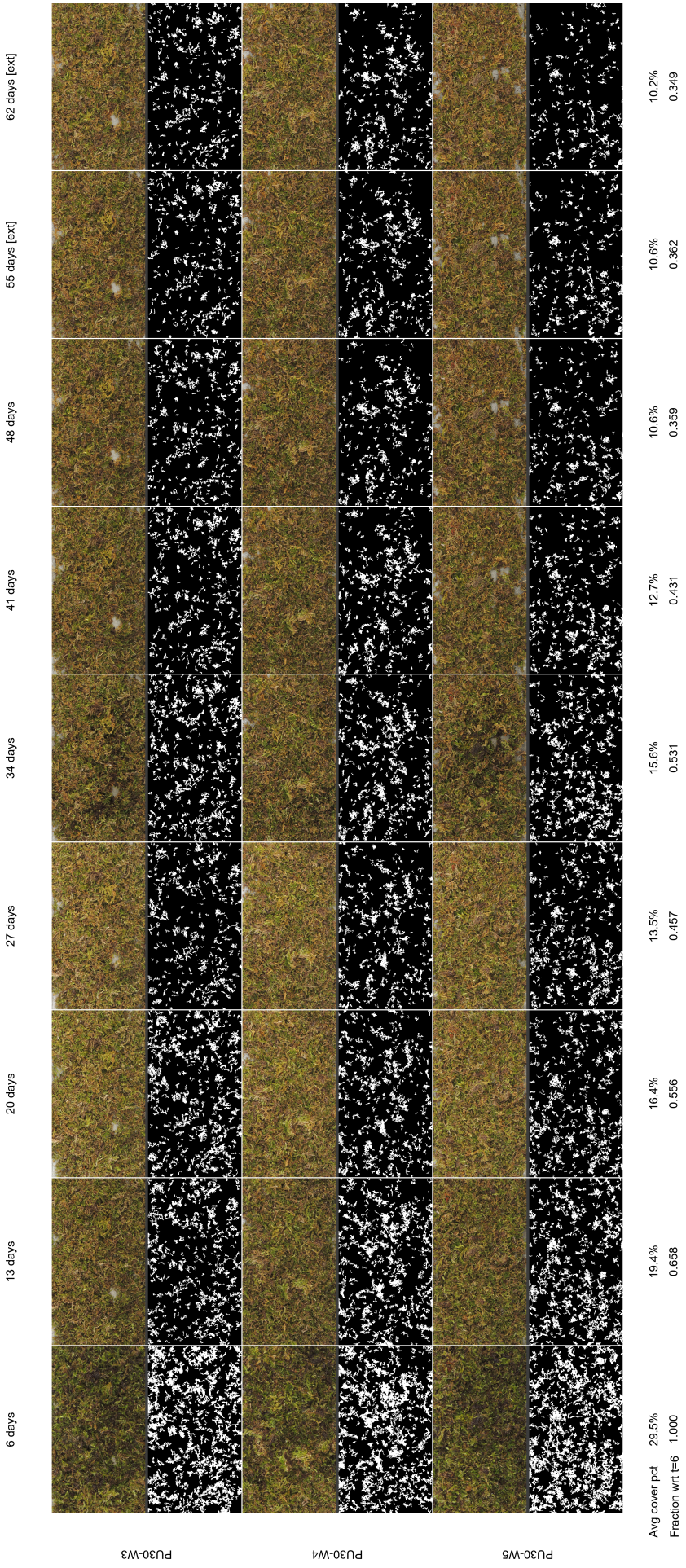


Figure 4.26: PU30 growth pictures and black-white image of green-indexed pixels by Canopeo

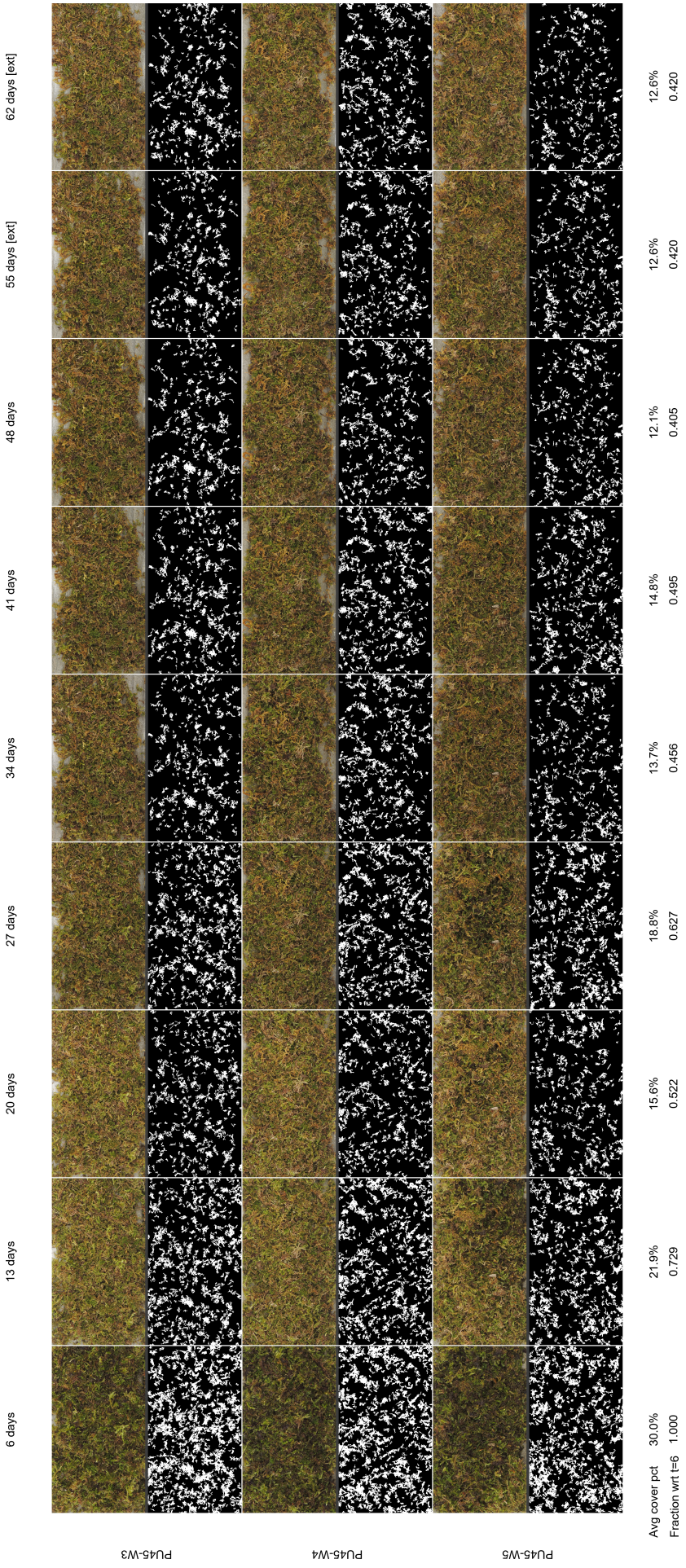


Figure 4.27: PU45 growth pictures and black-white image of green-indexed pixels by Canopeo

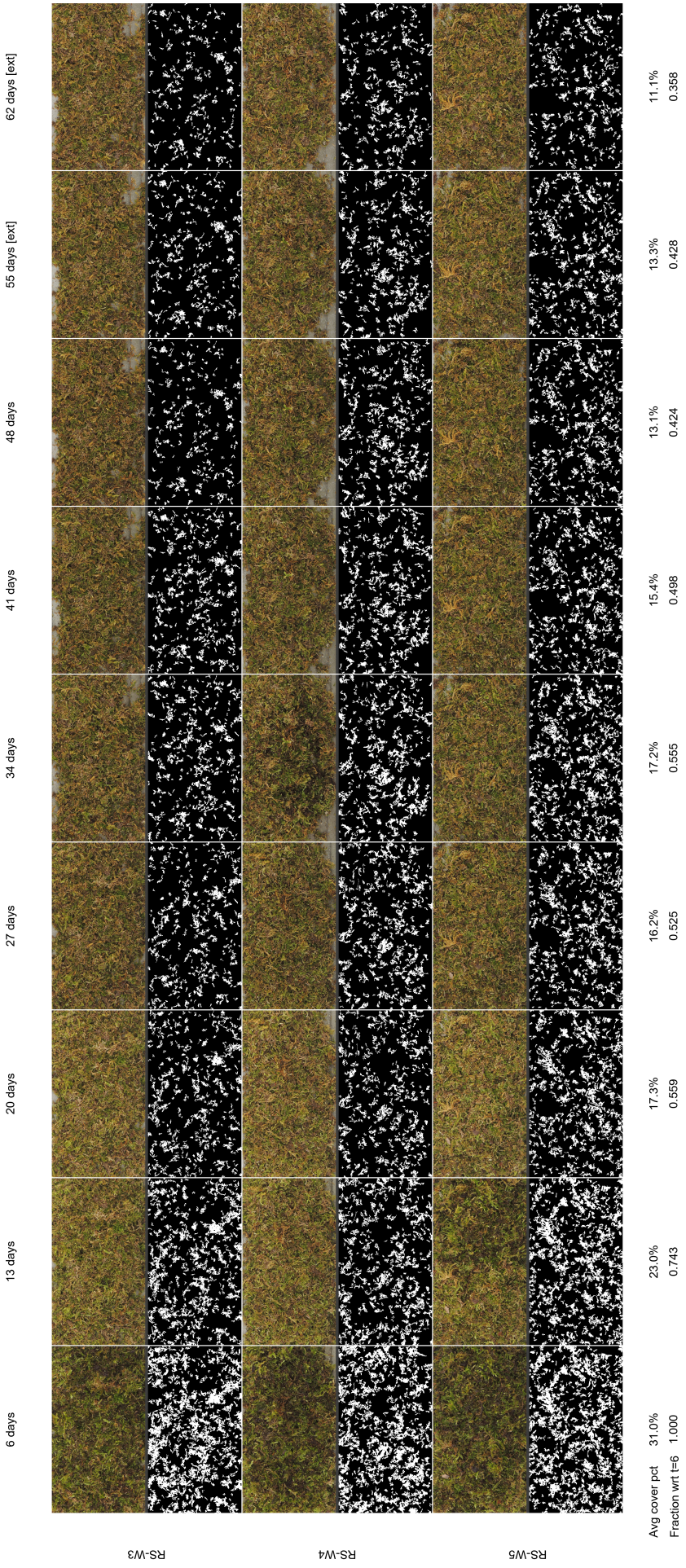


Figure 4.28: RS growth pictures and black-white image of green-indexed pixels by Canopeo

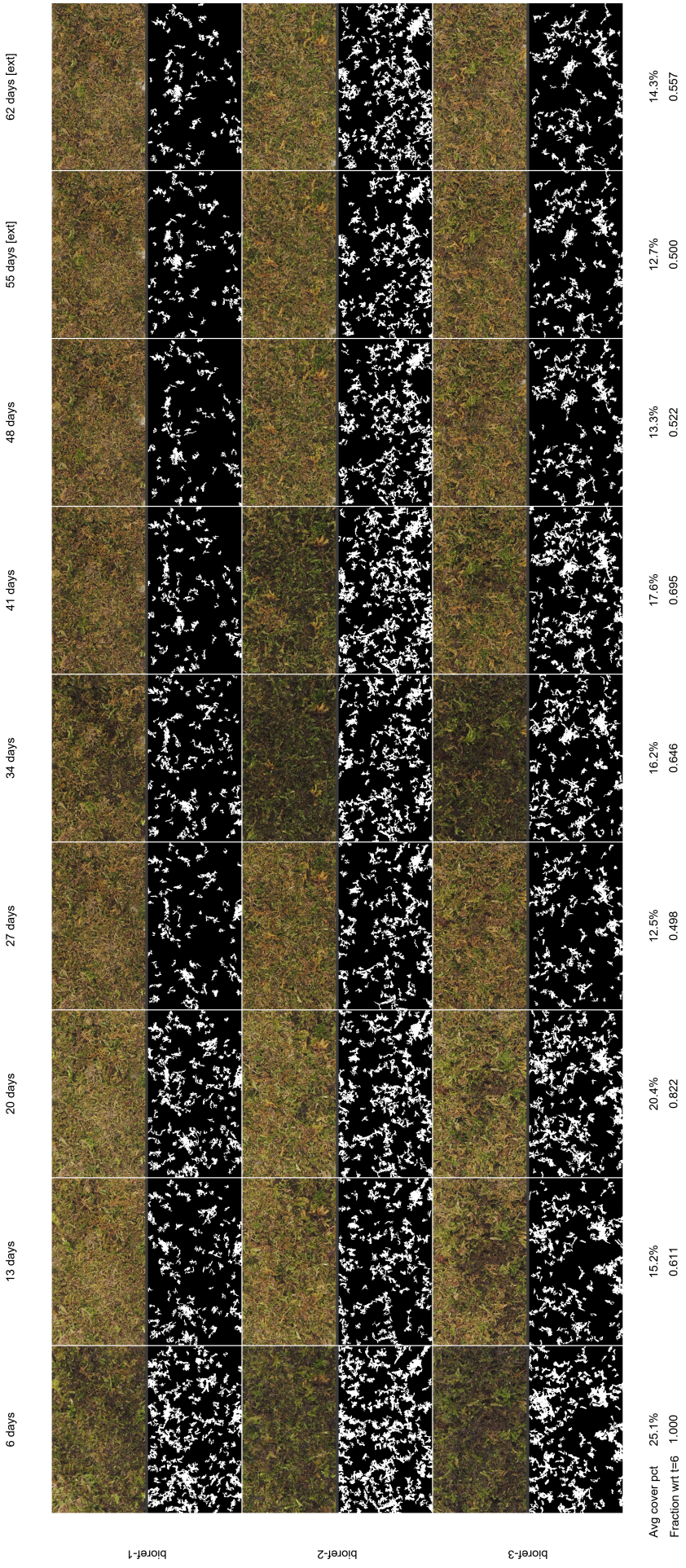


Figure 4.29: Bioref growth pictures and black-white image of green-indexed pixels by Canopeo

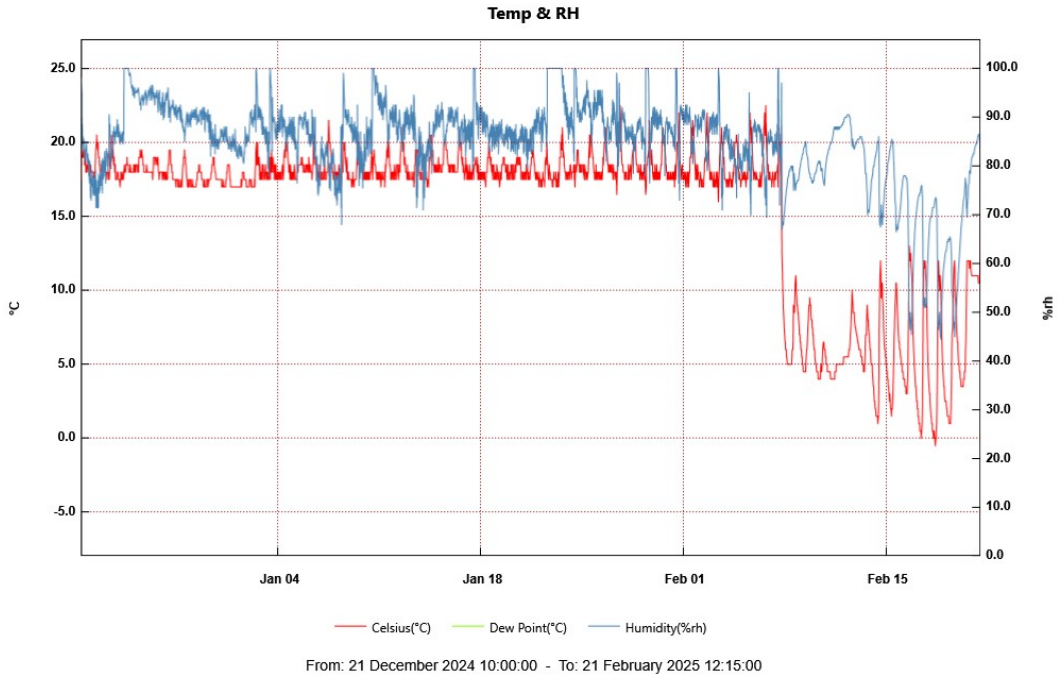


Figure 4.30: Temperature and relative humidity data during the growing experiment. The first 7 weeks represent the environment in the glass house, the last 2 weeks at the second 'exterior' location.

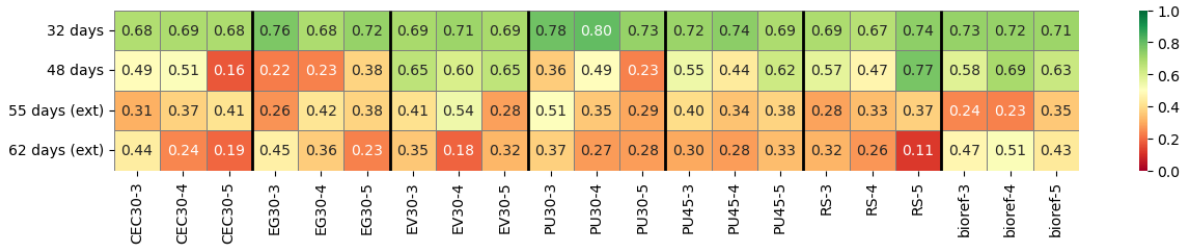


Figure 4.31: PAM-F quantum yield per sample

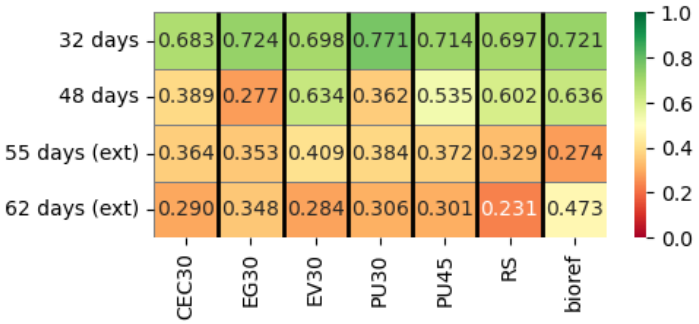


Figure 4.32: PAM-F quantum yield averaged per concrete type

4.5.2. Quantum yield

Complementing the green cover measurements, PAM showed a similar trend in the moss' survival over time. Within every three measurements done at one sample, values of the maximum quantum yield (F_v/F_m) could vary substantially, possible due to the arbitrary coverages of 'healthy' and 'unhealthy' parts. The results of measurements at 32 days and 48 days after planting are shown in figure 4.31 and the averages per concrete type in figure 4.32. At 32 days, the mosses exhibit still a solid quantum yield with average values being around 0.70. Remarkably, the mosses on PU30 samples were found to be in the best condition, higher than PU45 and bioref. However, at 48 days the values came out much lower. On none of the RS samples the moss showed a better condition than before. Often, the PAM-F measuring device displayed a message about a low PAM signal, indicating little chlorophyll amounts to base the values on. Values below 0.1 have been documented, which is not representative for living material. CEC30, EG30 and PU30 samples had the lowest averages, even far below RS. Specifically these three types were grouped at the right side in the glass house, while the samples of the other types were grouped at the left side.

The quantum yield after 1 and 2 weeks at the exterior location did generally not increase anymore. Only for bioref, a higher value was measured at the last stamp. RS showed the lowest plant health at this measurement.

5

Statistical analysis and Discussion

This chapter holds the interpretation and critical review of the results from the growth experiment and the tests regarding bioreceptive markers. Any implied relationships between LWA implementation and 3DPC characteristics are discussed. Some comments on the impact on printability are given. Lastly, a reflection is done by the author on this thesis and its experiments.

5.1 Growth experiment assessment

For both green cover and PAM-F results, an Independent Samples Kruskal-Wallis was employed, of which the results are shown in tables 5.1 and 5.2.

Table 5.1: Green cover Kruskal-Wallis: test statistic and significance per datapoint for 3DPC specimens and bioref

Green cover at	Test-statistic	p-value
t=13	10.926	0.091
t=20	10.199	0.117
t=27	8.398	0.210
t=34	6.303	0.390
t=41	5.991	0.424
t=48	5.818	0.444
t=55 [ext]	7.100	0.312
t=62 [ext]	7.861	0.248

Table 5.2: PAM-F Kruskal-Wallis: test statistic and significance per datapoint for 3DPC specimens and bioref

PAM-F at	Test-statistic	p-value
t=32	10.416	0.108
t=48	13.680	**0.033**
t=55 [ext]	5.524	0.479
t=62 [ext]	8.261	0.220

From the tables it becomes clear that there is no evidence that the green covers are much different from eachother across the different concrete types, as none of the p-values are below 0.05. Regarding PAM-F, at t=48 the p-value is below 0.05, suggesting that there is a difference between the distributions of results. The distribution of this measurement is shown in the boxplot in figure 5.1. When looking at the subsets that were created for this, the ranks of PU45, RS, EV30 and bioref are all clearly higher than the other ones, as can be seen in table 5.3.

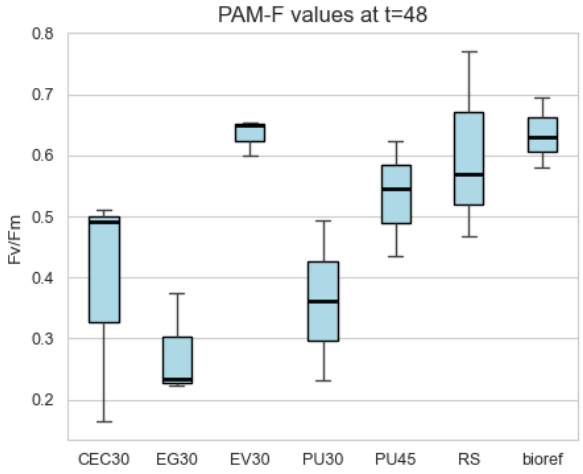


Figure 5.1: Boxplot of Fv/Fm values measured by PAM-F at t=48

Table 5.3: Homogeneous subsets per concrete type for the results of PAM-F measurement at t=48. Subsets are based on asymptotic significances. Each cell shows the sample average rank per concrete type.

	Subset	
Sample	**1**	**2**
EG30	4.000	
PU30	6.000	6.000
CEC30	7.000	7.000
PU45	11.667	11.667
RS	14.000	14.000
bioref	17.000	17.000
EV30		17.333
Test-statistic	10.778	10.216
p-value	0.056	0.069
Adjusted p-value	0.056	0.069

The origin in the higher test statistic can be found in the before mentioned placement of the specimens in the glass house. The four higher ranked concrete types were more or less grouped together on one side, where the other ones were grouped some distance further. This creates the impression that an unequal environmental treatment caused the observed differences. Slightly different convection induced air movement, or a dissimilar amount of daylight could be the cause for this, although assumed the same across all specimens. Some other present plants might have cast a partial shadow over the worse performing specimens. These factors were not measured, so no causes for this can be concluded, except that there is most likely an environmental difference. Thus, it should be noted that for future research the exact placement in the glass house does play a role regarding photosynthetic yield.

Concluding from these Kruskal-Wallis analyses, there is unfortunately not enough variation across the concrete types (even when bioref is included) to state which type of implemented LWA, and moreover LWA implementation in general, has the largest influence on bioreceptivity. The experiment yields not enough usable data to support any hypotheses. In the sections below, possible causes are discussed.

5.1.1. Initial moss quality

The moss showed rates of decease rather than growth, where growth was expected. Multiple causes can be reasoned, one of which is the possibility of moss use with insufficient initial quality. If the moss was already struggling for survival before being harvested, the sudden environmental changes would not have been comforting, eventually leading to decay. While the chances are there, this theory seems unlikely. The mosses were harvested from multiple sub-locations across a parking lot. These included varying exposures to wind and rain, and different (sun-)light intensities, which ensured that the mosses all dwelled in varying starting conditions. Some patches were bright-green, had sporangia and were attached quite well to the concrete substrate, indicating the presence of rhizoids as well. These are implicative factors for a healthy colonization. Before application on the 3DPC samples, the moss pieces were thoroughly mixed, which decreases the chance of similar parts being planted on one sample. These things combined make it seem very unlikely that the initial quality of the moss was the direct reason for the observed decease.

5.1.2. Substrate properties

5.1.2.1. Surface pH

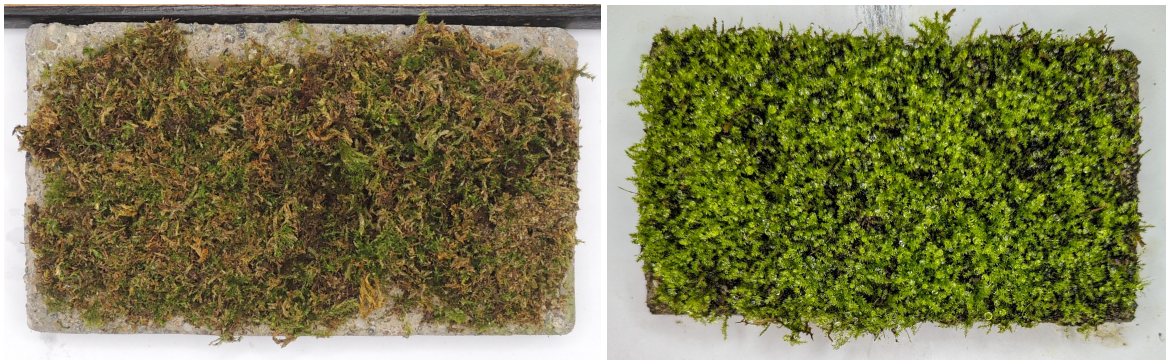
One of the strongest predicting factors for biological growth is the pH of the substrate surface. The pH values graphed in section 4.4.2 underscore the strong alkalinity that concrete can have. Over a period of around 14 weeks, the 3DPC specimens all showed a lower pH value, albeit barely reaching below 12.0. Pointed out before, the pH is strongly linked to the extent at which nutrients can be made available for the moss [17], where a low pH in the acidic region of 3.0 to 5.5 is ideal for most mosses.

In nature, some species of moss have been observed in limestone-rich areas [17], but substrate pH for those chalk-dwelling species almost never exceeds 8.0 [135]. Growth on very carbonated concrete has been reported often, of which the pH can be somewhat below 9.0. In the study from [20], algal growth on concrete with pH > 10 was observed, and from dialogue with that author it became clear that even growth on a surface with pH > 11 was feasible in ideal environment. Stretching the comfortable pH limit for mosses and other biological growth seems possible, but the pH on the surface of the 3DPC specimens could make this extremely difficult.

It is no surprise that the pH of the bioref samples is significantly lower. Some naturally adhered algal biomass was seen, underscoring the pH difference between bioref and 3DPC. The average pH is not determined exactly since only one measurement was done, but the obtained value would implicate a pH in the range of 9.5. This is not yet optimal, but in a controlled setting it should be sufficient enough to observe any strong difference in moss growth compared to the higher-pH 3DPC samples. In an other environment, a concrete sample from the same batch as bioref, covered with newly grown moss, clearly shows the potential of such concrete to act as a suitable habitat (figure 5.2b). This sample comes from unpublished research from the supervisor, and was stored in an optimized growth chamber for moss. The pH of that concrete at the moment of growing was arguably even higher than the pH of bioref, as bioref was comparatively older when used for this thesis and had more time to carbonate. Given this remarkable difference in moss growth performance, it can be stated that the pH is not solely accountable for the moss decay in this thesis. The largest influence likely came from environmental conditions.

5.1.2.2. Chemical effect

The chemical composition of the aggregates (table 4.1) shows that all LWAs contain aluminum, which is a toxin for mosses. But since CEC has the highest fraction of aluminum and particularly this LWA has had promising results in previous studies [20], it stands to reason that the toxic effect of incorporating LWA is negligible.



(a) (b)

Figure 5.2: Two identical cast concrete specimens with moss after 6 weeks of growth, both *Hypnales*-type mosses. Camera settings and lightning conditions differ. (a) A bioref sample from this thesis, stored in a glass house. (b) A sample from research from the supervisor [unpublished], stored in a 'growth chamber'.

Table 5.4: Differences between the glass house and growth chamber regarding environmental conditions and setup.

Condition	Glass house	Growth chamber
Temperature	Ranging between 16 and 22.5°C, with an average of 18.2°C.	20°C
Relative humidity	Ranging from 68 to 100%, averaging 87.8%.	50%
Lighting	During the growing period, not more than 9 hours of light per day. Incoming sunlight is diffused through roof panels. Other vegetation might be partially blocking light from reaching the moss. No (artificial) light at night.	Artificial LED lights emitting at a programmed 12 hour day-night cycle.
Watering	Watered almost every day using a plant sprayer. Humidity in the glass house is controlled with vapor-emitting sprinkler units, located near the ceiling.	Watered by fine water vapor, emitted from sprinkler units right above the samples.

5.1.3. Environmental conditions

The interior circumstances do affect the moss growth. In this thesis, it can already be said that slightly varying locations within the glass house apparently affect the photosynthetic yield of the moss. When comparing the results with the unpublished work of the supervisor, the influence becomes even more evident. The conditions in the glass house were not sufficient for growth, where the ones in the 'growth chamber' are. The most pronounced differences are shown in table 5.4. The composition of the air, concerning concentrations of CO_2, N, etc., was assumed equal for both locations.

Temperature at both locations is very similar. The relative humidity does differ: in the glass house, the air contained more water. However, the most distinct differences are seen for lighting and watering.

Regarding lighting, the light intensity between the locations is arguably different, and the glasshouse moss received light for a shorter duration each day. Mosses use sunlight to drive photosynthesis, which is essential for their energy production and growth [136]. There are some species that can adapt to lower light conditions by making more chlorophyll, but generally reduced light negatively impacts growth and photosynthetic efficiency [136]. This is true up to a certain extent, as it has also been found that continuous light negatively affects photosynthesis in mosses [137]. What the exact light intensities in the glass house and in the growth chamber were is not known. However, the glass house contains many other plant species for which the exposure to light is sufficient to drive photosynthesis and grow.

For that reason, it is presumed that the amount of received light was not the limiting factor for growth either.

Water application was also employed differently in the two setups. In the glass house, the samples were thoroughly watered to compensate for the high rates of evaporation. When taking weekly pictures, the mosses were almost always visibly dry, exceptions aside (such as bioref-3 at t=34). Drenching the mosses in water for extended periods can be disastrous for the moss' survival, as respiration (gas exchange) and photosynthesis are reduced [138]. In the employed experiment for this thesis, extensive amounts of water could presumably have interacted with the concrete surface, effectively flooding the moss with alkalinity. However, no measurements have been carried out to test this.

Besides the possibility of abundant amounts of water acting as an obstruction for basic plant functions, the daily alterations between wet and dry states in this experiment could also have been an important stressor. Although *Hypnales* are bryophytes that are desiccation tolerant, some studies suggest that many cycles of dehydration and rehydration can be impactful on plant functions [35, 36]. It could be argued that desiccation occurred more pronounced and in higher frequency in the glass house than in the growth chamber. Thus, excessive amounts of moisture when watering, too much desiccation between watering moments, or a combination of both did presumably diminish moss growth in the glass house.

The support for this thesis' Theoretical Framework originated from the statement that water availability is the single most-important factor for bio-colonization [22, 29]. The above mentioned issues suggest that simple presence of water is not enough for moss, and the statement should be nuanced to something that includes supply rates or optima.

To conclude, the carried out growth experiment of this thesis did not yield sufficient results in order to assess the bioreceptive effect of LWA implementation in 3DPC samples. Several factors have been considered to be the reason for the observed moss decease, where the environmental conditions and watering regime were presumably the most influential. Comparisons were made between the glass house and a growth chamber. For future research and conduction of similar experiments, the appointed differences should be taken into consideration in order to create a more comfortable habitat that stimulates moss growth.

5.2 Influence on intermediate variables

Now that no link can be made to moss growth, this section will discuss what the effect has been on 3DPC water retention and porosity. In other words, how the input variables have influenced the 'intermediate variables'. In figure 5.3, the variables as derived from the theoretical framework are presented.

It will not be possible to fundamentally link the influence of aggregate incorporation on the porosity and water retention of the respective concrete. This is because of the inadequate sample size for both porosity and water retention of the concrete. Measurements could therefore be prone to outliers. Moreover, statistical models cannot be applied due to the small quantity of samples. However, graphically visualizing the results has some implicative value. These findings can still partly reject or confirm the theoretical framework, and have value for future research.

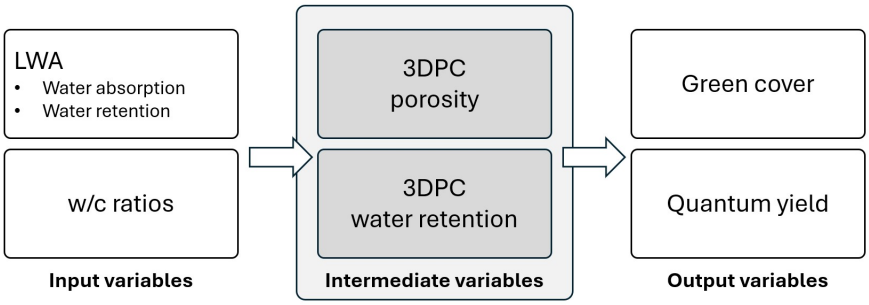


Figure 5.3: System overview derived from the theoretical framework and experiments. The output variables appeared not conclusive, hence the relation of input variables to intermediate ones will now be discussed.

5.2.1. Effect of aggregate water absorption

To start, the total water absorption of LWA is many times higher than that of sand with EV being even several times more absorbing than CEC and PU. Deriving from figures 5.4a, 5.4c and 5.4e, higher 3DPC open porosity, higher 3DPC bulk porosity and lesser 3DPC water retention are implied when the water absorbing capabilities of the aggregate increase. However, the datapoints are widely distributed and no perfect ranking is seen for any variable.

5.2.2. Effect of aggregate water retention

Ideally, the aggregate absorbs large quantities of water and consequently is able to hold on to it for extended periods. Kruskal-Wallis analysis on the LWA water retention data shows that the retained water fraction of absorbed water is significantly different between the types at 4 and 8 hours (table 5.5). At 24 hours, for all the LWA types, almost all the water has evaporated. However, when looking at the water loss per unit of volume LWA, the most significant finding is at 24hrs, where EV has lost by far the most water, as seen in figure 4.4a and table 5.6. Combined, these findings suggest that for a period of 24 hours, EV will lose most water in absolute terms, but also retain a larger part of it compared to the other LWA, meaning that EV as an aggregate has the best properties for water availability.

Table 5.5: Kruskal-Wallis test outcome of LWA water retention (by fractional water loss) at several timestamps

LWA fractional water loss at	Test-statistic	p-value
t = 1hr	6.282	0.099
t = 2hrs	7.667	0.053
t = 4hrs	9.462	**0.024**
t = 8hrs	8.538	**0.036**
t = 24hrs	7.205	0.066

Table 5.6: Kruskal-Wallis test outcome of LWA water retention (by volume-wise water loss) at several timestamps

Water loss per mL LWA at	Test-statistic	p-value
t = 1hr	2.744	0.433
t = 2hrs	0.744	0.863
t = 4hrs	0.333	0.954
t = 8hrs	4.641	0.200
t = 24hrs	10.385	**0.016**

Deriving from figures 5.4b, 5.4d and 5.4f, an increased 3DPC open porosity, increased 3DPC bulk porosity, and lesser 3DPC water retention capacities are implied with a decreasing water retention value (increasing water loss) of the LWA. However, the datapoints are widely distributed and no perfect ranking is seen for any variable.

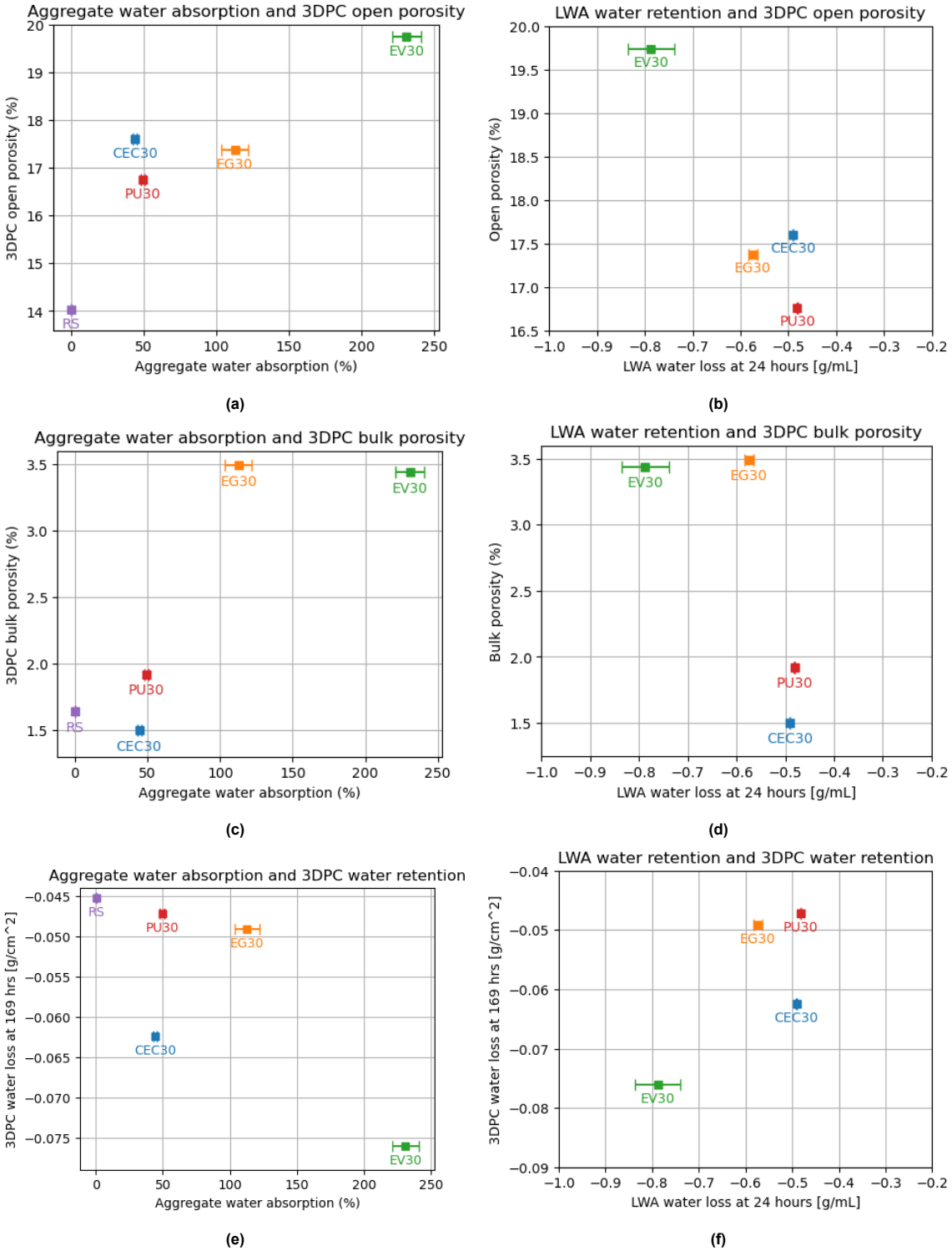


Figure 5.4: (a, c, e): water absorptions of LWA and sand compared to 3DPC properties. PU45 contains more LWA and is not depicted. **(b, d, f):** LWA water loss at 24 hours compared to 3DPC properties. PU45 contains more LWA and is not depicted. Water retention of sand was not measured.

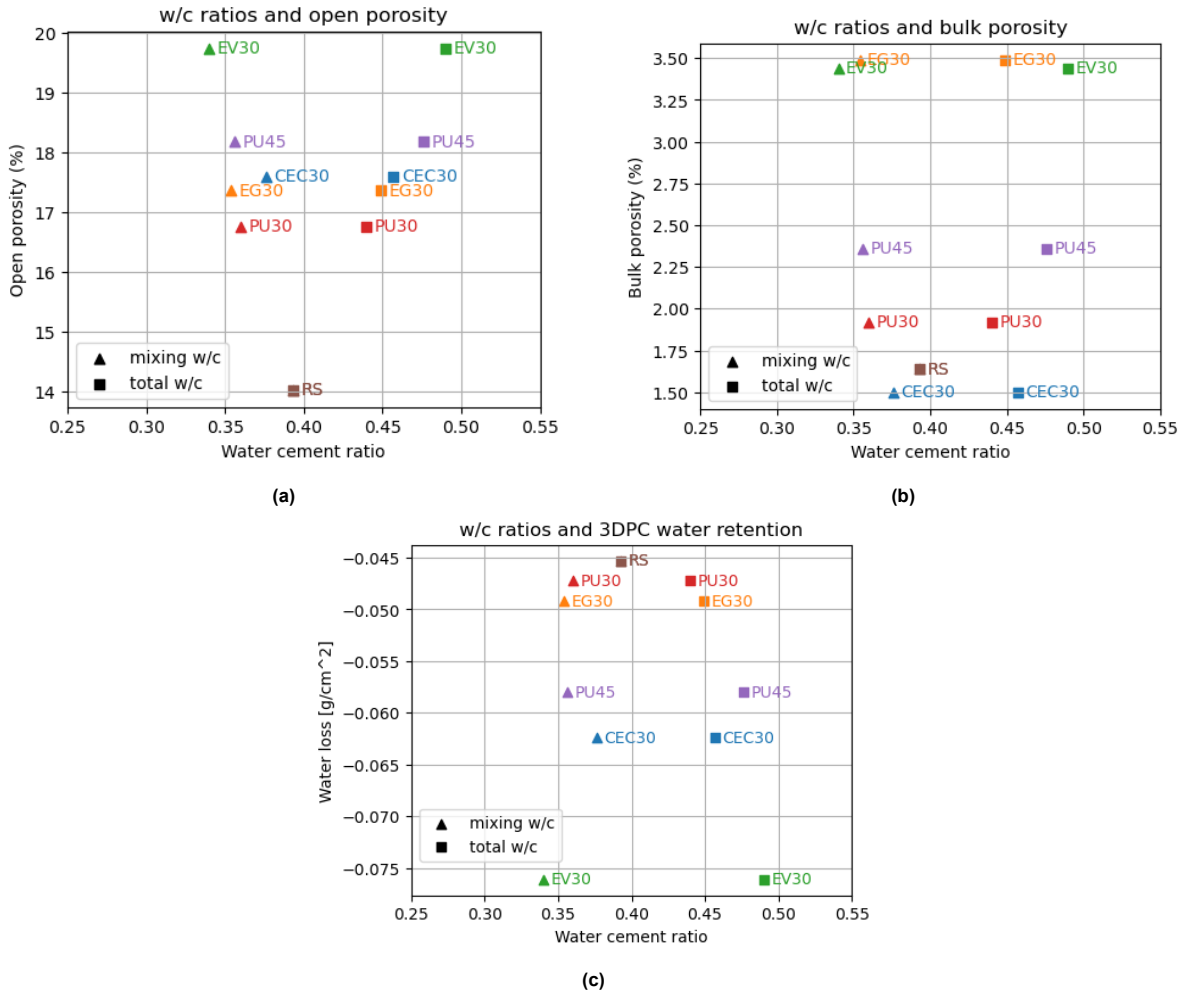


Figure 5.5: Mixing and total w/c ratios compared to open porosity (WAM), bulk porosity (CT) and water retention. The mixing and total w/c ratio for RS is equal.

5.2.3. Effect of water cement ratios

Deriving from figures 5.5a, 5.5b and 5.5c, an increased 3DPC open porosity, increased 3DPC bulk porosity, and lesser water retention (more water loss) is implied with a decreasing Mixing w/c ratio. The figures imply the contrary for a decreasing total w/c ratio, where also the absorbed water in the LWAs has been taken into calculation. However, the datapoints are widely distributed and no perfect ranking is seen for any variable, except for the relationship between total w/c ratio and open porosity. This could be coincidental, especially since only one measurement was done. Nonetheless, reasonably more water in the system results in a higher (capillary) porosity, although this is usually caused by the mixing water. A decreased mixing w/c ratio that implies higher open porosity could suggests some things. Either that the inherent porosity of the aggregates governs compared to the decreased capillary porosity, or that some water from the aggregates had seeped into the concrete matrix and therefore increased the capillary content. The latter is supported by [139], as they state that an equilibrium should exist between the Laplacian water pressures in the lightweight aggregates and the surrounding cement matrix. The theoretical model that [139] presents could be greatly helpful in future research, where the mixing water cement ratio can be kept more equal among batches, making comparisons more convenient.

5.2.4. Outlier: Expanded Vermiculite

Based on the results and the variable comparisons, it becomes clear that Expanded Vermiculite constantly forms (one of) the most outlying value. The absorptivity is undoubtedly the highest across all the

LWA types in this thesis, which is presumably an important explanation for the relatively high porosity and lesser water retention in 3DPC. Hereby it should be noted that the curing regime for the EV30 specimens was different from the other batches. After printing, the samples cured on the printbed for three days instead of one, before transfer to the curing room. Although the samples were carefully covered with foil to prevent loss of moisture, chances are that it had still affected the hydration and drying, leaving behind a more porous matrix compared to other batches [140]. The improper curing conditions could also have exaggerated shrinkage cracks, which effectively increases open porosity as well [73].

5.2.5. Effects of higher LWA content

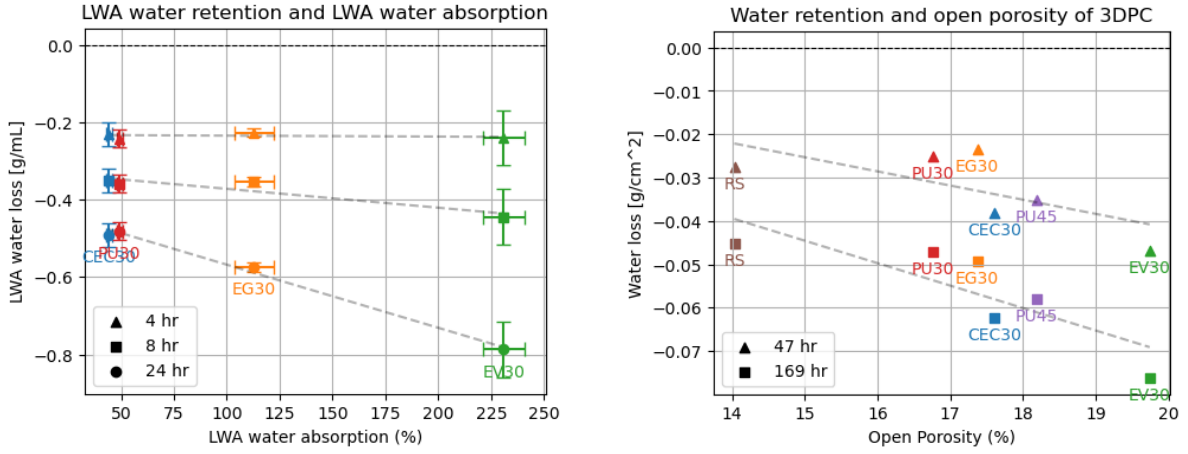
The porosity and water retention of PU30 and PU45 imply that a higher LWA content leads to an increased porosity, absorption and higher water release rate. This finding seems reasonable: implementing more of a certain aggregate will amplify its effects. Regarding strength (also discussed in section 5.3.3), it was found that PU45 had slightly lower mechanical performance compared to PU30. This is more or less in line with the findings from [83].

5.2.6. Reflection on Theoretical Framework

It was found that the used lightweight aggregates have a tremendously larger porosity and water absorption compared to sand. The incorporation of the lightweight aggregates was therefore expected to increase 3DPC porosity and water absorption as well. This was measured with the WAM method, plotted against the aggregate's absorption in figure 5.4a. A positive relationship is implied, but not confirmed due to the sample size.

The next assumption concerned an increased water retention with increasing porosity. Looking at figure 5.6a, the water retention for purely aggregates is mostly determined by how much it has absorbed, showing an inverse relationship. Based on [141, 142], a similar water release behaviour suggests similar internal pore structure. This is somewhat in line with the MIP results, as all LWA showed a peak at around the same pore size.

The relation between open porosity and water retention in 3DPC is less aligned, as seen in figure 5.6b. This graph implies that generally a larger open pore space leads to higher amounts of water loss over time. However, especially in concrete this relation appears to be more nuanced.



(a) (b)

Figure 5.6: (a): The LWA water absorption and it water release rate seem linearly connected. (b): Relation between 3DPC open porosity and water loss implies no linear alignment.

5.2.6.1. Pore specifics

Not just the implementation of porous and water absorbing compound, but more concrete characteristics can describe the water absorption and release rates. The pore size distribution is important.

Very small pores can retain water better due to capillary forces, but larger pores can serve as reservoirs. When not connected to many other pores, these larger pores can cause much water to be retained. The interconnectivity between pores does facilitate water movement, potentially leading to quicker drainage when the pore connectivity increases [143]. Lastly, the relative humidity plays a role in water release per pore size through the Kelvin equation, where larger pores tend to dry at higher RH, while the smaller ones remain saturated [144]. However, this holds for pores up to 100 nm. Pores larger than this size will drain regardless. Given that 3DPC contains relatively many larger pores due to the lack of compaction and the entrapments between layers, this might have contributed to part of the water absorption and consequent loss. Shortly, the total pore content is not fully responsible for the rate of water release. This depends on other pore structure specifics as well.

Concluding, the Theoretical Framework adopted for this thesis can be called partly plausible. It was implied that porosity increases with LWA addition. However, the higher porosity could not retain water better, as more or less the contrary was found. In order to retain more water, more attention should be given to the pore microstructure.

5.3 Influence on other factors

Although having no spot in the adopted Theoretical Framework, surface roughness and surface pH were measured as they are reportedly strong indicators for bioreceptivity. These findings are discussed based on value and impact. Flexural and compressive strength tests were also employed for practical feasibility of the 3DPC. The extent to which the input parameters have affected the mechanical performance is also evaluated.

5.3.1. Surface roughness

No specific treatment was applied in this thesis to change the structure of the surface. Regarding waviness and macro roughness, it was to be expected that no significant difference was found between the 6 concrete types, as seen in table 5.7. For the micro roughness, however, there is some significant difference between the concrete types. Whether such small scale differences will affect moss growth could be addressed in future research.

Sadly, due to the inadequate growth experiment it is also not known whether the waviness and macro roughness were sufficient for rhizoids to clamp and the moss to attach.

Table 5.7: Kruskal-Wallis test on surface roughness results, divided by scale.

Roughness scale	Test-statistic	p-value
Waviness	6.731	0.241
Macro roughness	3.173	0.673
Micro roughness	18.368	**0.003**

5.3.2. Surface pH

The 3DPC samples had a highly alkaline surface pH. Possibly, this was even too high for moss to thrive, even in an ideal setting. From the current experimental setup, it cannot be assessed whether growth on these surfaces was possible. However, literature recommends pH values of at most $\sim$10 [27], where the 3DPC stuck around 12. Fortunately, previous studies point out that carbonation in 3DPC occurs at a faster pace than in MC, and therefore the pH becomes lower more quickly [108].

Nonetheless, it is still worth exploring alkalinity mitigating treatments for 3DPC, which will lower the initial pH value, thus being more suitable as a convenient moss habitat.

5.3.3. Mechanical performance

A stepwise step-down Kruskal-Wallis statistic gives insight in the division of strength results. Displayed in table 5.8, there is for both flexural and compressive strength a significant difference visible between the groups, where the subsets indicate that EV30 outcomes are the least comparable to those of other types. Contrarily, CEC30, PU30, PU45 and RS are found to have statistically similar mechanical performance, despite incorporating weaker aggregates, and thereby introducing more water into the system. This suggests that there are other variables governing in the mechanical context.

Table 5.8: Kruskal-Wallis test on flexural and compressive strength, and derived subsets with corresponding concrete types. Within a subset, the types are ordered by rank

			Subset		
	Test-statistic	**p-value**	**1**	**2**	**3**
Flexural	14.570	**0.012**	EV30	EG30, RS, PU45, CEC30, PU30	-
Compressive	29.621	**<0.001**	EV30	EG30	PU45, PU30, RS, CEC30

Deriving from figures 5.7a to 5.7f, there is no clear indication why some of the concrete types exert similar mechanical response as RS. Found by [111], strength should decrease with LWA are applied,

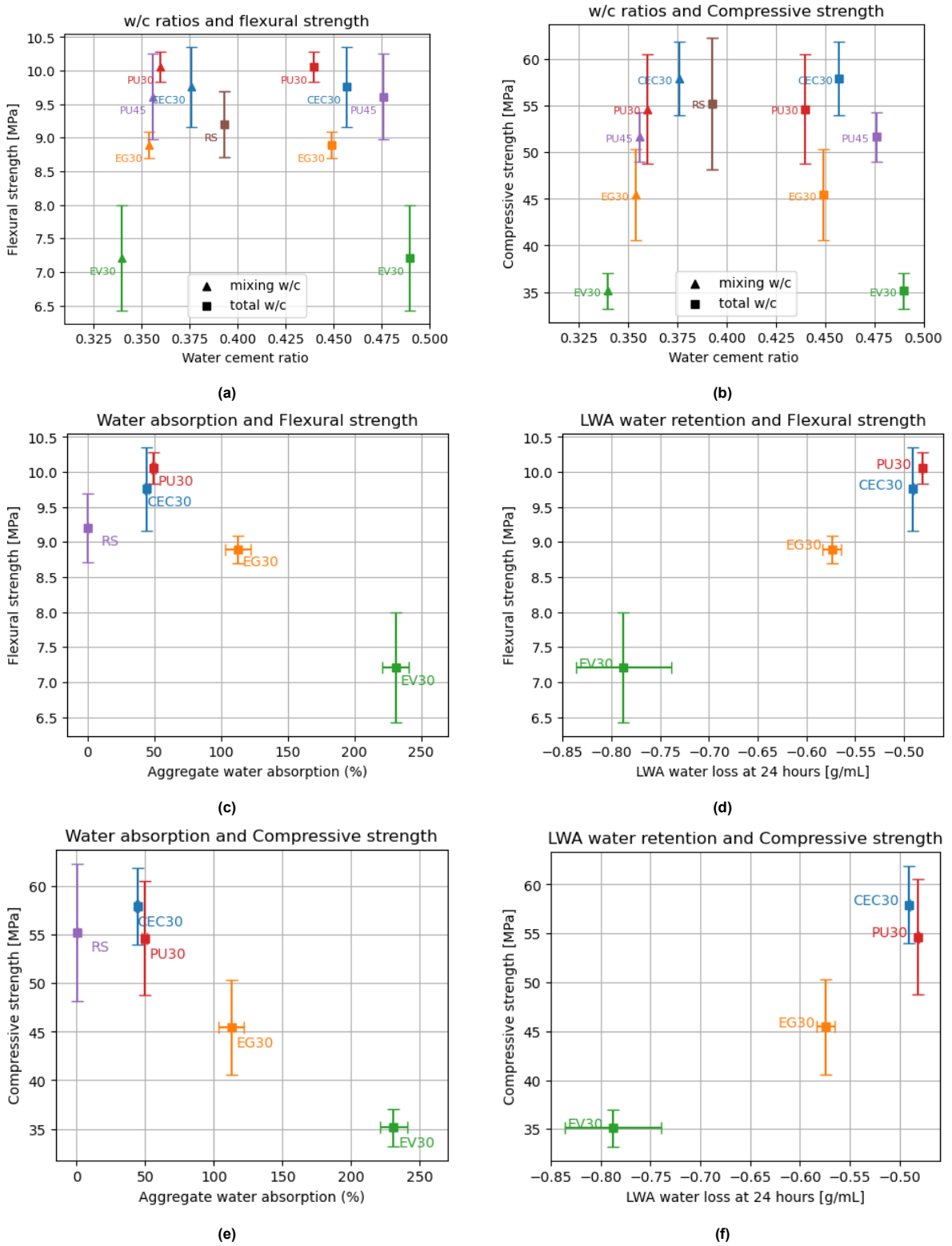


Figure 5.7: (a, b): Mixing w/c and total w/c compared to flexural and compressive strength. For RS, both values are the same. **(c, e):** LWA and sand water absorption compared to the flexural and compressive strength. PU45 contains more LWA and is not depicted. **(d, f):** LWA water retention compared to concrete flexural compressive strength. PU45 contains more LWA and is not depicted. Water retention of sand was not measured.

but these results imply a no reduction. Also, lower mixing water cement ratios are expected to increase strength [101], but such relation is not observed here for the group containing CEC30, PU30, PU45 and RS. This suggests that the amount of applied CEC and PU does not create a reduction in mechanical performance, given the treatments from the experiments in this thesis (print settings, curing conditions, etc.). Also, any occurrence of pozzolanic response from pumice or expanded clay cannot be ruled out [145].

When taking also EG30 and EV30 into account, a reduction in mechanical performance with increasing aggregate porosity is implied (figures 5.7c and 5.7e, which is in line with studies such as [44], stating that porosity of concrete is inversely correlated with the strength. Interestingly, the graphs also imply a lower mechanical performance when the water retention of the aggregates is reduced. This could again be linked to the water pressure equilibrium from [139]. Water bled out of the aggregates into the cement matrix, increasing the water content and consequently decreasing the strength [101]. This is still hypothetical, and it should be mentioned that the LWA water loss was measured for much different conditions than those inside the fresh or hardened cement matrix, questioning the applicability.Moreover, as stated before, the different curing regime of EV30 has likely also contributed to the lower mechanical properties.

When comparing the mechanical performance to other studies, the values from this thesis exceed most values reported by reference studies by a broad margin. Studies with almost similar conditions were not found, but 28 day compressive strength of fiber reinforced 3DPC found by [146] ranged from 22 - 25 MPa, and flexural near 6 MPa. The same loading conditions were used, but the cement fraction in the mix was lower than in this thesis. A similar result for compressive strength was obtained by [147], and a control mold-cast specimen reached 66 MPa, which is slightly higher than specimens from this thesis. Lastly, calcined clay based 3DPC samples from [97] with the same specimen size and loading direction reached around 50 MPa.

The flexural and compressive strengths of EV30 are the lowest of all sets, 7.2 MPa and 35.1 MPa respectively. One other study reported compressive strength on 7.5 wt% EV at 7 days was 4.88 MPa [120]. The tested cube with dimensions 100x100x100 mm was made of a cast block with the 3DPC concrete mix. The results are therefore not entirely comparable, but EV30 in this thesis shows relatively high strength even respective to beforementioned values.

5.4 Quality of printing

Adding saturated LWA to fresh concrete was found to significantly increase the slump flow and decrease shape retention. Presumably, water seeped out of the LWA particles because of a water pressure difference [139]. For future research it is recommended that the LWA is not added fully saturated. For this thesis, the workability issues were evaded through redeveloping the mixtures with a lower water content.

Regarding extrudability and open time no serious issues were encountered. The rheological nature of the mixtures allowed for a consistent flow of the concrete within the allowable electrical range of the pump.

The fresh concrete characteristics combined with aligned print parameters resulted in decent final specimens: the extrusion was continuous and no filament tearing or pressure induced segregation was observed. However, generally the LWA incorporated samples had slightly more deformation than RS. This suggests that the buildability can still be improved. Some effective solutions for this listed by [148] involve a print design with longer interlayer time gap, or the fine tuning of VMA addition.

The printability issues encountered with LWA incorporation in this thesis proved to be surmountable, as well as any further refinement issues. Using Pumice, expanded glass, expanded vermiculite and crushed expanded clay in 3DPC as replacement for sand is feasible, which aligns with the findings of [83, 120, 149].

5.5 Reflection on experiments

Given the formulated problem and corresponding research question, setting up a strategy is not the simplest task. The research fields of mosses, bioreceptivity on concrete, and concrete 3D printing had to be investigated sufficiently in order to pave an outline. Many facets of the undertaken actions in this thesis were not or limitedly documented before. Standards for the measuring of all bioreceptivity factors and growth monitoring are non-existent. Moreover, the quality of 3DPC structures is influenced in a complex way by many parameters, ranging from mixture ingredients, to print parameters, to curing conditions etc. Similarly, all the factors that could, to a certain extent, regulate the moss growth on concrete are abundant and incredibly interwoven as well. Many things rely on many other things. To come up with a strategy that addresses the major players while not diminishing others was the challenge. At the same time, long duration experiments such as moss growing should be fitted into a short timeframe, while ensuring sufficient data from those experiments is obtained. Many aspects of this thesis where therefore driven by fast pace actions.

5.5.1. Porosity approach

Although the porosity increase approach is arguably a fair method, the value from the experiments in this thesis would have been greater when mossgrowth instead of decease was observed. However, even if growth was visible on the specimens, drawing conclusions from the adopted experimental setup is not that straightforward. Growing regime and environment were controlled, so it can be argued that water availability was barely an issue for the mosses as they were watered almost every day. The water availability from the concrete specimens did not get a chance to make difference in the moss growth or decease rate. To get an actual fair result, the samples would have to be exposed for significant duration in an uncontrolled exterior setting. It is expected that only then the materialistic differences could be fully revealed.

5.5.2. Statistical significance

Limited time or resources have often been the reason to decide for a singular execution of certain experiments. Any measurement oversights or errors are therefore not always averaged out. In many experiments the statistical significance is questionable. Experiments such as slump flow and Vicat were carried out only once for a mixture, as those tests served in the goal for finding mixture characteristics similar to the control. Especially the WAM and water retention experiments would have been more valuable when performed in at least triplicate.

5.5.3. CT scanning

Porosity percentages that were obtained through CT scanning did not quite comply with outcomes of the WAM method. Several issues regarding this variance are addressed:

- The resolution of the CT scan did not allow for a sufficient estimation of the true porosity. Even the EG30 core that was scanned with higher resolution did not yield that much pore space. The equivalent smallest pore diameter was around 30 µm, which still largely exceeds the upper capillary pore limit defined by [45] of 10 µm. Capillary pores can therefore not be identified in the CT data. Since these pores can substantially impact the water absorption, it is a possible explanation for the variety in porosities from both methods
- Still, the segmentation of CT data remains a challenge too. Pore rich parts can still be identified as solid material when the pores are too small, and hence not be taken into calculation. More advanced segmentation, for example with picking lower density LWA particles as a separate intensity domain could improve overall porosity estimation. Also, for this particular set of scans, it is likely that water was still occupying some of the pore volume in either the matrix or the LWAs as the cores were not oven dried prior to the experiment. Doing this will likely empty most of the pore spaces and make division of pores to solid material less complicated.
- The water absorption method assesses the open pore spaces connected to the outside, while the

CT scanned cores are drilled from the inner part of the 3DPC. Fewer open spaces may be present in the mid section compared to the outer region. A water absorption test for porosity estimation of the cores should grant comprehensive information on this observation, but that was not part of this thesis.

6

Conclusions and recommendations

6.1 Conclusive statements

In this thesis, a 3DPC mix design was altered by adding lightweight aggregates (crushed expanded clay, expanded glass, expanded vermiculite and pumice), with the aim of increasing the receptivity to moss growth. Multiple specimens were 3D printed and a moss growth experiment was done to evaluate the quality of the substrate for moss to live on. This thesis was set up to answer the following research question:

How can 3D printable concrete mix design be altered to promote bioreceptivity, and how does that affect fresh and hardened 3D printed concrete properties?

After completion of this thesis, some conclusive remarks can made based on literature and the findings of the performed experiments.

The effectiveness of the measures to enhance bioreceptivity was evaluated by monitoring the green cover and the maximum quantum yield of moss on the samples. Over the course of 7 weeks interior and 2 weeks exterior, all samples showed moss decease. It is speculated that the prolonged exposure to abiotic stressors such as environmental conditions and watering regime became fatal, despite the moss species being relatively adaptive and desiccation tolerant. No conclusion about the effect of LWA input could therefore be drawn from this experiment.

The most important properties of concrete to evaluate whether biological growth can take place are (open) porosity and water retention, surface roughness and surface pH. The used LWA were tremendously more porous than the reference sand. Although having a small sample size, 30% and 45% replacement of the sand with LWA did imply an increase in open porosity of 3DPC samples compared to the reference. The highest porosity was observed for EV30, although the curing regime of EV samples is expected to have also played a role in this. Furthermore, the sample with 45% pumice showed higher porosity than the sample with 30%, which is an expected outcome. CT scan data of the bulk regions did point out the highest porosities for EV30 and EG30 samples, of which the LWAs are the most porous and water absorbent. However, the ranking for other samples was not conform the open porosity values which is likely due to CT scanning not being the optimal technique for this.

The consequent water retention capacities of the LWA did decrease with increasing open porosity. Aggregates that absorbed more water did show the highest release rates. When applied in 3DPC, more or less the same relationship was implied, albeit again based on a small sample size. Moreover, the dissimilar water cement ratios did presumably affect the porosity and pore size distribution of the 3DPC, leading to varying retention. The pore sizes in the LWA were addressed with MIP, and showed a relatively high quantity in the range of 100-300 µm, which are pore sizes related to fast drying. In order to create highly water retaining 3DPC, the microstructure of the concrete matrix is governing over the absorbing capacity of the aggregates.

For porosity and water retention, EV showed to be the most outlying, both as loose aggregate and included in 3DPC. Besides this aggregate being the most absorbent, the dissimilar curing regime presumably played a role in the observed behaviour.

The inclusion of any LWA did not seem to significantly influence surface roughness or surface pH. The pH value was found to decrease over a 10 week period to around 12, which still exceeds any viable range reported in literature. It is therefore questionable whether growth would have taken place in better environmental conditions.

In the fresh state, inclusion of saturated aggregates did cause the fresh mix to be highly more flowable and less shape retaining, for which had to be compensated by decreasing the added water amount. Still, some more deformation was observed on the final samples compared to the control, for which the most probable explanation is the higher total water content. Regarding hardened mechanical performance, all samples except for EV30 showed a relatively high compressive (45 MPa - 58 MPa) and flexural strength (8.9 MPa - 10.1 MPa), where EV30 averaged 35.1 MPa and 7.2 MPa respectively.

To answer the research question, replacement of sand with various types of lightweight aggregate can be used to alter characteristics of 3D printed concrete that are associated with bioreceptivity. Primarily in terms of open porosity, water absorption and water retention, the effect of LWA incorporation is clearly visible. To what extent this has an effect on the bioreceptivity could not be addressed in this thesis. The addition of saturated LWA in the fresh mix substantially increases flowability and decreases shape retention, for which had to be compensated by reducing the water content. Hardened mechanical performance appear to be reliant on aggregate type and replacement percentage, although most samples showed similar strength to the reference.

6.2 Recommendations

From this thesis some issues arose that can be addressed in future research. Moreover, the small knowledge base on this topic allows for a wide range of variables that can still be investigated. The most urgent topics for future research are listed below:

- This thesis shows that environmental conditions and watering regime are crucial for the growth and survival of moss. There is need for a better understanding on influential factors on moss growth, as to reduce the risk of decease in alike experimental setups.
- Since the samples sizes for porosity and water retention measurements in this thesis are small, it is recommended that similar tests are employed with a larger sample size, and if possible with varying specimen dimensions. This can confirm or reject the implied relationships found in this thesis.
- LWA incorporation improved porosity but did not enhance retention per se. Methods to mitigate the water release rate should therefore be explored, for example by the use of SAPs. It is recommended to look into the pore microstructure as well, and evaluate the pore size distribution with tests like MIP.

Furthermore, some other issues arose that might be interesting to investigate.

- Exploration of pH mitigators that reduce pH in primary state of 3DPC. Addition of SCMs or agents can be researched, as well as lowering the binder content or adopting a completely different binder with lower initial pH levels. The incorporation of waste sludges can be considered as well, as these were found to decrease pH. Else, carbonation in order to evade the alkaline barricade can be considered as well, especially since 3DPC is relatively carbonation prone.
- Incorporating a higher content of lightweight aggregates (up to 100% replacement) and investigate what it effects are on printability, water retention and strength. This might be the most interesting for CEC and PU, since a 30% and even 45% replacement of sand did not deviate from RS regarding mechanical properties. The theoretical model from [139] could be useful to find proper saturation levels for LWA.
- Micro roughness was found to be quite dissimilar across concrete types. It could be interesting to investigate the effects of this on bioreceptivity. Additionally, interlayer bond strength could be investigated as this is partially dependent on interfacial roughness.

Lastly, a tip for similar future research: Use a pH pen or some alike device to assess surface pH, that can be placed on the concrete surface and gives a pH value directly. It might not be entirely accurate but is very fast and one can take multiple measurements per sample. Grinding off surface material is slow and has a high risk of involving bulk pieces that influence the pH measurement

References

[1] UnitedNations. *World Urbanization Prospects: The 2018 Revision*. Report. 2019. URL: https://www.un.org/development/desa/pd/content/world-urbanization-prospects-2018-revision.

[2] Colin R. Gagg. “Cement and concrete as an engineering material: An historic appraisal and case study analysis”. In: *Engineering Failure Analysis* 40 (2014), pp. 114–140. ISSN: 1350-6307. DOI: https://doi.org/10.1016/j.engfailanal.2014.02.004. URL: https://www.sciencedirect.com/science/article/pii/S1350630714000387.

[3] Daniel B. Botkin and Charles E. Beveridge. “The Ecological Importance of Urban Vegetation”. In: (1992). URL: https://www.waterboards.ca.gov/waterrights/water_issues/programs/bay_delta/wq_control_plans/1995wqcp/admin_records/part05/405.pdf.

[4] Xiaohui Zhao et al. “Future projection of extreme precipitation using a pseudo-global warming method: A case study of the 2013 Alberta flooding event”. In: *Weather and Climate Extremes* 46 (2024). ISSN: 22120947. DOI: 10.1016/j.wace.2024.100721.

[5] Nitin Muttil, Tasnim Nasrin, and Ashok K. Sharma. *Impacts of Extreme Rainfalls on Sewer Overflows and WSUD-Based Mitigation Strategies: A Review*. Electronic Article. 2023. DOI: 10.3390/w15030429.

[6] V. Oquendo-Di Cosola, F. Olivieri, and L. Ruiz-García. “A systematic review of the impact of green walls on urban comfort: temperature reduction and noise attenuation”. In: *Renewable and Sustainable Energy Reviews* 162 (2022). ISSN: 13640321. DOI: 10.1016/j.rser.2022.112463.

[7] S. M. Sheweka and N. M. Mohamed. “Green Facades as a New Sustainable Approach Towards Climate Change”. In: *Energy Procedia* 18 (2012), pp. 507–520. ISSN: 18766102. DOI: 10.1016/j.egypro.2012.05.062.

[8] Samar Sheweka and Arch Nourhan Magdy. “The Living walls as an Approach for a Healthy Urban Environment”. In: *Energy Procedia* 6 (2011), pp. 592–599. ISSN: 1876-6102. DOI: https://doi.org/10.1016/j.egypro.2011.05.068. URL: https://www.sciencedirect.com/science/article/pii/S1876610211014792.

[9] Julià Coma et al. “Vertical greenery systems for energy savings in buildings: A comparative study between green walls and green facades”. In: *Building and Environment* 111 (2017), pp. 228–237. ISSN: 03601323. DOI: 10.1016/j.buildenv.2016.11.014.

[10] Rewaa Mahrous et al. “Review of key factors that affect the implementation of bio-receptive façades in a hot arid climate: Case study north Egypt”. In: *Building and Environment* 214 (2022). ISSN: 03601323. DOI: 10.1016/j.buildenv.2022.108920.

[11] Daniel R. Richards et al. “Global variation in contributions to human well-being from urban vegetation ecosystem services”. In: *One Earth* 5.5 (2022), pp. 522–533. ISSN: 2590-3322. DOI: https://doi.org/10.1016/j.oneear.2022.04.006. URL: https://www.sciencedirect.com/science/article/pii/S259033222200207X.

[12] Ralf-Uwe Syrbe and Jiang Chang. “Options and Challenges for Implementing Green Spaces in Urban Development”. In: 2018, pp. 105–173. ISBN: 978-3-319-58222-1. DOI: 10.1007/978-3-319-58223-8_4.

[13] Christine Haaland and Cecil Konijnendijk van den Bosch. “Challenges and strategies for urban green-space planning in cities undergoing densification: A review”. In: *Urban Forestry & Urban Greening* 14.4 (2015), pp. 760–771. ISSN: 1618-8667. DOI: https://doi.org/10.1016/j.ufug.2015.07.009. URL: https://www.sciencedirect.com/science/article/pii/S161886671500103X.

[14] O. Guillitte. “Bioreceptivity: a new concept for building ecology studies”. In: *Science of The Total Environment* 167.1 (1995), pp. 215–220. ISSN: 0048-9697. DOI: https://doi.org/10.1016/0048-9697(95)04582-L. URL: https://www.sciencedirect.com/science/article/pii/004896979504582L.

[15] Max Veeger et al. “Bioreceptive concrete: State of the art and potential benefits”. In: *Heron* 68 (2023), pp. 47–76.

[16] Katia Perini et al. “Experiencing innovative biomaterials for buildings: Potentialities of mosses”. In: *Building and Environment* 172 (2020). ISSN: 03601323. DOI: 10.1016/j.buildenv.2020.106708.

[17] Janice M. Glime. *Chapter 8 - Nutrients*. Electronic Book. 2017. URL: https://digitalcommons.mtu.edu/bryophyte-ecology1/7.

[18] J. Wood Andrew. “The nature and distribution of vegetative desiccation-tolerance in hornworts, liverworts and mosses”. In: *The Bryologist* 110.2 (2007), pp. 163–177. DOI: 10.1639/0007-2745(2007)110[163:IENFIB]2.0.CO;2. URL: https://doi.org/10.1639/0007-2745(2007)110[163:IENFIB]2.0.CO;2.

[19] Chameera Udawattha et al. “Mold growth and moss growth on tropical walls”. In: *Building and Environment* 137 (2018), pp. 268–279. ISSN: 03601323. DOI: 10.1016/j.buildenv.2018.04.018.

[20] Max Veeger, Marc Ottelé, and Alejandro Prieto. “Making bioreceptive concrete: Formulation and testing of bioreceptive concrete mixtures”. In: *Journal of Building Engineering* 44 (2021), p. 102545. ISSN: 2352-7102. DOI: 10.1016/j.jobe.2021.102545. URL: https://www.sciencedirect.com/science/article/pii/S2352710221004022.

[21] Sandra Manso et al. “Bioreceptivity evaluation of cementitious materials designed to stimulate biological growth”. In: *Science of The Total Environment* 481 (2014), pp. 232–241. ISSN: 0048-9697. DOI: https://doi.org/10.1016/j.scitotenv.2014.02.059. URL: https://www.sciencedirect.com/science/article/pii/S0048969714002332.

[22] Kazi Fahriba Mustafa, Alejandro Prieto, and Marc Ottele. “The Role of Geometry on a Self-Sustaining Bio-Receptive Concrete Panel for Facade Application”. In: *Sustainability* 13.13 (2021). ISSN: 2071-1050. DOI: 10.3390/su13137453.

[23] Intan Chairunnisa and Dalhar Susanto. “Living Material as a Building Façade: The Effect of Moss Growth toward Mechanical Performance on Pre-vegetated Concrete Panels”. In: *International Journal of Technology* 9.6 (2018). ISSN: 2087-2100 2086-9614. DOI: 10.14716/ijtech.v9i6.2445.

[24] Shajay Bhooshan et al. “The Striatus bridge”. In: *Architecture, Structures and Construction* 2.4 (2022), pp. 521–543. ISSN: 2730-9886. DOI: 10.1007/s44150-022-00051-y. URL: https://dx.doi.org/10.1007/s44150-022-00051-y.

[25] Manu K. Mohan et al. “Performance criteria, environmental impact and cost assessment for 3D printable concrete mixtures”. In: *Resources, Conservation and Recycling* 181 (2022). ISSN: 09213449. DOI: 10.1016/j.resconrec.2022.106255.

[26] F. P. Bos et al. “The realities of additively manufactured concrete structures in practice”. In: *Cement and Concrete Research* 156 (2022). ISSN: 00088846. DOI: 10.1016/j.cemconres.2022.106746.

[27] Leonie Stohl et al. “Bioreceptivity of concrete: A review”. In: *Journal of Building Engineering* 76 (2023), p. 107201. ISSN: 2352-7102. DOI: https://doi.org/10.1016/j.jobe.2023.107201. URL: https://www.sciencedirect.com/science/article/pii/S2352710223013815.

[28] S. Wang et al. “Digital planting: Fabrication of integrated concrete green wall via additive manufacturing”. In: *RE: Anthropocene, Design in the Age of Humans - Proceedings of the 25th International Conference on Computer-Aided Architectural Design Research in Asia, CAADRIA 2020*. Ed. by D. Holzer et al. Vol. 1. Export Date: 28 February 2024; Cited By: 0; Conference name: 25th International Conference on Computer-Aided Architectural Design Research in Asia, CAADRIA 2020; Conference date: 5 August 2020 through 6 August 2020; Conference code: 162806. The Association for Computer-Aided Architectural Design Research in Asia (CAADRIA), pp. 145–151. ISBN: 978-988789173-4 (ISBN). URL: https://www.scopus.com/inward/record.uri?eid=2-s2.0-85091328796&partnerID=40&md5=afff1d6d821d7782f3a8e4ed68a349b2.

[29] Ariel Cheng Sin Lim and Ayoub Lharchi. “Parameters for Bio-receptivity in 3D Printing”. In: *Design for Climate Adaptation*. Sustainable Development Goals Series. 2023. Chap. Chapter 44, pp. 701–715. ISBN: 978-3-031-36319-1. DOI: 10.1007/978-3-031-36320-7_44.

[30] P. Sochůrková et al. “Bioreceptivity as a Factor of Additive Fabrication: Material Research on 3D Printed Structures affecting Urban Spaces”. In: *Proceedings of the International Conference on Education and Research in Computer Aided Architectural Design in Europe*. Ed. by W. Dokonal et al. Vol. 2. Export Date: 28 February 2024; Cited By: 0; Conference name: 41st Conference on Education and Research in Computer Aided Architectural Design in Europe, eCAADe 2023; Conference date: 20 September 2023 through 22 September 2023; Conference code: 300449. Education and research in Computer Aided Architectural Design in Europe, pp. 115–124. ISBN: 978-949120735-8. URL: https://www.scopus.com/inward/record.uri?eid=2-s2.0-85172441427&partnerID=40&md5=06085645179c95879714b72ff3d27509.

[31] Janice M. Glime. *Chapter 7 - Water Relations*. Electronic Book. 2017. URL: https://digitalcommons.mtu.edu/bryophyte-ecology1/6.

[32] J. E. Park and H. Murase. “Evapotranspiration efficiency of sunagoke moss mat for the wall greening on the building”. In: *American Society of Agricultural and Biological Engineers Annual International Meeting 2008, ASABE 2008*. Vol. 6. Export Date: 23 January 2025; Cited By: 7. 2008, pp. 3612–3621. URL: https://www.scopus.com/inward/record.uri?eid=2-s2.0-63049120496&partnerID=40&md5=34510965eb48079104dd0f4e4ed50540.

[33] Todd N. Rosenstiel et al. “Sex-specific volatile compounds influence microarthropod-mediated fertilization of moss”. In: *Nature* 489.7416 (2012), pp. 431–433. ISSN: 1476-4687. DOI: 10.1038/nature11330. URL: https://doi.org/10.1038/nature11330.

[34] Janice M. Glime. *Chapter 3 - Sexual Strategies*. Vol. Bryophyte Ecology: Volume 1 - Physiological Ecology. Michigan Technological University, 2017. URL: https://digitalcommons.mtu.edu/bryophyte-ecology1/2/.

[35] A. J. Charron and R. S. Quatrano. “Between a rock and a dry place: the water-stressed moss”. In: *Mol Plant* 2.3 (2009). Charron, Audra J Quatrano, Ralph S eng Research Support, Non-U.S. Gov’t England 2009/10/15 Mol Plant. 2009 May;2(3):478-86. doi: 10.1093/mp/ssp018. Epub 2009 Mar 31., pp. 478–86. ISSN: 1674-2052 (Print) 1674-2052 (Linking). DOI: 10.1093/mp/ssp018. URL: https://www.ncbi.nlm.nih.gov/pubmed/19825631.

[36] Mandy L. Slate et al. “Desiccation and rehydration of mosses greatly increases resource fluxes that alter soil carbon and nitrogen cycling”. In: *Journal of Ecology* 107.4 (2019), pp. 1767–1778. ISSN: 0022-0477 1365-2745. DOI: 10.1111/1365-2745.13162.

[37] M. Veeger et al. “Moss species for bioreceptive concrete: A survey of epilithic urban moss communities and their dynamics”. In: *Ecological Engineering* 212 (2025). ISSN: 09258574. DOI: 10.1016/j.ecoleng.2024.107502.

[38] P. Sanmartín et al. “Revisiting and reanalysing the concept of bioreceptivity 25 years on”. In: *Science of The Total Environment* 770 (2021), p. 145314. ISSN: 0048-9697. DOI: https://doi.org/10.1016/j.scitotenv.2021.145314. URL: https://www.sciencedirect.com/science/article/pii/S0048969721003818.

[39] CROW. “C1008-Beton-en-mosaangroei”. In: (2018). URL: https://www.crow.nl/Download-PlaceHolder?downloadid=21423&product=28946.

[40] O. Guillitte and R. Dreesen. “Laboratory chamber studies and petrographical analysis as bioreceptivity assessment tools of building materials”. In: *Science of The Total Environment* 167.1 (1995), pp. 365–374. ISSN: 0048-9697. DOI: https://doi.org/10.1016/0048-9697(95)04596-S. URL: https://www.sciencedirect.com/science/article/pii/004896979504596S.

[41] Didier Snoeck et al. “The effect of (and the potential of recycled) superabsorbent polymers on the water retention capability and bio-receptivity of cementitious materials”. In: *Resources, Conservation and Recycling* 177 (2022). ISSN: 09213449. DOI: 10.1016/j.resconrec.2021.106016.

[42] Husam H. Elgaali, Marina Lopez-Arias, and Mirian Velay-Lizancos. “Accelerated CO2 exposure treatment to enhance bio-receptivity properties of mortars with natural and recycled concrete aggregate”. In: *Construction and Building Materials* 449 (2024). ISSN: 09500618. DOI: 10.1016/j.conbuildmat.2024.138423.

[43] K. M. A. Hossain, S. Ahmed, and M. Lachemi. “Lightweight concrete incorporating pumice based blended cement and aggregate: Mechanical and durability characteristics”. In: *Construction and Building Materials* 25.3 (2011), pp. 1186–1195. ISSN: 0950-0618. DOI: https://doi.org/10.1016/j.conbuildmat.2010.09.036. URL: https://www.sciencedirect.com/science/article/pii/S0950061810004691.

[44] Rakesh Kumar and B. Bhattacharjee. “Porosity, pore size distribution and in situ strength of concrete”. In: *Cement and Concrete Research* 33.1 (2003), pp. 155–164. ISSN: 0008-8846. DOI: https://doi.org/10.1016/S0008-8846(02)00942-0. URL: https://www.sciencedirect.com/science/article/pii/S0008884602009420.

[45] Sandra Manso Blanco et al. “Bioreceptivity optimisation of concrete substratum to stimulate biological colonisation”. Thesis. 2014.

[46] J. Rouquerol et al. “Recommendations for the characterization of porous solids (Technical Report)”. In: 66.8 (1994), pp. 1739–1758. DOI: doi:10.1351/pac199466081739. URL: https://doi.org/10.1351/pac199466081739.

[47] Max Veeger, Alejandro Prieto, and Marc Ottelé. “Exploring the Possibility of Using Bioreceptive Concrete in Building Façades”. In: *Journal of Facade Design and Engineering* 9 (2021), pp. 73–86. DOI: 10.7480/jfde.2021.1.5527.

[48] Mia Maltz et al. “Landscape Topography and Regional Drought Alters Dust Microbiomes in the Sierra Nevada of California”. In: *Frontiers in Microbiology* 13 (2022), p. 856454. DOI: 10.3389/fmicb.2022.856454.

[49] P. Holthuizen and O. Copuroglu. “Quantification of surface grinding during the sample preparation of cementitious materials by optical profilometry”. In: *J Microsc* 294.2 (2024). Holthuizen, Patrick Copuroglu, Oguzhan eng England 2023/12/18 J Microsc. 2024 May;294(2):128-136. doi: 10.1111/jmi.13256. Epub 2023 Dec 26., pp. 128–136. ISSN: 1365-2818 (Electronic) 0022-2720 (Linking). DOI: 10.1111/jmi.13256. URL: https://www.ncbi.nlm.nih.gov/pubmed/38108514.

[50] Kamil Leksycki and Jolanta B. Królczyk. “Comparative assessment of the surface topography for different optical profilometry techniques after dry turning of Ti6Al4V titanium alloy”. In: *Measurement* 169 (2021). ISSN: 02632241. DOI: 10.1016/j.measurement.2020.108378.

[51] D. Vazquez-Nion, B. Silva, and B. Prieto. “Influence of the properties of granitic rocks on their bioreceptivity to subaerial phototrophic biofilms”. In: *Sci Total Environ* 610-611 (2018). Vazquez-Nion, Daniel Silva, Benita Prieto, Beatriz eng Netherlands 2017/08/13 Sci Total Environ. 2018 Jan 1;610-611:44-54. doi: 10.1016/j.scitotenv.2017.08.015. Epub 2017 Aug 9., pp. 44–54. ISSN: 1879-1026 (Electronic) 0048-9697 (Linking). DOI: 10.1016/j.scitotenv.2017.08.015. URL: https://www.ncbi.nlm.nih.gov/pubmed/28802109.

[52] A. Garcia-Collado et al. “Studying the Effect of Short Carbon Fiber on Fused Filament Fabrication Parts Roughness via Machine Learning”. In: *3D Print Addit Manuf* 10.6 (2023). Garcia-Collado, Alberto Romero-Carrillo, Pablo Eduardo Dorado-Vicente, Ruben Gupta, Munish Kumar eng 2023/12/20 3D Print Addit Manuf. 2023 Dec 1;10(6):1336-1346. doi: 10.1089/3dp.2021.0304. Epub 2023 Dec 11., pp. 1336–1346. ISSN: 2329-7670 (Electronic) 2329-7662 (Print) 2329-7662 (Linking). DOI: 10.1089/3dp.2021.0304. URL: https://www.ncbi.nlm.nih.gov/pubmed/38116221.

[53] H. Gimmler and B. Degenhard. “Alkaliphilic and Alkali-Tolerant Algae”. In: 2001, pp. 291–321. ISBN: 978-3-642-63996-8. DOI: 10.1007/978-3-642-59491-5_10.

[54] Branko Šavija and Mladena Luković. “Carbonation of cement paste: Understanding, challenges, and opportunities”. In: *Construction and Building Materials* 117 (2016), pp. 285–301. ISSN: 09500618. DOI: 10.1016/j.conbuildmat.2016.04.138.

[55] Thu Hien Tran et al. “Influence of the intrinsic characteristics of mortars on their biofouling by pigmented organisms: Comparison between laboratory and field-scale experiments”. In: *International Biodeterioration & Biodegradation* 86 (2014), pp. 334–342. ISSN: 0964-8305. DOI: https://doi.org/10.1016/j.ibiod.2013.10.005. URL: https://www.sciencedirect.com/science/article/pii/S0964830513003600.

[56] Estelle Dalod et al. *INFLUENCE OF THE CHEMICAL COMPOSITION OF MORTARS ON ALGAL BIOFOULING*. 2014. DOI: 10.13140/2.1.5143.2327.

[57] Suzan Ibrahim et al. “Marwit Rod El Leqah Quartz Deposits as a Strategic Source of High Purity Quartz”. In: *Journal of Geoscience and Environment Protection* volume 3 (Sept. 2015), pp 41–47. DOI: 10.4236/gep.2015.37005.

[58] Yu Chen et al. “3D printing of calcined clay-limestone-based cementitious materials”. In: *Cement and Concrete Research* 149 (2021). ISSN: 00088846. DOI: 10.1016/j.cemconres.2021.106553.

[59] Payam Shafigh et al. “Influence of fly ash and GGBFS on the pH value of cement mortar in different curing conditions”. In: *Advances in concrete construction* 11.5 (2021), pp. 419–428. ISSN: 2287-5301.

[60] Manuel Ilg and Johann Plank. “Synthesis and Properties of a Polycarboxylate Superplasticizer with a Jellyfish-Like Structure Comprising Hyperbranched Polyglycerols”. In: *Industrial & Engineering Chemistry Research* 58.29 (2019). doi: 10.1021/acs.iecr.9b02077, pp. 12913–12926. ISSN: 0888-5885. DOI: 10.1021/acs.iecr.9b02077. URL: https://doi.org/10.1021/acs.iecr.9b02077.

[61] W.J. Brownlie et al. *Our Phosphorus Future*. Report. UK Centre for Ecology & Hydrology, 2022. DOI: 10.13140/RG.2.2.17834.08645.

[62] Jasmina Kurepa and Jan A. Smalle. “Plant Hormone Modularity and the Survival-Reproduction Trade-Off”. In: *Biology* 12.8 (2023), p. 1143. ISSN: 2079-7737. DOI: 10.3390/biology12081143. URL: https://dx.doi.org/10.3390/biology12081143.

[63] A. Eggert et al. “Quantification of algal biofilms colonising building materials: chlorophyll a measured by PAM-fluorometry as a biomass parameter”. In: *Biofouling* 22.1-2 (2006). Eggert, A Haubner, N Klausch, S Karsten, U Schumann, R eng Research Support, Non-U.S. Gov’t England 2006/04/04 Biofouling. 2006;22(1-2):79-90. doi: 10.1080/08927010600579090., pp. 79–90. ISSN: 0892-7014 (Print) 0892-7014 (Linking). DOI: 10.1080/08927010600579090. URL: https://www.ncbi.nlm.nih.gov/pubmed/16581672.

[64] Ulrich Schreiber. “Pulse-Amplitude-Modulation (PAM) Fluorometry and Saturation Pulse Method: An Overview”. In: *Chlorophyll a Fluorescence: A Signature of Photosynthesis*. Ed. by George Christos Papageorgiou and Govindjee. Dordrecht: Springer Netherlands, 2004, pp. 279–319. ISBN: 978-1-4020-3218-9. DOI: 10.1007/978-1-4020-3218-9_11. URL: https://doi.org/10.1007/978-1-4020-3218-9_11.

[65] Annika K. Jägerbrand and Gaku Kudo. *Short-Term Responses in Maximum Quantum Yield of PSII (Fv/Fm) to ex situ Temperature Treatment of Populations of Bryophytes Originating from Different Sites in Hokkaido, Northern Japan*. Electronic Article. 2016. DOI: 10.3390/plants5020022.

[66] D. Wakefield Rachael and S. Jones Melanie. “An introduction to stone colonizing micro-organisms and biodeterioration of building stone”. In: *Quarterly Journal of Engineering Geology* 31.4 (1998), pp. 301–313. DOI: 10.1144/GSL.QJEG.1998.031.P4.03. URL: https://doi.org/10.1144/GSL.QJEG.1998.031.P4.03.

[67] Maria Filomena Macedo et al. “Biodiversity of cyanobacteria and green algae on monuments in the Mediterranean Basin: an overview”. In: *Microbiology* 155.11 (2009), pp. 3476–3490. ISSN: 1350-0872. DOI: 10.1099/mic.0.032508-0. URL: https://dx.doi.org/10.1099/mic.0.032508-0.

[68] C. Saiz-Jimenez. “Deposition of anthropogenic compounds on monuments and their effect on airborne microorganisms”. In: *Aerobiologia* 11.3 (1995), pp. 161–175. ISSN: 0393-5965. DOI: 10.1007/bf02450035. URL: https://dx.doi.org/10.1007/bf02450035.

[69] M. A. Kaufman. “A Feasibility Growth Study of Native Mosses Associated with Self-Sustaining Flora on Vertical Infrastructure”. In: *International Conference on Transportation and Development 2016*. Proceedings. doi:10.1061/9780784479926.063. 2016, pp. 683–695. DOI: doi:10.1061/9780784479926.06310.1061/9780784479926.063. URL: https://doi.org/10.1061/9780784479926.063.

[70] Dawei Liu et al. “3D printing concrete structures: State of the art, challenges, and opportunities”. In: *Construction and Building Materials* 405 (2023). ISSN: 09500618. DOI: 10.1016/j.conbuildmat.2023.133364.

[71] CROW-CUR. *Richtlijn 5: 3D-betonprinten*. 2023. URL: https://kennisbank.crow.nl/kennismodule/publicationdetail/655#119565.

[72] Suvash Chandra Paul et al. “A review of 3D concrete printing systems and materials properties: current status and future research prospects”. In: *Rapid Prototyping Journal* 24.4 (2018), pp. 784–798. ISSN: 1355-2546. DOI: 10.1108/rpj-09-2016-0154.

[73] A. U. Rehman and J. H. Kim. “3D Concrete Printing: A Systematic Review of Rheology, Mix Designs, Mechanical, Microstructural, and Durability Characteristics”. In: *Materials (Basel)* 14.14 (2021). Rehman, Atta Ur Kim, Jung-Hoon eng 2021R1A2C2013522/National Research Foundation (NRF) Korea/ 2021-12-0027/Yonsei University Research Fund/ Review Switzerland 2021/07/25 Materials (Basel). 2021 Jul 7;14(14):3800. doi: 10.3390/ma14143800. ISSN: 1996-1944 (Print) 1996-1944 (Electronic) 1996-1944 (Linking). DOI: 10.3390/ma14143800. URL: https://www.ncbi.nlm.nih.gov/pubmed/34300719.

[74] Jianzhuang Xiao et al. “Large-scale 3D printing concrete technology: Current status and future opportunities”. In: *Cement and Concrete Composites* 122 (2021). ISSN: 09589465. DOI: 10.1016/j.cemconcomp.2021.104115.

[75] Zeina Malaeb, Fatima AlSakka, and Farook Hamzeh. “3D Concrete Printing: Machine Design, Mix Proportioning, and Mix Comparison Between Different Machine Setups”. In: *3D Concrete Printing Technology*. 2019, pp. 115–136. ISBN: 9780128154816. DOI: 10.1016/b978-0-12-815481-6.00006-3.

[76] Yi Wei Daniel Tay, Ye Qian, and Ming Jen Tan. “Printability region for 3D concrete printing using slump and slump flow test”. In: *Composites Part B: Engineering* 174 (2019). ISSN: 13598368. DOI: 10.1016/j.compositesb.2019.106968.

[77] Seung Cho et al. “A Compendious Rheo-Mechanical Test for Printability Assessment of 3D Printable Concrete”. In: *Second RILEM International Conference on Concrete and Digital Fabrication*. Ed. by Freek P. Bos et al. Springer International Publishing, pp. 196–205. ISBN: 978-3-030-49916-7.

[78] Stefan Chaves Figueiredo et al. “An approach to develop printable strain hardening cementitious composites”. In: *Materials & Design* 169 (2019). ISSN: 02641275. DOI: 10.1016/j.matdes.2019.107651.

[79] Ali Kazemian et al. “Cementitious materials for construction-scale 3D printing: Laboratory testing of fresh printing mixture”. In: *Construction and Building Materials* 145 (2017), pp. 639–647. ISSN: 09500618. DOI: 10.1016/j.conbuildmat.2017.04.015.

[80] Yu Chen et al. “Improving printability of limestone-calcined clay-based cementitious materials by using viscosity-modifying admixture”. In: *Cement and Concrete Research* 132 (2020). ISSN: 00088846. DOI: 10.1016/j.cemconres.2020.106040.

[81] Shaodan Hou et al. “A review of 3D printed concrete: Performance requirements, testing measurements and mix design”. In: *Construction and Building Materials* 273 (2021). ISSN: 09500618. DOI: 10.1016/j.conbuildmat.2020.121745.

[82] Chao Zhang et al. “Design of 3D printable concrete based on the relationship between flowability of cement paste and optimum aggregate content”. In: *Cement and Concrete Composites* 104 (2019), p. 103406. ISSN: 0958-9465. DOI: https://doi.org/10.1016/j.cemconcomp.2019.103406. URL: https://www.sciencedirect.com/science/article/pii/S0958946519305025.

[83] Reza Sedghi, Muhammad Saeed Zafar, and Maryam Hojati. “Exploring Fresh and Hardened Properties of Sustainable 3D-Printed Lightweight Cementitious Mixtures”. In: *Sustainability* 15.19 (2023). ISSN: 2071-1050. DOI: 10.3390/su151914425.

[84] T. T. Le et al. “Mix design and fresh properties for high-performance printing concrete”. In: *Materials and Structures* 45.8 (2012), pp. 1221–1232. ISSN: 1871-6873. DOI: 10.1617/s11527-012-9828-z. URL: https://doi.org/10.1617/s11527-012-9828-z.

[85] A. V. Rahul et al. “3D printable concrete: Mixture design and test methods”. In: *Cement and Concrete Composites* 97 (2019), pp. 13–23. ISSN: 09589465. DOI: 10.1016/j.cemconcomp.2018.12.014.

[86] A. V. Rahul and Manu Santhanam. “Evaluating the printability of concretes containing lightweight coarse aggregates”. In: *Cement and Concrete Composites* 109 (2020). ISSN: 09589465. DOI: 10.1016/j.cemconcomp.2020.103570.

[87] Wen Zhou et al. “Low-carbon, expansive engineered cementitious composites (ECC) in the context of 3D printing”. In: *Cement and Concrete Composites* 148 (2024). ISSN: 09589465. DOI: 10.1016/j.cemconcomp.2024.105473.

[88] Anne Linde van Overmeir et al. “Effects of 3D Concrete Printing Phases on the Mechanical Performance of Printable Strain-Hardening Cementitious Composites”. In: *Buildings* 13.10 (2023). ISSN: 2075-5309. DOI: 10.3390/buildings13102483.

[89] A. S. J. Suiker et al. “Elastic buckling and plastic collapse during 3D concrete printing”. In: *Cement and Concrete Research* 135 (2020). ISSN: 00088846. DOI: 10.1016/j.cemconres.2020.106016.

[90] Jun Ho Jo et al. “Development of a 3D Printer for Concrete Structures: Laboratory Testing of Cementitious Materials”. In: *International Journal of Concrete Structures and Materials* 14.1 (2020), p. 13. ISSN: 2234-1315. DOI: 10.1186/s40069-019-0388-2. URL: https://doi.org/10.1186/s40069-019-0388-2.

[91] R. A. Buswell et al. “3D printing using concrete extrusion: A roadmap for research”. In: *Cement and Concrete Research* 112 (2018), pp. 37–49. ISSN: 0008-8846. DOI: https://doi.org/10.1016/j.cemconres.2018.05.006. URL: https://www.sciencedirect.com/science/article/pii/S0008884617311924.

[92] Aktham S. Alchaar and Adil K. Al-Tamimi. “Mechanical properties of 3D printed concrete in hot temperatures”. In: *Construction and Building Materials* 266 (2021), p. 120991. ISSN: 0950-0618. DOI: https://doi.org/10.1016/j.conbuildmat.2020.120991. URL: https://www.sciencedirect.com/science/article/pii/S0950061820329950.

[93] Guowei Ma, Zhijian Li, and Li Wang. “Printable properties of cementitious material containing copper tailings for extrusion based 3D printing”. In: *Construction and Building Materials* 162 (2018), pp. 613–627. ISSN: 09500618. DOI: 10.1016/j.conbuildmat.2017.12.051.

[94] Senthil Kumar Kaliyavaradhan et al. “Test methods for 3D printable concrete”. In: *Automation in Construction* 142 (2022). ISSN: 09265805. DOI: 10.1016/j.autcon.2022.104529.

[95] Huawei Liu et al. “Hardened properties of 3D printed concrete with recycled coarse aggregate”. In: *Cement and Concrete Research* 159 (2022). ISSN: 00088846. DOI: 10.1016/j.cemconres.2022.106868.

[96] Marchant van den Heever et al. “Evaluating the effects of porosity on the mechanical properties of extrusion-based 3D printed concrete”. In: *Cement and Concrete Research* 153 (2022). ISSN: 00088846. DOI: 10.1016/j.cemconres.2021.106695.

[97] Yu Chen et al. “Characterization of air-void systems in 3D printed cementitious materials using optical image scanning and X-ray computed tomography”. In: *Materials Characterization* 173 (2021). ISSN: 10445803. DOI: 10.1016/j.matchar.2021.110948.

[98] X. Sun et al. “Influence of Extruded Strip Shape and Dimension on the Mechanical Properties of 3D Printed Concrete”. In: *Jianzhu Cailiao Xuebao/Journal of Building Materials* 23.6 (2020). Export Date: 27 January 2025; Cited By: 15, pp. 1313–1320. DOI: 10.3969/j.issn.1007-9629.2020.06.008. URL: https://www.scopus.com/inward/record.uri?eid=2-s2.0-85099012132&doi=10.3969%2fj.issn.1007-9629.2020.06.008&partnerID=40&md5=f4e01c070d464599472fd9100150d787.

[99] Liming Yang et al. “Nozzle criteria for enhancing extrudability, buildability and interlayer bonding in 3D printing concrete”. In: *Automation in Construction* 146 (2023), p. 104671. ISSN: 0926-5805. DOI: https://doi.org/10.1016/j.autcon.2022.104671. URL: https://www.sciencedirect.com/science/article/pii/S0926580522005416.

[100] Biranchi Panda et al. *The Effect of Material Fresh Properties and Process Parameters on Buildability and Interlayer Adhesion of 3D Printed Concrete*. Electronic Article. 2019. DOI: 10.3390/ma12132149.

[101] Marwah M. Thajeel and György L. Balázs. “3D Printed Concrete: Fresh and Hardened Properties”. In: *Periodica Polytechnica Civil Engineering* 69.1 (2024), pp. 12–27. ISSN: 1587-3773 0553-6626. DOI: 10.3311/PPci.37602.

[102] Patrick Bedarf. “Architected Porosity: Foam 3D Printing for Lightweight and Insulating Building Elements”. Thesis. ETZ Zurich, 2023. DOI: https://doi.org/10.3929/ethz-b-000643980.

[103] Yi W. Tay, Ming J. Tan, and Teck N. Wong. *Tailoring Light-Weight Aggregates for Concrete 3D Printing Applications*. Electronic Article. 2023. DOI: 10.3390/ma16072822.

[104] Jolien Van Der Putten, Geert De Schutter, and Kim Tittelboom. *Surface modification as a technique to improve inter-layer bonding strength in 3D printed cementitious materials*. Vol. 4. 2019. DOI: 10.21809/rilemtechlett.2019.84.

[105] Xiao-Sheng Li, Long Li, and Shuai Zou. “Developing Low-pH 3D Printing Concrete Using Solid Wastes”. In: *Buildings* 13.2 (2023). ISSN: 2075-5309. DOI: 10.3390/buildings13020454.

[106] Xiaoyan Sun et al. “PVA fibre reinforced high-strength cementitious composite for 3D printing: Mechanical properties and durability”. In: *Additive Manufacturing* 49 (2022), p. 102500. ISSN: 2214-8604. DOI: https://doi.org/10.1016/j.addma.2021.102500. URL: https://www.sciencedirect.com/science/article/pii/S2214860421006473.

[107] Jolien Van Der Putten et al. “Influence of the Print Process on the Durability of Printed Cementitious Materials”. In: *Third RILEM International Conference on Concrete and Digital Fabrication*. Ed. by Richard Buswell et al. Springer International Publishing, pp. 194–199. ISBN: 978-3-031-06116-5.

[108] Jean De’M Malan, Algurnon Steve van Rooyen, and Gideon P. A. G. van Zijl. “Chloride Induced Corrosion and Carbonation in 3D Printed Concrete”. In: *Infrastructures* 7.1 (2021). ISSN: 2412-3811. DOI: 10.3390/infrastructures7010001.

[109] Kee-Hong Ler et al. “Porosity and durability tests on 3D printing concrete: A review”. In: *Construction and Building Materials* 446 (2024). ISSN: 09500618. DOI: 10.1016/j.conbuildmat.2024.137973.

[110] Yiwei Weng et al. “Feasibility study on sustainable magnesium potassium phosphate cement paste for 3D printing”. In: *Construction and Building Materials* 221 (2019), pp. 595–603. ISSN: 0950-0618. DOI: https://doi.org/10.1016/j.conbuildmat.2019.05.053. URL: https://www.sciencedirect.com/science/article/pii/S0950061819312127.

[111] Alaa M. Rashad. “A short manual on natural pumice as a lightweight aggregate”. In: *Journal of Building Engineering* 25 (2019). ISSN: 23527102. DOI: 10.1016/j.jobe.2019.100802.

[112] Suman Kumar Adhikary, Deepankar Kumar Ashish, and Žymantas Rudžionis. “Expanded glass as lightweight aggregate in concrete – A review”. In: *Journal of Cleaner Production* 313 (2021). ISSN: 09596526. DOI: 10.1016/j.jclepro.2021.127848.

[113] Escsi. *ESCSI - Lightweight Aggregate*. en-US. July 2018. URL: https://www.escsi.org/escs-lwa/.

[114] Bekir Karasu et al. *Properties of Expanded Clay Aggregates*. 2006.

[115] Mikuláš Šveda and Radomir Sokolar. “The effect of firing temperature on the irreversible expansion, water absorption and pore structure of a brick body during freeze-thaw cycles”. In: *Materials Science* 19 (2013). DOI: 10.5755/j01.ms.19.4.2741.

[116] J. Alexandre Bogas, Augusto Gomes, and M. F. C. Pereira. “Self-compacting lightweight concrete produced with expanded clay aggregate”. In: *Construction and Building Materials* 35 (2012), pp. 1013–1022. ISSN: 0950-0618. DOI: https://doi.org/10.1016/j.conbuildmat.2012.04.111. URL: https://www.sciencedirect.com/science/article/pii/S0950061812003133.

[117] Boris Goltsman and N. S. Goltsman. “Study of Recycling Processes of Mixed Waste Glass to Obtain Expanded Glass when Using Glycerol Blowing Agent”. In: *Ecology and Industry of Russia* 26 (2022), pp. 27–33. DOI: 10.18412/1816-0395-2022-6-27-33.

[118] Suman Kumar Adhikary and Zymantas Rudzionis. “Influence of expanded glass aggregate size, aerogel and binding materials volume on the properties of lightweight concrete”. In: *Materials Today: Proceedings* 32 (2020), pp. 712–718. ISSN: 22147853. DOI: 10.1016/j.matpr.2020.03.323.

[119] B. Lubelli et al. “Influence of brick and mortar properties on bioreceptivity of masonry – Results from experimental research”. In: *Construction and Building Materials* 266 (2021). ISSN: 09500618. DOI: 10.1016/j.conbuildmat.2020.121036.

[120] Kyle B Stebbing and Algurnon S Van Rooyen. “The development of a vermiculite based 3D printable fire-resistant concrete and an assessment of its fresh state and mechanical properties”. In: ().

[121] Alaa M. Rashad. “An Overview of Pumice Stone as a Cementitious Material – the Best Manual for Civil Engineer”. In: *Silicon* 13.2 (2020), pp. 551–572. ISSN: 1876-990X 1876-9918. DOI: 10.1007/s12633-020-00469-3.

[122] Degirmenci Nurhayat and Arin Yilmaz. “Use of pumice fine aggregate as an alternative to standard sand in production of lightweight cement mortar”. In: *Indian Journal of Engineering & Materials Sciences* 18.1 (2011), pp. 61–68.

[123] V Bhaskar Desai, K Mallik Arjunappa, and A Sathyam. “An Experimental Investigation on Mode-II Fracture of Light Weight Pumice Aggregate Concrete”. In: *Int. J. Mod. Trends Eng. Res.(IJMER)* 4.12 (2014).

[124] N Sivalinga Rao et al. “Fibre reinforced light weight aggregate (Natural Pumice Stone) concrete”. In: *CONTRIBUTORY PAPERS* 155 (2013).

[125] Yu Chen. “Investigation of limestone-calcined clay-based cementitious materials for sustainable 3d concrete printing.” Thesis. DOI: 10.4233/uuid:a0d9289b-9f24-4805-86ab-09f12714a946.

[126] A. L. van Overmeir et al. “3D printable strain hardening cementitious composites (3DP-SHCC), tailoring fresh and hardened state properties”. In: *Construction and Building Materials* 403 (2023). ISSN: 09500618. DOI: 10.1016/j.conbuildmat.2023.132924.

[127] NEN. *NEN-EN 196-2: 2013 - Methods of testing cement - Part 2: Chemical analysis of cement*. European Standard. Available from NEN or through the European Union’s standards website. 2013.

[128] NEN. *NEN-EN 933-1 - Tests for geometrical properties of aggregates - Part 1: Determination of particle size distribution - Sieving method*. European Standard. Available from NEN or through the European Union’s standards website. 2012.

[129] NEN. *NEN-EN 1097-6: 2022 - Tests for mechanical and physical properties of aggregates - Part 6: Determination of particle density and water absorption*. European Standard. Available from NEN or through the European Union’s standards website. 2022.

[130] NEN. *NEN-EN 1015-3: 1999 - Methods of test for mortar for masonry - Part 3: Determination of consistence of fresh mortar (by flow table)*. European Standard. Available from NEN or through the European Union’s standards website. 1999.

[131] NEN. *NEN-EN 480-2: 2006 - Admixtures for concrete, mortar and grout - Test methods - Part 2: Determination of setting time*. European Standard. Available from NEN or through the European Union’s standards website. 2006.

[132] NEN. *NEN-EN 1015-11: 2019 - Methods of test for mortar for masonry - Part 11: Determination of flexural and compressive strength of hardened mortar*. European Standard. Available from NEN or through the European Union’s standards website. 2019.

[133] Andres Patrignani and Tyson E. Ochsner. “Canopeo: A Powerful New Tool for Measuring Fractional Green Canopy Cover”. In: *Agronomy Journal* 107.6 (2015), pp. 2312–2320. ISSN: 0002-1962 1435-0645. DOI: 10.2134/agronj15.0150.

[134] L. Korat et al. “Characterisation of the pore-forming process in lightweight aggregate based on silica sludge by means of X-ray micro-tomography (micro-CT) and mercury intrusion porosimetry (MIP)”. In: *Ceramics International* 39.6 (2013), pp. 6997–7005. ISSN: 02728842. DOI: 10.1016/j.ceramint.2013.02.037.

[135] Lars Hedenäs and Ole Bennike. “Moss Remains from the Last Interglacial at Thule, NW Greenland”. In: *Lindbergia* 28 (2003), pp. 52–58. DOI: 10.2307/20150125.

[136] Tomáš Hájek et al. “Light responses of mire mosses - A key to survival after water-level drawdown?” In: *Oikos* 118 (2009), pp. 240–250. DOI: 10.1111/j.1600-0706.2008.16528.x.

[137] P. Kallio and N. Valanne. “On the Effect of Continuous Light on Photosynthesis in Mosses”. In: *Fennoscandian Tundra Ecosystems: Part 1 Plants and Microorganisms*. Ed. by F. E. Wielgolaski. Berlin, Heidelberg: Springer Berlin Heidelberg, 1975, pp. 149–162. ISBN: 978-3-642-80937-8. DOI: 10.1007/978-3-642-80937-8_17. URL: https://doi.org/10.1007/978-3-642-80937-8_17.

[138] Małgorzata Romańska. “Impact of water stress on physiological processes of moss Polytrichum piliferum Hedw”. In: *Annales Universitatis Paedagogicae Cracoviensis Studia Naturae* 5 (2020), pp. 129–141. DOI: 10.24917/25438832.5.9. URL: https://aupcstudianaturae.uken.krakow.pl/article/view/7523.

[139] Jae Hong Kim, Jin Hyun Lee, and Yong-Hyok Kim. “Equilibrium of capillary and pore water pressure in lightweight aggregates concrete”. In: *Mechanics of Advanced Materials and Structures* 29.26 (2022). doi: 10.1080/15376494.2021.1949510, pp. 5156–5162. ISSN: 1537-6494. DOI: 10.1080/15376494.2021.1949510. URL: https://doi.org/10.1080/15376494.2021.1949510.

[140] Firmin Anewuoh, Kennedy Appiadu-Boakye, and Francis Kwesi Nsakwa Gabriel-Wettey. “Impact of Curing Methods on the Porosity and Compressive Strength of Concrete”. In: *Journal of Engineering Research and Reports* (2021), pp. 18–30. ISSN: 2582-2926. DOI: 10.9734/jerr/2021/v20i917371.

[141] María Camila Olarte and Juan Carlos Ruge. “Analysis of the relationship between the water retention curve, particle size and pore size distribution in the characterization of a collapsible porous clay”. In: *Respuestas* 25.1 (2020), pp. 33–43. ISSN: 2422-5053 0122-820X. DOI: 10.22463/0122820x.2403.

[142] Zi Yu et al. *Research on the Water Absorption and Release Characteristics of a Carbonized γ-C2S Lightweight Aggregate in Lightweight and High-Strength Concrete*. Electronic Article. 2024. DOI: 10.3390/coatings14081056.

[143] Xiangqun Ding et al. *Capillary Water Absorption and Micro Pore Connectivity of Concrete with Fractal Analysis*. Electronic Article. 2020. DOI: 10.3390/cryst10100892.

[144] Hamlin Jennings et al. *Relating the nanostructure of concrete to engineering properties*. 2006.

[145] Hayati Ulusu et al. “Mechanical, durability and microstructural characteristics of Portland pozzolan cement (PPC) produced with high volume pumice: Green, cleaner and sustainable cement development”. In: *Construction and Building Materials* 378 (2023), p. 131070. DOI: 10.1016/j.conbuildmat.2023.131070.

[146] Mattias Põldaru et al. “The Effect of Printing Direction on the Strength Characteristics of a 3D Printed Concrete Wall Section”. In: *Buildings* 13.12 (2023). ISSN: 2075-5309. DOI: 10.3390/buildings13122917.

[147] Hojae Lee et al. *Evaluation of the Mechanical Properties of a 3D-Printed Mortar*. Electronic Article. 2019. DOI: 10.3390/ma12244104.

[148] Jairon Gomes da Silveira Júnior et al. “Influence of Time Gap on the Buildability of Cement Mixtures Designed for 3D Printing”. In: *Buildings* 14.4 (2024). ISSN: 2075-5309. DOI: 10.3390/buildings14041070.

[149] Zhicong Deng et al. “3D printing lightweight aggregate concrete prepared with shell-packing-aggregate method - Printability, mechanical properties and pore structure”. In: *Journal of Building Engineering* 62 (2022). ISSN: 23527102. DOI: 10.1016/j.jobe.2022.105404.

A

Geometrical code

The full code can be copied from: `https://gitfront.io/r/Coen1997/eNWoj2jr8rKm/3DPC/`

The settings and path for the first wall structure:

```
;reset g2 g3 motion to XY plane
G17
;reset back to mm mode
G21
;cancel radius compensation
G40
;cancel height compensation
G49
;smooth motion mode 0.1mm radius allowed (only when needed)
G64P0.1
;revert back to absolute programming
G90
;revert back to units per minute mode
G94

; to start point
G00 F4000 X0 Y0 Z0

; AROUND PART OF THE THE TABLE (INCREMENTAL)
; MAX DIMENSIONS (X1000 Y700)
G91
G01 F4000 X-725
G02 F4000 X-15 Y15 J15
G01 F4000 Y670
G02 F4000 X15 Y15 I15
G01 F4000 X320
G02 F4000 X15 Y-15 J-15
G01 F4000 Y-80
G02 F4000 X-15 Y-15 I-15

G01 F4000 X-60
G02 F4000 X-12 Y12 J12
G03 F4000 X-12 Y12 I-12


;RECTANGLE STRUCTURE I
G01 F4000 X-160
G02 F4000 Y24 J12
G01 F4000 X170
G02 F4000 Y-24 J-12

G18
G03 F4000 X-5 Z5 I0 K5
G01 F4000 Z1
G02 F4000 X-5 Z5 I-5 K0
G17
```

```
47
48 G01 F4000 X-160
49 G02 F4000 Y24 J12
50 G01 F4000 X170
51 G02 F4000 Y-24 J-12
52
53 G18
54 G03 F4000 X-5 Z5 I0 K5
55 G01 F4000 Z1
56 G02 F4000 X-5 Z5 I-5 K0
57 G17
58
59 G01 F4000 X-160
60 G02 F4000 Y24 J12
61 G01 F4000 X170
62 G02 F4000 Y-24 J-12
63
64 G18
65 G03 F4000 X-5 Z5 I0 K5
66 G01 F4000 Z1
67 G02 F4000 X-5 Z5 I-5 K0
68 G17
69
70 G01 F4000 X-160
71 G02 F4000 Y24 J12
72 G01 F4000 X170
73 G02 F4000 Y-24 J-12
74
75 G18
76 G03 F4000 X-5 Z5 I0 K5
77 G01 F4000 Z1
78 G02 F4000 X-5 Z5 I-5 K0
79 G17
80
81 G01 F4000 X-160
82 G02 F4000 Y24 J12
83 G01 F4000 X170
84 G02 F4000 Y-24 J-12
85
86 G18
87 G03 F4000 X-5 Z5 I0 K5
88 G01 F4000 Z1
89 G02 F4000 X-5 Z5 I-5 K0
90 G17
91
92 G01 F4000 X-160
93 G02 F4000 Y24 J12
94 G01 F4000 X170
95 G02 F4000 Y-24 J-12
96
97 G18
98 G03 F4000 X-5 Z5 I0 K5
99 G01 F4000 Z1
100 G02 F4000 X-5 Z5 I-5 K0
101 G17
102
103 G01 F4000 X-160
104 G02 F4000 Y24 J12
105 G01 F4000 X170
106 G02 F4000 Y-24 J-12
107
108 G18
109 G03 F4000 X-5 Z5 I0 K5
110 G01 F4000 Z1
111 G02 F4000 X-5 Z5 I-5 K0
112 G17
113
114 G01 F4000 X-160
115 G02 F4000 Y24 J12
116 G01 F4000 X170
117 G02 F4000 Y-24 J-12
```

```
118
119 G18
120 G03 F4000 X-5 Z5 I0 K5
121 G01 F4000 Z1
122 G02 F4000 X-5 Z5 I-5 K0
123 G17
124
125 G01 F4000 X-160
126 G02 F4000 Y24 J12
127 G01 F4000 X170
128 G02 F4000 Y-24 J-12
129
130 G18
131 G03 F4000 X-5 Z5 I0 K5
132 G01 F4000 Z1
133 G02 F4000 X-5 Z5 I-5 K0
134 G17
135
136 G01 F4000 X-160
137 G02 F4000 Y24 J12
138 G01 F4000 X170
139 G02 F4000 Y-24 J-12
140
141 G18
142 G03 F4000 X-5 Z5 I0 K5
143 G01 F4000 Z50
144 G17
145
146 G90
147 G00 X-390 Y524 Z0
148 G91
149
150 G00 Y-70
151 G02 F4000 X-12 Y-12 I-12
152 G01 F4000 X-60
153 G02 F4000 X-12 Y12 J12
154 G03 F4000 X-12 Y12 I-12
```

B

CT Acquisition settings

```
[Scantype]
name = "smooth take and save"
data format = ""

[Sample info]
Sample name = "3DPC cylinder "
Project = "MicroLab"
Application area = "CT"
Owner = "MicroLab"
Comment = "1.5mm Al Filter\0A\0A\0A\0A"
Contact person = "Arjan Thijssen"
Diameter (mm) = 14.824993
Height (mm) = 63.199972

[Scan info]
Scan name = "3DPC cylinder"
scanID = "241219_012"
Operator = "admin"
Acquila version = "release_16x\0D\0A    release 164\0D\0
    A883d1e127ca40a02733b66aa7a5b13ac2cad810b"
scanner type = "CoreTOM"
scanner S/N = "122-0078"
BatchID = "3DPC cylinder"
Start = "2024-12-19 10:54:43.2098455 UTC"
Stop = "2024-12-19 11:03:28.9921054 UTC"
Duration = "00:08:45"
Succeeded = TRUE
Error = "No error"
Scanner name = "CoreTOM TU-Delft"

[Tube settings]
Tube name = "xraysource"
Focus mode = "Microfocus"
Output mode = "Target power"
Current set value = 175.942245
Current actual value = 174.950577
kV set value = 160.000000
kV actual value = 160.246765
Target current set value = 156.249924
Target current actual value = 156.073151
Target power set value = 24.999989
Target power actual value = 25.010218
Vacuum level = "1.421379E-6"
Filament status = "OK"
Interlock = "CLOSED"
Defocussed = TRUE
Xray stable = TRUE
SerialNumber = "P20-839"
Filter = ""
```

```
49
50 [Camera settings]
51 Camera name = "XRD4343_2856x2856"
52 Imaging mode = "1_HW1SW1LOW"
53 Exposure time (ms) = 179.998590
54 Nr. of averages = 1
55 Nr. of frames = 2274
56 Unbinned pixelsize (mm) = 0.150000
57 Binning value = 1.000000
58 Binned pixelsize (mm) = 0.150000
59 ROI = "683;12;2199;2867"
60 Columns = 1517
61 Rows = 2856
62 SerialNumber = "896"
63
64 [Acquisition settings]
65 script settings set = TRUE
66 Vertical mode = "Cone beam"
67 Rotation mode = "Smooth"
68 CTaxis = "rot_obj"
69 Path = "/E/Civil Engineering/Microlab/Coen/EG30-W1-C1"
70 File base name = "scan_"
71 projs_per_360 = 2274
72 CT start angle = 0.000000
73 CT stop angle = 360.000000
74 total projections = 2274
75 nr of sections = 1
76 DI frequency = "Once"
77 nr DI before = 25
78 nr DI after = 0
79 IO frequency = "Once"
80 nr IO before = 50
81 nr IO after = 0
82 Refs frequency = "Never"
83 nr refs before = 0
84 nr refs after = 0
85 nr averages refs = 1
86 time lapse pause (s) = 0.000000
87 pause before scan (s) = 5.000000
88 pause before DI (s) = 5.000000
89 pause before IO (s) = 5.000000
90 set kV = FALSE
91 tube kV = 160.000000
92 set power = FALSE
93 tube power = 24.999989
94 set focus mode = FALSE
95 Focus Mode = "Microfocus"
96 Keep X-ray on = TRUE
97 Conditioning frequency = "Never"
98 Refresh tube = FALSE
99 Filament adjust = FALSE
100 AutocenterkV = TRUE
101 Exposure time (ms) = 179.998590
102 readout time (ms) = 0.000000
103 nr of averages = 1
104 Imaging mode = "1_HW1SW1LOW"
105 ROI = "683;12;2199;2867"
106 VOI name = "3DPC cylinder"
107 Set sample position = TRUE
108 PI_X = 0.041375
109 PI_Y = 1.746736
110 ver_obj = 846.385875
111 mag_obj = 86.417175
112 tra_obj = 17.875488
113 Flat field axis = "ver_obj"
114 Flat Field position = 750.000000
115 Scan position = 846.385875
116 ver_det = 161.917686
117 mag_det = 665.219604
118 tra_det = -4.684021
119 ver_tube = 75.498009
```

```
mag_tube = 0.000000
tra_tube = 0.000000
Top at VC = 814.785889
Bottom at VC = 877.985861
rotation speed = 0.879919
rotation acc = 11.250000
vertical speed = 2.000000
vertical acc = 62.500000
Goto ref after scan = FALSE
Log tubestatus = TRUE
vertical step = 0.203997
script generator = "script generator generic_newUI"

[Data set settings]
time = "12/19/2024 11:56:09 AM"
number offset images = "1"
number gain images = "1"
number projections = "2274"
data path = "E:\\Civil Engineering\\Microlab\\Coen\\EG30-W1-C1"
basename = "scan_"
import ROI = "0;0;1517;2856;"
import binning = "1.000000"
import binning method = "none"
import use slope/offset = "False"
import first projection = "0"
import last projection = "2273"
import projections = "2274"
import decimate value = "1"
X-position = "0.041250"
X-direction = "1"
Y-position = "1.746625"
Y-direction = "-1"
Z-position = "846.386963"
Z-direction = "1"
projection pixel size = ""
recon path = ""
BitsPerSample = "16"
Slope = "1.000000"
Offset = "0.000000"

[CT-parameters IN]
Start angle = "0.000000"
Last angle = "360.000000"
SOD = "108.332977"
SDD = "649.997375"
COR = "757.008179"
VC = "1429.111084"
Direction = "0.000000"
Pixel size = "0.150000"
bhc = "0.000000"
Tilt = "0.000000"
zmin = "251.000000"
zmax = "2606.000000"
x_start = "0.000000"
x_end = "1516.000000"
y_start = "0.000000"
y_end = "1516.000000"
Interpolate = "1.000000"
Resolution = "1.000000"
Voxel size = "0.025000"
z_start = "251.000000"
z_end = "2606.000000"
Min grey value = "0.000000"
Max grey value = "0.000000"
Recon mode = "0.000000"
ZP factor = "3.000000"
Filter type = "0.000000"
Filter level = "0.000000"
Min CT value = "-3.000000"
Max CT value = "20.000000"
Spot filter = "10.000000"
```

```
HC = "757.008667"
bhc2 = "0.000000"
Ring level = "0.960000"
Ring kernel = "5.000000"
Ring blocks = "4.000000"
Prompt scaling = "0.000000"
Spot kernel = "0.000000"
Phase mu = "0.000000"
Phase delta = "0.000000"
Edge correction factor = "0.800000"
Square recon = "0.000000"
Scatter = "0.000000"
Clipping value = "0.000000"
EFOV filter = "0.000000"
Original number of columns = "0.000000"
EFOV axis = "0.000000"
FilterEdgeWidth = "3.000000"

[motor positions]
ver_obj = 846.386991
mag_obj = 86.417175
mag_det = 665.219604
rot_obj = 0.000000
PI_X = 0.041250
PI_Y = 1.746625
tra_obj = 17.875488
tra_det = -4.684021
ver_tube = 75.499125
ver_det = 161.922580
```